

Rapidity distribution of pseudo-scalar Higgs boson to $\text{NNLO}_A + \overline{\text{NNLL}}$

V. Ravindran,^{a,b} Aparna Sankar^{a,b,c,d} and Surabhi Tiwari^{a,b,e}

^a*The Institute of Mathematical Sciences,
IV Cross Road, Taramani, Chennai 600 113, India*

^b*Homi Bhabha National Institute,
Training School Complex, Anushakti Nagar, Mumbai 400085, India*

^c*Physik Department T31, James-Franck-Straße 1,
Technische Universität München, D-85748 Garching, Germany*

^d*Max-Planck-Institut für Physik, Föhringer Ring 6, 80805 München, Germany*

^e*Institut für Theoretische Teilchenphysik, Karlsruhe Institute of Technology (KIT), Wolfgang-
Gaede Straße 1, 76128 Karlsruhe, Germany*

E-mail: ravindra@imsc.res.in, aparna@mpp.mpg.de,
surabhi.tiwari@kit.edu

ABSTRACT: We present the differential predictions for the rapidity distribution of pseudo-scalar Higgs boson through gluon fusion at the LHC. These results are obtained taking into account the soft-virtual (SV) as well as the next-to-soft virtual (NSV) resummation effects to next-to-next-to-leading- logarithmic ($\overline{\text{NNLL}}$) accuracy and matching them to the approximate fixed order next-to-next-to-leading- order (NNLO_A) computation. We perform the resummation in two dimensional Mellin space using our recent formalism [1] by limiting ourselves to the contributions only from gluon- gluon (gg) initiated channels. The NNLO_A rapidity distribution of pseudo-scalar Higgs is obtained by applying a ratio method on the NNLO rapidity distribution of the scalar Higgs boson. We also present the first analytical results of N^3LO rapidity distribution of pseudo-scalar Higgs at $\text{SV}+\text{NSV}$ accuracy. The phenomenological impacts of $\text{NNLO}_A + \overline{\text{NNLL}}$ predictions for 13 TeV LHC are studied. We observe that, for $m_A = 125(700)$ GeV, the $\text{SV}+\text{NSV}$ resummation at $\overline{\text{NNLL}}$ level brings about 14.76% (11.48%) corrections to the NNLO_A results at the central scale value of $\mu_R = \mu_F = m_A$. Further, we find that the sensitivity to the renormalisation scale gets improved substantially by the inclusion of NSV resummed predictions at $\overline{\text{NNLL}}$ accuracy.

KEYWORDS: Higgs Physics, Pseudo-scalar Higgs, QCD, gluon fusion, Radiative corrections, Resummation

Contents

1	Introduction	2
2	Pseudo-scalar Higgs effective field theory	5
3	Fixed order formalism	6
3.1	Fixed order results at NLO and NNLO _A	8
4	SV+NSV Formalism	12
4.1	Operator Renormalisation Constant	14
4.2	Form Factor	15
4.3	Mass factorisation kernel	18
4.4	Soft-collinear function	19
5	Matching with the inclusive	24
6	Results of the SV and NSV rapidity distributions	25
7	More on the \vec{z} space solution $\Phi_{d,g}^A$	27
8	Resummation in the Mellin \vec{N} space	29
9	Numerical analysis	30
10	Discussions and Conclusions	46
11	Acknowledgments	47
A	QCD β functions	47
B	NLO Results	48
C	Anomalous dimensions	50
D	Results of SV rapidity distribution to third order	51
E	The Resummation constant $\tilde{g}_{d,g,0}^A$	52
F	NSV Resummation exponents $\bar{g}_{d,g,i}^A(\omega)$	55
G	NSV Resummation exponents $h_{d,g,ij}^A(\omega)$ and $\tilde{h}_{d,g,ij}^A(\omega, \omega_l)$	56

1 Introduction

Measurement of a variety of observables to very high precision is one of the thrust areas in the physics programme of the Large Hadron Collider (LHC). Precision studies based on these measurements provide crucial tests of the consistency of the Standard Model (SM) and any significant deviation can also hint towards new physics beyond SM. The discovery of the Higgs boson [2, 3], one of the major milestones in particle physics, led to a better understanding of the dynamics behind the electroweak symmetry breaking [4–8], and in larger picture, opened up a plenty of opportunities to unravel hidden physics behind various phenomena. Despite this successes, the SM lacks in fronts in not providing satisfactory explanations for phenomena such as baryon asymmetry in the universe, the existence of the dark matter, the neutrino mass etc, and hence falls short of being a complete theory of fundamental interactions. Unravelling these phenomena demands one to go beyond the borderline of the SM. One of the possible extensions of the SM is the supersymmetric theories which provide an elegant solution to the above mentioned problems. Supersymmetric theories generally predict a richer Higgs sector than the Standard Model (SM). In the Minimal Supersymmetric Standard Model (MSSM) for instance one introduces two complex Higgs doublets, which originate five physical Higgs bosons: two CP-even Higgs bosons (h, H) two charged Higgs bosons (H^\pm) and, finally, a CP-odd (pseudo-scalar) Higgs boson (A) [9–16].

Ever since the Higgs boson was discovered at the LHC [2, 17], there exists curiosity among the high energy physics community to understand whether it is the Higgs boson of the SM or not. This leads to a physics program aiming at probing its interaction with other SM particles with extreme precision that will determine its properties. This can shed light on whether the discovered Higgs boson is the scalar or pseudo-scalar Higgs bosons of extended models. Such a study requires precise predictions for their production cross sections and the decay rates. In particular, the production of CP-odd Higgs boson/pseudo-scalar at the LHC has been studied in detail, taking into account the higher order QCD radiative corrections, owing to similarities with its CP-even counter part. Among other channels, it is desirable to look for pseudo-scalar Higgs boson in the gluon fusion through heavy fermions due to its appreciable coupling in the small and moderate $\tan\beta$ in the minimal version of SUSY model, where $\tan\beta$ is the ratio of vacuum expectation values $v_i, i = 1, 2$. Furthermore, the large gluon flux leads to an enhancement in the cross section.

Perturbative QCD (pQCD) provides the most successful framework to compute the observables that can be measured at the LHC. The production of a pseudo-scalar Higgs boson through gluon fusion at leading order suffers from large theoretical uncertainties, particularly due to the presence of renormalisation scale μ_R arising from the strong coupling constant. It also contains mild theoretical uncertainties which result from the factorisation scale μ_F in the parton distribution functions. In order to deal with these scale uncertainties as well as to uplift the accuracy of theoretical predictions, one has to go beyond the wall of leading-order (LO) computations.

The QCD higher order corrections to the production of CP-even scalar as well as CP-odd pseudo-scalar bosons through gluon fusion are known for a long time in the literature.

For the case of a scalar Higgs boson, results for the inclusive production cross section are available up to next-to-next-to-next-to-leading order(N³LO) QCD [18–21], within the framework of an effective theory that results from the integration of top quark degrees of freedom. This leads to variety of new interactions of the Higgs boson directly with the gluons [22–24]. On the other hand, for the pseudo-scalar case, only next-to-next-to-leading order(NNLO) QCD results [20, 25–28] in the effective theory [29] are known. The exact quark mass dependence for scalar and pseudo-scalar production is known to next-to-leading order(NLO) QCD [30, 31]. For N³LO predictions of pseudo-scalar cross section, both three loop form factors and real emission contributions are required. The computation of form factors is technically cumbersome[32] as pseudo-scalar Higgs boson couples to SM fields through two composite operators that mix under renormalisation due to the axial anomaly and additionally, a finite renormalisation constant needs to be introduced in order to restore the chiral Ward identities. Moreover, these operators involve Levi-Civita tensor and γ_5 which are not very straightforward to define in dimensional regularisation. The three loop form factor obtained in [32] was later combined with suitable soft distribution function [33–35] and mass factorisation kernels for the computation of the soft plus virtual (SV) contribution at N³LO in [36]. Later, in [37], a new determination of approximate N³LO pseudo-scalar boson cross section has been introduced, based on the N³LO results of scalar Higgs boson [38].

In addition to the the inclusive production cross section, the differential rapidity distribution is among the most important observables, which is expected to be measured in upcoming days. This demands for very precise theoretical predictions of this observable. The computation of the transverse momentum and rapidity distributions for the scalar Higgs boson up to NLO has been done in [39, 40] and for the pseudo-scalar Higgs boson in [41]. Both inclusive cross section and differential rapidity distribution get large contributions from logarithms arising from certain kinematic regions, thus spoiling the reliability of the fixed order predictions. This usually occurs at the threshold region, namely when the mass of pseudo-scalar Higgs boson becomes equal to the partonic center of mass energy, due to the presence of soft gluons. Hence, the large logarithms resulting from soft gluons in the perturbative series need to be resummed to provide sensible predictions. In the pioneering works of Sterman [42] and of Catani and Trentadue [43], resummation of leading large logarithms for the inclusive rates in the Mellin space and also to differential x_F distribution [43] using double Mellin moments were achieved. Soft gluon resummation of the gluon fusion cross section has been performed to next-to-next-to-next-to-leading logarithmic(N³LL) accuracy for the scalar Higgs case [33, 34, 44–50] and to next-to-next-to-leading logarithmic(NNLL) accuracy for the pseudo-scalar case [51]. In [52], the resummed transverse momentum distribution has been calculated up to NNLO_A + NNLL for the pseudo-scalar Higgs boson.

A generic threshold resummation formula valid to N³LL accuracy for colour-neutral final states was derived in [50], requiring only the virtual three-loop amplitudes as process-dependent input. Exploiting the factorization properties of differential cross sections as well as the renormalisation group (RG) invariance, an all order z -space formalism was also developed in [53], to study the threshold-enhanced contribution to rapidity distribution of

any colorless particle. In [54], the same formalism [53] was used to study the threshold resummation of rapidity distribution of Higgs boson and later to the Drell-Yan (DY) process [55]. For different approaches and their applications, see [56–64].

The resummed predictions played a crucial role to understand the experimental data in the threshold regions. Besides the threshold enhanced logarithms which are also called as the soft virtual (SV) logarithms, the subleading logarithms, called the next-to-soft virtual (NSV) logarithms, are also present in the partonic channels beyond leading order in perturbation theory. There have been a surge of interests in the community of theoretical physicists to understand the nature of these subleading logarithms by using various methods [65–77]. Recently, the well-established ideas of collinear factorisation and renormalisation group invariance have been implemented to understand the perturbative structure of NSV logarithms for inclusive processes in [78, 79]. Following the same formalism of [78, 79], in a series of articles [80–82], we studied variety of inclusive reactions to understand the impact of NSV logarithms and found a systematic way to sum them up to all orders in z as well as in the Mellin N spaces. We have also studied the perturbative structure of the NSV logarithms in the context of rapidity distributions of DY and Higgs productions in [1]. In addition, for the first time, a procedure to resum them in a systematic manner in the double Mellin space beyond the SV accuracy has also been developed in [1]. Further, we have studied the phenomenological relevance of the NSV resummation in the context of both DY and Higgs rapidity distributions in [83, 84] respectively. For the pseudo-scalar Higgs, the resummed predictions including both SV and NSV are recently available to NNLO+NNLL accuracy in [85] for the inclusive cross section case. However, similar predictions for the differential case is not available in the literature.

In this article, we explore the role of SV and NSV resummed contributions for the differential rapidity distribution of pseudo-scalar Higgs boson in gluon fusion channel by employing the formalism developed in [1]. In particular, we compute the SV and NSV resummed terms to NNLL accuracy in the double Mellin N -space. Further, we study the phenomenological impact of adding these resummed predictions to the fixed order results through a matching procedure.

The paper is structured as follows: The first section deals with the theoretical description for the interaction of a pseudo-scalar Higgs with the QCD particles. In the next section, we discuss the computation of the rapidity distribution at the fixed order level. We explicitly show the computational steps at NLO and discuss a procedure to obtain an approximate NNLO which is denoted as NNLO_A. In section 4, we review the framework given in [1] for computing the SV+NSV contributions to the rapidity distribution of a pseudo-scalar Higgs in gluon fusion. The following subsections are devoted to the discussions on the ingredients that are required to compute the rapidity distribution at SV+NSV approximation to N³LO accuracy. In section 5, a relation between inclusive cross section and rapidity distribution has been exploited to determine the unknown coefficients of certain logarithms which contribute to the SV+NSV rapidity distribution. The results of SV+NSV rapidity distribution for pseudo-scalar Higgs in gluon fusion at the partonic level are presented up to N³LO in section 6. In section 7, we focus on the characteristic structure of the NSV soft-collinear function along with some of its peculiar features. In section 8,

we review the formalism to resum the NSV logarithms to $\overline{\text{NNLL}}$ accuracy followed by the phenomenological studies of the resummed predictions in section 9. Finally, we conclude our findings in section 10.

2 Pseudo-scalar Higgs effective field theory

We begin with setting up the theoretical framework for our analysis. The coupling of a pseudo-scalar Higgs boson with gluons occurs only indirectly through a virtual heavy quark loop which can be integrated out in the infinite quark mass limit. The interaction between pseudo-scalar Higgs boson χ^A and the QCD particles in the infinitely large top quark mass limit can be described by an effective Lagrangian [29] and it is given by

$$\mathcal{L}_{\text{eff}}^A = \chi^A(x) \left[-\frac{1}{8} C_G O_G(x) - \frac{1}{2} C_J O_J(x) \right] \quad (2.1)$$

where the two operators are defined as

$$O_G(x) = G_a^{\mu\nu} \tilde{G}_a^{\rho\sigma} \equiv \epsilon_{\mu\nu\rho\sigma} G_a^{\mu\nu} G_a^{\rho\sigma}, \quad O_J(x) = \partial_\mu (\bar{\psi} \gamma^\mu \gamma_5 \psi). \quad (2.2)$$

Here, $G_{\mu\nu}^a = \partial_\mu G_\nu^a - \partial_\nu G_\mu^a + g_s f^{abc} G_\mu^b G_\nu^c$ is the colour-field-strength tensor and $\tilde{G}^{a\mu\nu} = \epsilon^{\mu\nu\rho\sigma} G_{\rho\sigma}^a$ is its dual with $\epsilon_{\mu\nu\rho\sigma}$ being the Levi-Civita tensor; G_μ^a are the gluon fields, $g_s = \sqrt{4\pi\alpha_s}$ is the QCD gauge coupling, and f^{abc} are the structure constants of the $SU(N)$ algebra. The symbols ψ and $\bar{\psi}$ represent fields related to quarks and anti-quarks, respectively. The Wilson coefficients C_G and C_J of the two operators originate from integrating out the heavy quark loop in effective theory. The coefficient C_G does not receive any QCD corrections beyond one loop due to Adler-Bardeen theorem [86], whereas C_J starts only at second order in the strong coupling constant. These Wilson coefficients are given by [29]

$$C_G = -a_s 2^{\frac{5}{4}} G_F^{\frac{1}{2}} \cot\beta, \quad C_J = - \left[a_s C_F \left(\frac{3}{2} - 3 \ln \frac{\mu_R^2}{m_t^2} \right) + a_s^2 C_J^{(2)} + \dots \right] C_G, \quad (2.3)$$

where $a_s = g_s^2/16\pi^2$. Here, G_F denotes the Fermi constant, $\cot\beta$ is the mixing angle in the Two-Higgs-Doublet model and C_F is the quadratic Casimir in the fundamental representation of QCD. The symbols m_A and m_t stand for the masses of the pseudo-scalar Higgs boson and top quark (heavy quark), respectively. The bare strong coupling constant in the regularized theory is denoted by \hat{a}_s which is related to its renormalised counter-part by

$$\hat{a}_s S_\epsilon = \left(\frac{\mu^2}{\mu_R^2} \right)^{\epsilon/2} Z_{a_s} a_s \quad (2.4)$$

where $S_\epsilon = \exp\left(\frac{\epsilon}{2}[\gamma_E - \ln(4\pi)]\right)$ with γ_E being the Euler-Mascheroni constant. In the above expression, μ_R is the mass scale at which the strong coupling constant is renormalised. The scale μ is introduced to keep the unrenormalised strong coupling constant dimensionless in

$d = 4 + \epsilon$ space-time dimensions. The renormalisation constant Z_{a_s} up to $\mathcal{O}(a_s^3)$ is given by

$$Z_{a_s} = 1 + a_s \left[\frac{2}{\epsilon} \beta_0 \right] + a_s^2 \left[\frac{4}{\epsilon^2} \beta_0^2 + \frac{1}{\epsilon} \beta_1 \right] + a_s^3 \left[\frac{8}{\epsilon^3} \beta_0^3 + \frac{14}{3\epsilon^2} \beta_0 \beta_1 + \frac{2}{3\epsilon} \beta_2 \right]. \quad (2.5)$$

The coefficient of the QCD β function β_i [87] are given in Appendix A.

3 Fixed order formalism

The rapidity distribution for the production of a pseudo-scalar Higgs boson at the hadron colliders can be computed using

$$\frac{d}{dY} \sigma^A(\tau, m_A^2, Y) = \sigma^{A,(0)}(\tau, m_A^2) W(\tau, m_A^2, Y)$$

with

$$W = \sum_{a,b=q,\bar{q},g} \int_0^1 dx_1 \int_0^1 dx_2 \hat{f}_a(x_1) \hat{f}_b(x_2) \int_0^1 dz \delta(\tau - zx_1 x_2) \times \int [dPS_{1+m}] |\overline{\mathcal{M}}_{ab}|^2 \times \delta\left(Y - \frac{1}{2} \ln\left(\frac{P_2 \cdot q}{P_1 \cdot q}\right)\right). \quad (3.1)$$

Here, $\sigma^{A,(0)}(\tau, m_A^2)$ is the born cross section corresponding to the leading order(LO) process: $g(p1) + g(p2) \rightarrow A(q)$ at the parton level. The hadronic scaling variable τ is defined by $\tau \equiv m_A^2/S$ where S is the square of hadronic centre of mass energy and the dimensionless variable z is defined as $z \equiv m_A^2/\hat{s}$, where \hat{s} is the square of partonic centre of mass energy. $\hat{f}_{a(b)}$ are the bare parton distribution functions (PDF) with $x_{1(2)}$ being the fraction of the initial state hadronic momentum carried by the partons (a, b) that take part in the scattering at the partonic level. $\overline{\mathcal{M}}_{ab}$ denotes the scattering amplitude at the partonic level and the overline signifies the sum and average over all the quantum numbers for the final and initial state particles, respectively. $[dPS_{1+m}]$ is the phase space element for the $A+m$ -system where the integer m depends on the number of radiated partons. The symbol Y in Eq.(3.1) stands for the rapidity of the pseudo-scalar Higgs boson and it is defined as

$$Y \equiv \frac{1}{2} \ln\left(\frac{P_2 \cdot q}{P_1 \cdot q}\right), \quad (3.2)$$

where P_l ($l = 1, 2$) is the momenta of incoming hadrons and q denotes the momentum of pseudo-scalar Higgs boson. In order to define the threshold limit at the partonic level and to express the hadronic rapidity distribution in terms of the partonic one through convolution integrals, we choose to work with the symmetric scaling variables x_1^0 and x_2^0

$$Y \equiv \frac{1}{2} \ln\left(\frac{x_1^0}{x_2^0}\right) \quad \text{and} \quad \tau \equiv x_1^0 x_2^0. \quad (3.3)$$

In terms of these variables, the partonic contributions arising from the subprocesses are found to depend on the ratios

$$z_i \equiv \frac{x_i^0}{x_i}, \quad i = 1, 2, \quad (3.4)$$

which play the role of scaling variables at the partonic level.

The partonic rapidity distribution can be computed, within the framework of perturbative QCD, order by order in strong coupling constant. The contributions arising from beyond leading order contain the UV, soft and collinear divergences. Upon performing dimensional regularisation, the true nature of the UV divergences arises as poles in ε , and such divergences go away when the renormalisation of coupling, masses and fields are performed in modified minimal subtraction (\overline{MS}) scheme. The UV renormalised partonic rapidity distribution denoted by $\hat{\Delta}_{d,ab}^A$ is identified as,

$$\frac{1}{x_1 x_2} \hat{\Delta}_{d,ab}^A(z_1, z_2, \hat{a}_s, \mu^2, m_A^2, \mu_R^2) = \int [dPS_{1+m}] \int_0^1 dz |\overline{\mathcal{M}}_{ab}|^2 \times \delta(\tau - z x_1 x_2) \delta\left(Y - \frac{1}{2} \ln\left(\frac{P_2 \cdot q}{P_1 \cdot q}\right)\right). \quad (3.5)$$

The soft and collinear divergences are collectively called as infrared (IR) divergences. The soft divergences come from zero momentum gluons in the loops of virtual contributions and real gluons in the gluon emission processes. The massless or light partons are responsible for collinear divergences. Due to the KLN theorem [88, 89], soft and collinear divergences resulting from final state partons cancel independently after summing up contributions from all possible degenerate states. However, the collinear singularities arising from the collinear configurations involving initial state particles remain. Those are removed at the hadronic level through the technique, known as mass factorisation. The infrared safe partonic rapidity distribution which is also termed as the partonic coefficient function (CF) can be obtained by using the factorisation formula given below

$$\Delta_{d,ac}^A(z_1, z_2, a_s(\mu_R^2), m_A^2, \mu_F^2, \mu_R^2) = \int_{z_1}^1 \frac{dy_1}{y_1} \int_{z_2}^1 \frac{dy_2}{y_2} \Gamma_{aa'}^{-1}(\hat{a}_s, \mu^2, \mu_F^2, y_1, \epsilon) \times \hat{\Delta}_{d,a'c'}^A\left(\frac{z_1}{y_1}, \frac{z_2}{y_2}, \hat{a}_s, \mu^2, m_A^2, \mu_R^2, \epsilon\right) \times \Gamma_{cc'}^{-1}(\hat{a}_s, \mu^2, \mu_F^2, y_2, \epsilon), \quad (3.6)$$

where Γ_{ab} are the Altarelli-Parisi (AP) [90] kernels which essentially absorb the initial state collinear singularities. The factored out initial state collinear divergences get absorbed into the bare PDFs to give a finite renormalised value at the scale μ_F . Using Eq.(3.6) and substituting it in Eq.(3.1), we obtain the expression for the rapidity distribution in terms of renormalised PDFs and finite CF as given below.

$$\frac{d\sigma^A}{dY} = \sigma^{A,(0)}(\tau, m_A^2) \sum_{a,b=q,\bar{q},g} \int_{x_1^0}^1 \frac{dz_1}{z_1} \int_{x_2^0}^1 \frac{dz_2}{z_2} f_a\left(\frac{x_1^0}{z_1}, \mu_F^2\right) f_b\left(\frac{x_2^0}{z_2}, \mu_F^2\right) \times \Delta_{d,ab}^A(z_1, z_2, m_A^2, \mu_F^2, \mu_R^2). \quad (3.7)$$

The perturbative expansion of the infrared safe CF in powers of strong coupling constant read as,

$$\Delta_{d,c}^A(z_1, z_2, m_A^2, \mu_F^2, \mu_R^2) = \sum_{i=0}^{\infty} a_s^i(\mu_R^2) \Delta_{d,c}^{A,(i)}(z_1, z_2, m_A^2, \mu_F^2, \mu_R^2), \quad c = q, \bar{q}, g. \quad (3.8)$$

In this article, we have computed $\frac{d\sigma^A}{dY}$ in Eq. (3.7) explicitly up to next-to leading order (NLO) for the production of pseudo-scalar Higgs boson in gluon fusion channel, which will be discussed in the following sub-section. We will also discuss how an approximate NNLO which is denoted as NNLO_A can be obtained by using the NNLO results of a scalar Higgs boson.

3.1 Fixed order results at NLO and NNLO_A

Here, we begin with the computation of the rapidity distribution $\frac{d\sigma^A}{dY}$ given in Eq. (3.7) at NLO accuracy. Note that the NLO contribution arises from the one loop virtual corrections to born process $g + g \rightarrow A$ and from the real emission processes, namely $g + g \rightarrow A + g$, $q + g \rightarrow A + q$ and $q + \bar{q} \rightarrow A + g$. In order to obtain $\frac{d\sigma^A}{dY}$ at NLO, the first step is to calculate $\hat{\Delta}_{d,ab}^{A,(i)}$ given in Eq. (3.5) for $i = 1$ for the aforementioned processes. One of the ingredients to find $\hat{\Delta}_{d,ab}^{A,(1)}$ is the phase space element dPS_{1+m} which is relevant for the processes at NLO. For the virtual contributions to the born process, $dPS_{1+m} = dPS_1$ which is given as

$$dPS_1 = \frac{2\pi}{m_A^2} \delta(1 - z_1) \delta(1 - z_2), \quad (3.9)$$

and for the real emission processes, we have two body phase space element $dPS_{1+m} = dPS_2$, which takes the following form:

$$dPS_2 = \frac{1}{8\pi x_1 x_2} \frac{1}{\Gamma(1 + \frac{\epsilon}{2})} \left(\frac{m_A^2}{4\pi} \right)^{\epsilon/2} \frac{2z_1 z_2 (1 + z_1 z_2)}{(z_1 + z_2)^{2-\epsilon}} \left((1 - z_1^2)(1 - z_2^2) \right)^{\epsilon/2}. \quad (3.10)$$

Next, we need to determine the square of the matrix element $|\overline{\mathcal{M}}_{ab}|^2$ which is averaged over spin, polarisation and color for the NLO processes mentioned above. For the one loop correction to the LO process, we obtain

$$\begin{aligned} |\overline{\mathcal{M}}|_{g+g \rightarrow A}^2 \Big|_{\text{one loop}} &= a_s \frac{C_A G_F^2 Q^4}{(N^2 - 1)} \left[\frac{1}{\epsilon^2} \left\{ -2 \right\} + \frac{1}{\epsilon} \left\{ -1 - L_{QF} \right\} + \left\{ \frac{3}{2} + \frac{7}{4} \zeta_2 - \frac{1}{2} L_{QF} \right. \right. \\ &\quad \left. \left. - \frac{1}{4} L_{QF}^2 \right\} + \epsilon \left\{ -\frac{5}{4} - \frac{7}{12} \zeta_3 + \frac{7}{8} \zeta_2 + \frac{3}{4} L_{QF} + \frac{7}{8} L_{QF} \zeta_2 - \frac{1}{8} L_{QF}^2 \right. \right. \\ &\quad \left. \left. - \frac{1}{24} L_{QF}^3 \right\} + \epsilon^2 \left\{ \frac{7}{8} - \frac{7}{24} \zeta_3 - \frac{21}{16} \zeta_2 - \frac{73}{320} \zeta_2^2 - \frac{5}{8} L_{QF} - \frac{7}{24} L_{QF} \zeta_3 \right. \right. \\ &\quad \left. \left. + \frac{7}{16} L_{QF} \zeta_2 + \frac{3}{16} L_{QF}^2 + \frac{7}{32} L_{QF}^2 \zeta_2 - \frac{1}{48} L_{QF}^3 \right\} + \epsilon^3 \left\{ -\frac{9}{16} + \frac{7}{16} \zeta_3 \right. \right. \\ &\quad \left. \left. + \frac{35}{32} \zeta_2 + \frac{1}{6} \zeta_2 \zeta_3 - \frac{73}{640} \zeta_2^2 + \frac{7}{16} L_{QF} - \frac{7}{48} L_{QF} \zeta_3 - \frac{21}{32} L_{QF} \zeta_2 \right. \right. \\ &\quad \left. \left. - \frac{73}{640} L_{QF} \zeta_2^2 - \frac{5}{32} L_{QF}^2 - \frac{7}{96} L_{QF}^2 \zeta_3 + \frac{7}{64} L_{QF}^2 \zeta_2 + \frac{1}{32} L_{QF}^3 \right. \right. \\ &\quad \left. \left. + \frac{7}{192} L_{QF}^3 \zeta_2 \right\} + \epsilon^4 \left\{ \frac{5}{16} - \frac{35}{96} \zeta_3 + \frac{37}{144} \zeta_3^2 - \frac{49}{64} \zeta_2 + \frac{1}{12} \zeta_2 \zeta_3 + \frac{219}{1280} \zeta_2^2 \right. \right. \\ &\quad \left. \left. - \frac{39}{640} \zeta_2^3 - \frac{9}{32} L_{QF} + \frac{7}{32} L_{QF} \zeta_3 + \frac{35}{64} L_{QF} \zeta_2 + \frac{1}{12} L_{QF} \zeta_2 \zeta_3 \right. \right. \end{aligned}$$

$$\begin{aligned}
& -\frac{73}{1280}L_{QF}\zeta_2^2 + \frac{7}{64}L_{QF}^2 - \frac{7}{192}L_{QF}^2\zeta_3 - \frac{21}{128}L_{QF}^2\zeta_2 - \frac{73}{2560}L_{QF}^2\zeta_2^2 \\
& - \left. \frac{5}{192}L_{QF}^3 - \frac{7}{576}L_{QF}^3\zeta_3 + \frac{7}{384}L_{QF}^3\zeta_2 \right\}, \tag{3.11}
\end{aligned}$$

where $L_{QF} = \log\left(\frac{Q^2}{\mu_F^2}\right)$ and ζ_i are the Riemann zeta functions. Here, $Q^2 = m_A^2$. For the real emission process $g + g \rightarrow A + g$, we find

$$\begin{aligned}
|\overline{\mathcal{M}}|_{g+g \rightarrow A+g}^2 &= \frac{a_s}{(\mu_R)^{\epsilon/2}} \frac{\pi^2 C_A G_F^2}{(N^2 - 1)} \left[\frac{1}{D_1 D_2} (8s^3) + Q^2(32) + \frac{Q^2}{D_2}(16s) + \frac{Q^2}{D_1}(16s) + Q^4 \left(\right. \right. \\
& - \frac{16}{s} \left. \right) + \frac{Q^4}{D_2}(-8) + \frac{Q^4}{D_1}(-8) + \frac{Q^6}{D_2}\left(\frac{8}{s}\right) + \frac{Q^6}{D_1}\left(\frac{8}{s}\right) + D_1(-8) \\
& + D_1 Q^2\left(\frac{8}{s}\right) + D_1^2\left(-\frac{8}{s}\right) - 16s + \epsilon \left\{ \frac{1}{D_1 D_2}(4s^3) + Q^2(8) + \frac{Q^2}{D_2}(8s) \right. \\
& + \frac{Q^2}{D_1}(8s) + Q^4\left(-\frac{8}{s}\right) + \frac{Q^4}{D_2}(-4) + \frac{Q^4}{D_1}(-4) + \frac{Q^6}{D_2}\left(\frac{4}{s}\right) + \frac{Q^6}{D_1}\left(\frac{4}{s}\right) \\
& \left. + D_1(-4) + D_1 Q^2\left(\frac{4}{s}\right) + D_1^2\left(-\frac{4}{s}\right) - 8s \right\} + \epsilon^2 \left\{ \frac{1}{D_1 D_2}(-2s^3) + Q^2 \left(\right. \right. \\
& - 4) + \frac{Q^2}{D_2}(-4s) + \frac{Q^2}{D_1}(-4s) + Q^4\left(\frac{4}{s}\right) + \frac{Q^4}{D_2}(2) + \frac{Q^4}{D_1}(2) + \frac{Q^6}{D_2} \left(\right. \\
& \left. - \frac{2}{s} \right) + \frac{Q^6}{D_1}\left(-\frac{2}{s}\right) + D_1(2) + D_1 Q^2\left(-\frac{2}{s}\right) + D_1^2\left(\frac{2}{s}\right) + 4s \left. \right\} \\
& + \epsilon^3 \left\{ \frac{1}{D_1 D_2}(s^3) + Q^2(6) + \frac{Q^2}{D_2}(2s) + \frac{Q^2}{D_1}(2s) + Q^4\left(-\frac{2}{s}\right) - \frac{Q^4}{D_2} \right. \\
& \left. - \frac{Q^4}{D_1} + \frac{Q^6}{D_2}\left(\frac{1}{s}\right) + \frac{Q^6}{D_1}\left(\frac{1}{s}\right) - D_1 + D_1 Q^2\left(\frac{1}{s}\right) + D_1^2\left(-\frac{1}{s}\right) - 2s \right\} \\
& + \epsilon^4 \left\{ \frac{1}{D_1 D_2}\left(-\frac{1}{2}s^3\right) + Q^2(-5) + \frac{Q^2}{D_2}(-s) + \frac{Q^2}{D_1}(-s) + Q^4\left(\frac{1}{s}\right) \right. \\
& + \frac{Q^4}{D_2}\left(\frac{1}{2}\right) + \frac{Q^4}{D_1}\left(\frac{1}{2}\right) + \frac{Q^6}{D_2}\left(-\frac{1}{2s}\right) + \frac{Q^6}{D_1}\left(-\frac{1}{2s}\right) + D_1\left(\frac{1}{2}\right) + D_1 Q^2 \left(\right. \\
& \left. \left. - \frac{1}{2s} \right) + D_1^2\left(\frac{1}{2s}\right) + s \right\}, \tag{3.12}
\end{aligned}$$

with $D_1 = \frac{-Q^2}{z}(1-z)(1-y)$ and $D_2 = \frac{-Q^2}{z}(1-z)y$, where

$$z = \frac{x_1^0 x_2^0}{x_1 x_2}, \quad y = \frac{x_2 x_2^0 (x_1 + x_1^0)(x_1 - x_1^0)}{(x_1 x_2^0 + x_2 x_1^0)(x_1 x_2 - x_1^0 x_2^0)}. \tag{3.13}$$

For the real emission process $q + g \rightarrow A + q$, we obtain

$$|\overline{\mathcal{M}}|_{q+g \rightarrow A+q}^2 = \frac{a_s}{(\mu_R)^{\epsilon/2}} \frac{\pi^2 C_F G_F^2}{(N^2 - 1)} \left[(-4s) + \frac{1}{D_1}(-8s^2) + Q^2(4) + Q^2 \frac{1}{D_1}(8s) + Q^4 \frac{1}{D_1} \left(\right. \right.$$

$$\begin{aligned}
& -4) + D_2(4) + \epsilon \left\{ \frac{1}{D_1}(-4s^2) + Q^2(4) + Q^2 \frac{1}{D_1}(4s) + Q^4 \frac{1}{D_1}(-4) \right. \\
& \left. + D_2(4) \right\} + \epsilon^2 \left\{ (2s) + \frac{1}{D_1}(2s^2) + Q^2 \frac{1}{D_1}(-2s) \right\} + \epsilon^3 \left\{ (-s) + \frac{1}{D_1}(-s^2) \right. \\
& \left. + Q^2 \frac{1}{D_1}(s) \right\} + \epsilon^4 \left\{ \left(\frac{1}{2}s \right) + \frac{1}{D_1} \left(\frac{1}{2}s^2 \right) + Q^2 \frac{1}{D_1} \left(-\frac{1}{2}s \right) \right\} \Big],
\end{aligned} \tag{3.14}$$

and for $g + q \rightarrow A + q$, we have

$$|\overline{\mathcal{M}}|_{g+q \rightarrow A+q}^2 = |\overline{\mathcal{M}}|_{q+g \rightarrow A+q|_{D_1 \leftrightarrow D_2}}^2. \tag{3.15}$$

Finally, for the real emission process $q + \bar{q} \rightarrow A + g$, we find

$$\begin{aligned}
|\overline{\mathcal{M}}|_{q+\bar{q} \rightarrow A+g}^2 &= \frac{a_s}{(\mu_R)^{\epsilon/2}} \frac{\pi^2 C_F G_F^2}{N} \left[(4s) + Q^2(-8) + Q^4 \left(\frac{4}{s} \right) + D_1(8) + D_1 Q^2 \left(-\frac{8}{s} \right) \right. \\
&+ D_1^2 \left(\frac{8}{s} \right) + \epsilon \left\{ (6s) + Q^2(-12) + Q^4 \left(\frac{6}{s} \right) + D_1(8) + D_1 Q^2 \left(-\frac{8}{s} \right) \right. \\
&\left. \left. + D_1^2 \left(\frac{8}{s} \right) \right\} + \epsilon^2 \left\{ (2s) + Q^2(-4) + Q^4 \left(\frac{2}{s} \right) \right\} \right].
\end{aligned} \tag{3.16}$$

Now, we can compute the NLO hadronic rapidity distribution $\frac{d\sigma^A}{dY}$ in Eq. (3.7) by performing the convolution of $\Delta_{d,ab}^A$ for all the contributing processes at NLO discussed above with the corresponding PDFs. Note that $\Delta_{d,ab}^A$ can be obtained by substituting for $\hat{\Delta}_{d,a'b'}^A$ in the factorisation formula (3.6) which requires the phase space element as well as the matrix element square computed above according to Eq. (3.5). We express the NLO rapidity distribution at the hadronic level as

$$\frac{d\sigma^{A,\text{NLO}}}{dY} = \sigma^{A,(0)}(\tau, m_A^2) \left\{ \frac{d\sigma_{gg}^{A,(0)}}{dY} + a_s \frac{d\sigma_{gg}^{A,(1)}}{dY} + a_s \frac{d\sigma_{qg}^{A,(1)}}{dY} + a_s \frac{d\sigma_{q\bar{q}}^{A,(1)}}{dY} + a_s \frac{d\sigma_{q\bar{q}}^{A,(1)}}{dY} \right\}, \tag{3.17}$$

where

$$\frac{d\sigma_{gg}^{A,(0)}}{dY} = H_{gg}(x_1^0, x_2^0, \mu_F^2) = f_g(x_1^0, \mu_F^2) f_g(x_2^0, \mu_F^2). \tag{3.18}$$

The full result of $\frac{d\sigma^{A,\text{NLO}}}{dY}$ is provided in Appendix B. Here, we would like to mention one interesting observation of the NLO result of pseudo-scalar Higgs rapidity distribution. As already noted in [91], the NLO result of rapidity distribution of pseudo-scalar is related to that of scalar Higgs at partonic level as follows:

$$\begin{aligned}
\Delta_{d,gg}^{A,(1)} &= \Delta_{d,gg}^{H,(1)} + a_s 8C_A \delta(1-z_1)\delta(1-z_2), \\
\Delta_{d,qg}^{A,(1)} &= \Delta_{d,qg}^{H,(1)}, \quad \Delta_{d,q\bar{q}}^{A,(1)} = \Delta_{d,q\bar{q}}^{H,(1)},
\end{aligned} \tag{3.19}$$

where H stands for the scalar Higgs boson. From a detailed analysis of the above results, it has been found that the difference in the rapidity distribution of scalar and pseudo-scalar Higgs at NLO for gg -channel arises only from the one loop virtual contribution to the respective born processes which is also termed as one loop form factor(FF). Note that the FFs of both scalar and pseudo-scalar Higgs bosons are different due to the presence of different Wilson coefficients corresponding to ggA (pseudo-scalar) and ggH (scalar) vertices in the Higgs effective field theory[29]. However, we note that the full hadronic NLO rapidity distribution of pseudo-scalar Higgs can be correctly obtained from that of scalar Higgs by using the formula given below

$$\frac{d\sigma^{A,\text{NLO}}}{dY} = \mathcal{R}_{\mathcal{AH}} \times \left(\frac{\sigma^{A,(0)}}{\sigma^{H,(0)}} \right) \times \frac{1}{C_H^2} \frac{d\sigma^{H,\text{NLO}}}{dY}, \quad (3.20)$$

with $\sigma^{H,(0)}$ being the born cross section for scalar Higgs and C_H is the Wilson coefficient for ggH effective vertex [92]. In the above formula, $\mathcal{R}_{\mathcal{AH}}$ is the ratio of the modulus square of the finite form factors (FF) corresponding to pseudo-scalar and scalar Higgs [32, 93], that means $\mathcal{R}_{\mathcal{AH}} = \frac{|FF_A|^2}{|FF_H|^2}$. We provide the expression of the ratio factor $\mathcal{R}_{\mathcal{AH}}$ up to a_s^3 below

$$\begin{aligned} \mathcal{R}_{\mathcal{AH}} = & \left[1 + a_s \{8C_A\} + a_s^2 \left\{ n_f C_F \left(-31 + 12L_{rmt} - 4L_{qr} \right) + C_A n_f \left(-\frac{2}{3} - \frac{4}{3}L_{qr} \right) \right. \right. \\ & + C_A^2 \left(\frac{215}{3} - \frac{20}{3}L_{qr} \right) \left. \right\} + a_s^3 \left\{ n_f \left(-4C_J^{(2)} \right) + n_f C_F^2 \left(\frac{763}{9} + 4L_{qr} + \frac{32}{3}\zeta_3 \right) \right. \\ & + n_f^2 C_F \left(\frac{4520}{81} - \frac{328}{9}L_{qr} + 16L_{qr}L_{rmt} - \frac{8}{3}L_{qr}^2 + 16\zeta_2 \right) + C_A n_f C_F \left(-\frac{67094}{81} \right. \\ & + 96L_{rmt} + \frac{1492}{9}L_{qr} - 88L_{qr}L_{rmt} + \frac{44}{3}L_{qr}^2 + \frac{224}{3}\zeta_3 - 88\zeta_2 \left. \right) + C_A n_f^2 \left(-\frac{631}{81} \right. \\ & + \frac{134}{27}L_{qr} - \frac{8}{9}L_{qr}^2 + \frac{16}{3}\zeta_2 \left. \right) + C_A^2 n_f \left(\frac{1973}{81} - \frac{838}{27}L_{qr} + \frac{4}{9}L_{qr}^2 - 16\zeta_3 - \frac{8}{3}\zeta_2 \right) \\ & \left. \left. + C_A^3 \left(\frac{68309}{81} - \frac{6028}{27}L_{qr} + \frac{220}{9}L_{qr}^2 - \frac{208}{3}\zeta_3 - \frac{440}{3}\zeta_2 \right) \right\} \right], \quad (3.21) \end{aligned}$$

where $L_{qr} = \ln\left(\frac{q^2}{\mu_R^2}\right)$ and $L_{rmt} = \ln\left(\frac{\mu_R^2}{m_t^2}\right)$.

Now we ask the following question: can this ratio factor $\mathcal{R}_{\mathcal{AH}}$ be used for computing the rapidity distribution of pseudo-scalar from that of scalar Higgs beyond NLO accuracy? In [37], one of the authors of this article had studied the applicability of this ratio method in obtaining the inclusive cross section of pseudo-scalar from that of scalar Higgs beyond NLO. In [37], it has been established that an approximate NNLO result can be obtained for the inclusive cross section of pseudo-scalar from that of scalar Higgs by using this ratio method. In that case, the difference between the exact and approximate results are found to be in terms of next-to-next-to-soft contributions which are suppressed by $(1-z)^2$ with respect to the leading soft terms that means they vanish in the threshold limit $z \rightarrow 1$. In addition, there are no $\log(1-z)$ terms present in the difference of exact and approximate

NNLO results. This suggests that one can compute the inclusive cross section of pseudo-scalar Higgs from that of scalar Higgs by employing the ratio method up to next-to soft terms or NSV terms correctly. In addition, in [37], it has been shown that the approximate NNLO results provide an excellent approximation to the exact one where the discrepancy is at most 2% for high mass region whereas it is around 1% for the low mass case.

Drawing inspiration from the above observation for the inclusive case at NNLO, in this article, we attempt to go beyond NLO for uplifting the theoretical accuracy of the predictions for pseudo-scalar Higgs rapidity distribution. We begin with computing the approximate NNLO rapidity distribution of the pseudo-scalar from the exact NNLO result of scalar Higgs available in [94] by using a formula which is equivalent to Eq. (3.20) for the NNLO case. We denote this approximate NNLO result by NNLO_A. The analytic expression of this result is too big to be presented in this article, nevertheless, we reserve a section for the detailed numerical analysis of the results we computed. Further, in principle, one can extend the same ratio method discussed here to obtain the approximate results at N³LO for the rapidity distribution of the pseudo-scalar Higgs. However, since the complete N³LO results for the Higgs rapidity distribution [95] are not yet available publicly, it is not possible to compute approximate N³LO results for the rapidity distribution of the pseudo-scalar Higgs using the ratio method mentioned above. Needless to say, computing the corrections beyond NNLO is not easy and the complexity level of the computation increases significantly which often prevents us from achieving it. Hence, we resort to an alternate method based on soft-virtual and next-to-soft-virtual approximation [1] which essentially captures the dominant contribution at the threshold to go beyond the NNLO accuracy, which will be the topic of the next section.

4 SV+NSV Formalism

The goal of this section is to study the rapidity distribution of pseudo-scalar Higgs in gluon fusion at the soft-virtual(SV) + next-to-soft-virtual(NSV) approximation. To be more precise, we consider the contributions to the partonic CF corresponding to the rapidity distribution of a pseudo-scalar Higgs boson in gluon fusion in the limit $z_l \rightarrow 1$ by keeping only SV and NSV terms, hence we denote them by $\Delta_{d,g}^{A,SV+NSV}$. Since we restrict ourselves to SV terms namely distributions of the kind $\delta(1-z_i)$ and $\mathcal{D}_k(z_i)$ and NSV terms $\log^k(1-z_i)$ for the CF with gluon-gluon initiated channel, the expansion coefficients in Eq. 3.8 can be expressed as follows

$$\begin{aligned} \Delta_{d,g}^{A,(i)} &= \Delta_{d,g,\delta\delta}^{A,(i)} \delta(\bar{z}_1)\delta(\bar{z}_2) + \sum \Delta_{d,g,\delta\mathcal{D}_j}^{A,(i)} \delta(\bar{z}_1)\mathcal{D}_j(z_2) + \sum \Delta_{d,g,\delta L_j}^{A,(i)} \delta(\bar{z}_1)L_j(z_2) \\ &+ \sum \Delta_{d,g,\mathcal{D}_j\mathcal{D}_k}^{A,(i)} \mathcal{D}_j(z_1)\mathcal{D}_k(z_2) + \sum \Delta_{d,g,\mathcal{D}_j L_k}^{A,(i)} \mathcal{D}_j(z_1)L_k(z_2) + (z_1 \leftrightarrow z_2), \end{aligned}$$

$$\text{with } \mathcal{D}_j(z_l) = \left[\frac{\ln^j(1-z_l)}{(1-z_l)} \right]_+, \delta(\bar{z}_l) = \delta(1-z_l) \text{ and } L_j(z_l) = \log^j(1-z_l) \text{ for } l = 1, 2. \quad (4.1)$$

In [1], it has been already shown that, the SV+NSV contributions to the differential distributions arising from diagonal partonic channels which is the gluon-gluon channel in our case, can be factorised in terms of the overall operator UV renormalization constant Z_g^A , the bare form factor \hat{F}_g^A (FF), a function $\mathcal{S}_{d,g}^A$ that is sensitive to real emission contributions and the collinear singular AP kernels Γ_{gg} . This is always possible as $(Z_g^A)^2$ and $|\hat{F}_g^A|^2$ are simply proportional to $\delta(\bar{z}_1)\delta(\bar{z}_2)$ and can be factored out from these partonic channels. Hence, near threshold we obtain, for $\Delta_{d,g}^{A,SV+NSV}$

$$\begin{aligned} \Delta_{d,g}^{A,SV+NSV}(z_1, z_2, m_A^2, \mu_F^2, \mu_R^2, \epsilon) &= \sigma^{A,(0)}(\mu_R^2) (Z_g^A(\hat{a}_s, \mu_R^2, \mu^2, \epsilon))^2 |\hat{F}_g^A(\hat{a}_s, \mu^2, m_A^2, \epsilon)|^2 \\ &\times \delta(\bar{z}_2)\delta(\bar{z}_1) \otimes \mathcal{S}_{d,g}^A(\hat{a}_s, \mu^2, m_A^2, z_1, z_2, \epsilon) \\ &\otimes \Gamma_{gg}^{-1}(\hat{a}_s, \mu^2, \mu_F^2, z_1, \epsilon) \delta(\bar{z}_2) \\ &\otimes \Gamma_{gg}^{-1}(\hat{a}_s, \mu^2, \mu_F^2, z_2, \epsilon) \delta(\bar{z}_1). \end{aligned} \quad (4.2)$$

The symbol \otimes refers to convolution, which is defined for functions, $f_i(x_i), i = 1, 2, \dots, n$, as,

$$(f_1 \otimes f_2 \otimes \dots \otimes f_n)(z) = \prod_{i=1}^n \left(\int dx_i f_i(x_i) \right) \delta(z - x_1 x_2 \dots x_n). \quad (4.3)$$

As long as we are interested in computing the SV+NSV parts of the rapidity distribution, that is those resulting from the phase space region where $z_{1(2)} \rightarrow 1$, we keep only those terms that are proportional to distributions $\delta(\bar{z}_l)$, $\mathcal{D}_i(z_l)$ and NSV terms $\log^i(1 - z_l)$ with $l = 1, 2$ and $i = 0, 1, \dots$ and drop the rest of the terms resulting from the convolutions. Hence, we have kept only diagonal part of AP kernel Γ_{ab} in Eq. 4.2 and dropped the non-diagonal AP kernels. In addition, the diagonal kernels get contributions only from the diagonal splitting functions. The reason for the above simplification is due to the fact that the distributions and NSV logarithms can come only from convolutions of two or more distributions or a distribution with NSV logarithms. In summary, since our main focus here is on SV and NSV terms resulting from gluon initiated pseudo-scalar Higgs production, we have dropped contributions from non-diagonal partonic channels in the mass factorised result of $\Delta_{d,g}^A$. All the ingredients in Eq. 4.2 that are required to get a finite CF, namely Z_g^A , \hat{F}_g^A , $\mathcal{S}_{d,g}^A$ and Γ_{gg} are known to satisfy certain differential equations with respect to some mass scales [1, 33, 79, 80]. The form of solutions to the respective differential equations which will be discussed in the subsequent sections along with the well-established ideas of collinear factorisation lead to an all order formula for computing $\Delta_{d,g}^{A,SV+NSV}$ in z -space

$$\Delta_{d,g}^{A,SV+NSV}(q^2, \mu_R^2, \mu_F^2, z_1, z_2) = \mathcal{C} \exp \left(\Psi_{d,g}^A(q^2, \mu_R^2, \mu_F^2, z_1, z_2, \epsilon) \right) \Big|_{\epsilon=0}, \quad (4.4)$$

where the function $\Psi_{d,g}^A$ is given by

$$\Psi_{d,g}^A(q^2, \mu_R^2, \mu_F^2, z_1, z_2, \epsilon) = \left(\ln(Z_g^A(\hat{a}_s, \mu^2, \mu_R^2, \epsilon))^2 + \ln |\hat{F}_g^A(\hat{a}_s, \mu^2, Q^2, \epsilon)|^2 \right) \delta(\bar{z}_1)\delta(\bar{z}_2)$$

$$\begin{aligned}
& + \mathcal{C} \ln \mathcal{S}_{d,g}^A(\hat{a}_s, \mu^2, q^2, z_1, z_2, \epsilon) - \mathcal{C} \ln \Gamma_{gg}(\hat{a}_s, \mu^2, \mu_F^2, z_1, \epsilon) \delta(\bar{z}_2) \\
& - \mathcal{C} \ln \Gamma_{gg}(\hat{a}_s, \mu^2, \mu_F^2, z_2, \epsilon) \delta(\bar{z}_1). \tag{4.5}
\end{aligned}$$

The symbol ‘‘ \mathcal{C} ’’ stands for the convolution whose actions on a distribution $g(z_1, z_2)$ is defined as

$$\mathcal{C}e^{g(z_1, z_2)} = \delta(1 - z_1)\delta(1 - z_2) + \frac{1}{1!}g(z_1, z_2) + \frac{1}{2!}(g \otimes g)(z_1, z_2) + \dots, \tag{4.6}$$

where \otimes denotes the Mellin convolution. Though the constituents of $\Psi_{d,g}^A$ contain UV and IR divergent terms, the sum of all these terms is finite and is regular in the variable ϵ . It contains the distributions such as $\delta(1 - z_l)$, $\mathcal{D}_i(z_l)$ and the logarithms of the form $\log^i(1 - z_l)$, $l = 1, 2, i = 0, 1, \dots$.

4.1 Operator Renormalisation Constant

Besides coupling constant renormalisation, the form factor also requires the renormalisation of the effective operators in the effective Lagrangian, Eq.(2.1). This additional renormalisation is called the overall operator renormalisation which is performed through the constant Z_g^A . In Eq. 4.2, the overall operator renormalisation Z_g^A is determined by solving the underlying renormalisation group (RG) equation:

$$\mu_R^2 \frac{d}{d\mu_R^2} \ln Z_g^A(\hat{a}_s, \mu_R^2, \mu^2, \epsilon) = \sum_{i=1}^{\infty} a_s^i \gamma_{g,i}^A. \tag{4.7}$$

Using the results of $\gamma_{g,i}^A$ given in Appendix A and solving the above RG equation, we obtain the overall renormalisation constant up to three loop level as

$$\begin{aligned}
Z_g^A = & 1 + a_s \left[\frac{22}{3\epsilon} C_A - \frac{4}{3\epsilon} n_f \right] + a_s^2 \left[\frac{1}{\epsilon^2} \left\{ \frac{484}{9} C_A^2 - \frac{176}{9} C_A n_f + \frac{16}{9} n_f^2 \right\} + \frac{1}{\epsilon} \left\{ \frac{34}{3} C_A^2 \right. \right. \\
& \left. \left. - \frac{10}{3} C_A n_f - 2 C_F n_f \right\} \right] + a_s^3 \left[\frac{1}{\epsilon^3} \left\{ \frac{10648}{27} C_A^3 - \frac{1936}{9} C_A^2 n_f + \frac{352}{9} C_A n_f^2 - \frac{64}{27} n_f^3 \right\} \right. \\
& \left. + \frac{1}{\epsilon^2} \left\{ \frac{5236}{27} C_A^3 - \frac{2492}{27} C_A^2 n_f - \frac{308}{9} C_A C_F n_f + \frac{280}{27} C_A n_f^2 + \frac{56}{9} C_F n_f^2 \right\} \right. \\
& \left. + \frac{1}{\epsilon} \left\{ \frac{2857}{81} C_A^3 - \frac{1415}{81} C_A^2 n_f - \frac{205}{27} C_A C_F n_f + \frac{2}{3} C_F^2 n_f + \frac{79}{81} C_A n_f^2 + \frac{22}{27} C_F n_f^2 \right\} \right], \tag{4.8}
\end{aligned}$$

with the $SU(N)$ QCD color factors

$$C_A = N, \quad C_F = \frac{N^2 - 1}{2N}. \tag{4.9}$$

Here, n_f is the number of active light quark flavors. It is to be noted that $Z_g^A = Z_{GG}$ which is given in Eq.(3.49) of [32] has been discussed extensively in [32].

4.2 Form Factor

The unrenormalised form factor $F_g^A(\hat{a}_s, Q^2, \mu^2, \epsilon)$ satisfies the so-called K + G differential equation [96–99] which is dictated by the factorization property, gauge and renormalisation group (RG) invariances:

$$Q^2 \frac{d}{dQ^2} \ln \hat{F}_g^A(\hat{a}_s, Q^2, \mu^2, \epsilon) = \frac{1}{2} \left[K_g^A\left(\hat{a}_s, \frac{\mu_R^2}{\mu^2}, \epsilon\right) + G_g^A\left(\hat{a}_s, \frac{Q^2}{\mu_R^2}, \frac{\mu_R^2}{\mu^2}, \epsilon\right) \right], \quad (4.10)$$

where all poles in the dimensional regulator ϵ are contained in the Q^2 independent function K_g^A and the finite terms in $\epsilon \rightarrow 0$ are encapsulated in G_g^A . RG invariance of the form factor implies

$$\mu_R^2 \frac{d}{d\mu_R^2} K_g^A\left(\hat{a}_s, \frac{\mu_R^2}{\mu^2}, \epsilon\right) = -\mu_R^2 \frac{d}{d\mu_R^2} G_g^A\left(\hat{a}_s, \frac{Q^2}{\mu_R^2}, \frac{\mu_R^2}{\mu^2}, \epsilon\right) = -\sum_{i=1}^{\infty} a_s^i(\mu_R^2) A_{g,i}^A. \quad (4.11)$$

The cusp anomalous dimensions $A_{g,i}^A$ [43, 100–103] are given in Appendix A. Solving the above renormalisation group equation (RGE) satisfied by K_g^A we get

$$K_g^A(\hat{a}_s, \mu^2, \mu_R^2, \epsilon) = \sum_{i=1}^{\infty} \hat{a}_s^i \left(\frac{\mu_R^2}{\mu^2} \right)^{i \frac{\epsilon}{2}} S_\epsilon^i K_g^{A,(i)}(\epsilon) \quad (4.12)$$

with

$$\begin{aligned} K_g^{A,(1)}(\epsilon) &= \frac{1}{\epsilon} \left\{ -2A_{g,1}^A \right\}, \quad K_g^{A,(2)}(\epsilon) = \frac{1}{\epsilon^2} \left\{ 2\beta_0 A_{g,1}^A \right\} + \frac{1}{\epsilon} \left\{ -A_{g,2}^A \right\}, \\ K_g^{A,(3)}(\epsilon) &= \frac{1}{\epsilon^3} \left\{ -\frac{8}{3}\beta_0^2 A_{g,1}^A \right\} + \frac{1}{\epsilon^2} \left\{ \frac{2}{3}\beta_1 A_{g,1}^A + \frac{8}{3}\beta_0 A_{g,2}^A \right\} + \frac{1}{\epsilon} \left\{ -\frac{2}{3}A_{g,3}^A \right\}. \end{aligned} \quad (4.13)$$

Similarly upon solving the RGE in (4.11) for G_g^A , we obtain

$$\begin{aligned} G_g^A\left(\hat{a}_s, \frac{Q^2}{\mu_R^2}, \frac{\mu_R^2}{\mu^2}, \epsilon\right) &= G_g^A(a_s(\mu_R^2), \frac{Q^2}{\mu_R^2}, \epsilon) \\ &= G_g^A(a_s(Q^2), 1, \epsilon) + \int_{Q^2/\mu_R^2}^1 \frac{d\lambda^2}{\lambda^2} A_g^A(a_s(\lambda^2 \mu_R^2)) \\ &= G_g^A(a_s(Q^2), 1, \epsilon) + \sum_{i=1}^{\infty} S_\epsilon^i \hat{a}_s^i \left(\frac{\mu_R^2}{\mu^2} \right)^{i \frac{\epsilon}{2}} \left[\left(\frac{Q^2}{\mu_R^2} \right)^{i \frac{\epsilon}{2}} - 1 \right] K_g^{A,(i)}(\epsilon). \end{aligned} \quad (4.14)$$

We expand the finite function $G_g^A(a_s(Q^2), 1, \epsilon)$ in powers of $a_s(Q^2)$ as

$$G_g^A(a_s(Q^2), 1, \epsilon) = \sum_{i=1}^{\infty} a_s^i(Q^2) G_{g,i}^A(\epsilon). \quad (4.15)$$

After substituting these solutions in (4.10) and performing the final integration, we obtain the following solution for the form factor

$$\ln \hat{F}_g^A(\hat{a}_s, Q^2, \mu^2, \epsilon) = \sum_{i=1}^{\infty} \hat{a}_s^i \left(\frac{Q^2}{\mu^2} \right)^{i \frac{\epsilon}{2}} S_\epsilon^i \hat{\mathcal{L}}_{g,F}^{A,(i)}(\epsilon), \quad (4.16)$$

where

$$\begin{aligned}
\hat{\mathcal{L}}_{g,F}^{A,(1)} &= \frac{1}{\epsilon^2} \left(-2A_{g,1}^A \right) + \frac{1}{\epsilon} \left(G_{g,1}^A(\epsilon) \right) \\
\hat{\mathcal{L}}_{g,F}^{A,(2)} &= \frac{1}{\epsilon^3} \left(\beta_0 A_{g,1}^A \right) + \frac{1}{\epsilon^2} \left(-\frac{1}{2} A_{g,2}^A - \beta_0 G_{g,1}^A(\epsilon) \right) + \frac{1}{2\epsilon} G_{g,2}^A(\epsilon) \\
\hat{\mathcal{L}}_{g,F}^{A,(3)} &= \frac{1}{\epsilon^4} \left(-\frac{8}{9} \beta_0^2 A_{g,1}^A \right) + \frac{1}{\epsilon^3} \left(\frac{2}{9} \beta_1 A_{g,1}^A + \frac{8}{9} \beta_0 A_{g,2}^A + \frac{4}{3} \beta_0^2 G_{g,1}^A(\epsilon) \right) \\
&\quad + \frac{1}{\epsilon^2} \left(-\frac{2}{9} A_{g,3}^A - \frac{1}{3} \beta_1 G_{g,1}^A(\epsilon) - \frac{4}{3} \beta_0 G_{g,2}^A(\epsilon) \right) + \frac{1}{\epsilon} \left(\frac{1}{3} G_{g,3}^A(\epsilon) \right), \quad (4.17)
\end{aligned}$$

One finds that $G_{g,i}^A$ can be expressed in terms of collinear B_i^q and soft f_i^q anomalous dimensions through the relation [39, 104, 105]

$$G_{g,i}^A(\epsilon) = 2(B_{g,i}^A - \gamma_{g,i}^A) + f_{g,i}^A + \sum_{k=0}^{\infty} \epsilon^k g_{g,i}^{A,k}. \quad (4.18)$$

Note that the single pole term of the form factor depends on three different anomalous dimensions, namely the collinear anomalous dimension $B_{g,i}^A$, anomalous dimension of the coupling constant $\gamma_{g,i}^A$ and the soft anomalous dimension $f_{g,i}^A$. $B_{g,i}^A$ can be obtained from the $\delta(1-z)$ part of the diagonal splitting function known up to three loop level [100, 101] which are given in Appendix A. The $f_{g,i}^A$ for $i=1,2$ can be found in [39] and in [100] for $i=3$. We list them in Appendix A. The constants $g_{g,i}^{A,0}$ are controlled by the beta function of the strong coupling constant through renormalization group invariance of the bare form factor as

$$g_{g,1}^{A,0} = 0, \quad g_{g,2}^{A,0} = -2\beta_0 g_{g,1}^{A,1}, \quad g_{g,3}^{A,0} = -2\beta_1 g_{g,1}^{A,1} - 2\beta_0 (g_{g,2}^{A,1} + 2\beta_0 g_{g,1}^{A,2}). \quad (4.19)$$

Below, we give the expressions of $g_{g,j}^{A,i}$ which are required to calculate the form factor up to a_s^3 .

$$\begin{aligned}
g_{g,1}^{A,1} &= C_A \left\{ 4 + \zeta_2 \right\}, \\
g_{g,1}^{A,2} &= C_A \left\{ -6 - \frac{7}{3} \zeta_3 \right\}, \\
g_{g,1}^{A,3} &= C_A \left\{ 7 - \frac{1}{2} \zeta_2 + \frac{47}{80} \zeta_2^2 \right\}, \\
g_{g,2}^{A,1} &= C_A^2 \left\{ \frac{11882}{81} + \frac{67}{3} \zeta_2 - \frac{44}{3} \zeta_3 \right\} + C_A n_f \left\{ -\frac{2534}{81} - \frac{10}{3} \zeta_2 - \frac{40}{3} \zeta_3 \right\} + C_F n_f \left\{ -\frac{160}{3} \right. \\
&\quad \left. + 12 \ln \left(\frac{\mu_R^2}{m_t^2} \right) + 16 \zeta_3 \right\},
\end{aligned}$$

$$\begin{aligned}
g_{g,2}^{A,2} &= C_F n_f \left\{ \frac{2827}{18} - 18 \ln \left(\frac{\mu_R^2}{m_t^2} \right) - \frac{19}{3} \zeta_2 - \frac{16}{3} \zeta_2^2 - \frac{128}{3} \zeta_3 \right\} + C_A n_f \left\{ \frac{21839}{243} - \frac{17}{9} \zeta_2 \right. \\
&\quad \left. + \frac{259}{60} \zeta_2^2 + \frac{766}{27} \zeta_3 \right\} + C_A^2 \left\{ -\frac{223861}{486} + \frac{80}{9} \zeta_2 + \frac{671}{120} \zeta_2^2 + \frac{2111}{27} \zeta_3 + \frac{5}{3} \zeta_2 \zeta_3 - 39 \zeta_5 \right\}, \\
g_{g,3}^{A,1} &= n_f C_J^{(2)} \left\{ -6 \right\} + C_F n_f^2 \left\{ \frac{12395}{27} - \frac{136}{9} \zeta_2 - \frac{368}{45} \zeta_2^2 - \frac{1520}{9} \zeta_3 - 24 \ln \left(\frac{\mu_R^2}{m_t^2} \right) \right\} \\
&\quad + C_F^2 n_f \left\{ \frac{457}{2} + 312 \zeta_3 - 480 \zeta_5 \right\} + C_A^2 n_f \left\{ -\frac{12480497}{4374} - \frac{2075}{243} \zeta_2 - \frac{128}{45} \zeta_2^2 \right. \\
&\quad \left. - \frac{12992}{81} \zeta_3 - \frac{88}{9} \zeta_2 \zeta_3 + \frac{272}{3} \zeta_5 \right\} + C_A^3 \left\{ \frac{62867783}{8748} + \frac{146677}{486} \zeta_2 - \frac{5744}{45} \zeta_2^2 - \frac{12352}{315} \zeta_3 \right. \\
&\quad \left. - \frac{67766}{27} \zeta_3 - \frac{1496}{9} \zeta_2 \zeta_3 - \frac{104}{3} \zeta_3^2 + \frac{3080}{3} \zeta_5 \right\} + C_A n_f^2 \left\{ \frac{514997}{2187} - \frac{8}{27} \zeta_2 + \frac{232}{45} \zeta_2^2 \right. \\
&\quad \left. + \frac{7640}{81} \zeta_3 \right\} + C_A C_F n_f \left\{ -\frac{1004195}{324} + \frac{1031}{18} \zeta_2 + \frac{1568}{45} \zeta_2^2 + \frac{25784}{27} \zeta_3 + 40 \zeta_2 \zeta_3 + \frac{608}{3} \zeta_5 \right. \\
&\quad \left. + 132 \ln \left(\frac{\mu_R^2}{m_t^2} \right) \right\}. \tag{4.20}
\end{aligned}$$

After substituting the above expressions in (4.10) and performing the final integration, we obtain the UV renormalised form factor up to $\mathcal{O}(a_s^3)$ as

$$\begin{aligned}
\ln |\hat{F}_g^A|^2(-q^2, \epsilon) &= a_s(q^2) \left\{ -\frac{1}{\epsilon^2} 16 C_A + C_A (8 + 14 \zeta_2) \right\} + a_s(q^2)^2 \left\{ \frac{1}{\epsilon^3} \left[16 C_A n_f - 88 C_A^2 \right] \right. \\
&\quad + \frac{1}{\epsilon^2} \left[C_A n_f \left(\frac{40}{9} \right) + C_A^2 \left(-\frac{268}{9} + 8 \zeta_2 \right) \right] + \frac{1}{\epsilon} \left[C_A n_f \left(-\frac{76}{27} + \frac{4}{3} \zeta_2 \right) \right. \\
&\quad + C_A^2 \left(\frac{772}{27} - 4 \zeta_3 - \frac{22}{3} \zeta_2 \right) \left. \right] + C_F n_f \left(-\frac{160}{3} + 12 \ln \left(\frac{\mu_R^2}{m_t^2} \right) + 16 \zeta_3 \right) \\
&\quad + C_A n_f \left(-\frac{1886}{81} - \frac{92}{9} \zeta_3 - \frac{50}{3} \zeta_2 \right) + C_A^2 \left(\frac{8318}{81} - \frac{286}{9} \zeta_3 + \frac{335}{3} \zeta_2 - 24 \zeta_2^2 \right) \left. \right\} \\
&\quad + a_s(q^2)^3 \left\{ \frac{1}{\epsilon^4} \left[C_A n_f^2 \left(-\frac{1408}{81} \right) + C_A^2 n_f \left(\frac{15488}{81} \right) + C_A^3 \left(-\frac{42592}{81} \right) \right] \right. \\
&\quad + \frac{1}{\epsilon^3} \left[C_A n_f^2 \left(-\frac{1600}{243} \right) + C_A C_F n_f \left(\frac{256}{9} \right) + C_A^2 n_f \left(\frac{31040}{243} - \frac{320}{27} \zeta_2 \right) \right. \\
&\quad + C_A^3 \left(-\frac{98128}{243} + \frac{1760}{27} \zeta_2 \right) \left. \right] + \frac{1}{\epsilon^2} \left[C_A n_f^2 \left(\frac{224}{81} - \frac{32}{27} \zeta_2 \right) \right. \\
&\quad + C_A C_F n_f \left(\frac{440}{27} - \frac{128}{9} \zeta_3 \right) - C_A^2 n_f \left(\frac{6176}{243} - \frac{544}{27} \zeta_3 - \frac{416}{81} \zeta_2 \right) + C_A^3 \left(\frac{16328}{243} \right. \\
&\quad \left. - \frac{880}{27} \zeta_3 + \frac{1384}{81} \zeta_2 - \frac{704}{45} \zeta_2^2 \right) \left. \right] + \frac{1}{\epsilon} \left[C_A n_f^2 \left(-\frac{3728}{2187} + \frac{224}{81} \zeta_3 - \frac{80}{81} \zeta_2 \right) \right. \\
&\quad \left. - C_A C_F n_f \left(\frac{3638}{81} - \frac{608}{27} \zeta_3 - \frac{8}{3} \zeta_2 - \frac{64}{15} \zeta_2^2 \right) + C_A^2 n_f \left(\frac{14980}{2187} - \frac{1424}{81} \zeta_3 \right) \right.
\end{aligned}$$

$$\begin{aligned}
& + \frac{4792}{243} \zeta_2 - \frac{656}{45} \zeta_2^2 \Big) + C_A^3 \left(\frac{234466}{2187} + \frac{64}{3} \zeta_5 - \frac{488}{9} \zeta_3 - \frac{24436}{243} \zeta_2 + \frac{160}{9} \zeta_2 \zeta_3 \right. \\
& \left. + \frac{2552}{45} \zeta_2^2 \right) \Big] - n_f C_J^{(2)} + C_F n_f^2 \left(\frac{1498}{9} - \frac{224}{3} \zeta_3 - \frac{40}{9} \zeta_2 - \frac{32}{45} \zeta_2^2 \right) + C_F^2 n_f \left(\frac{457}{3} \right. \\
& \left. - 320 \zeta_5 + 208 \zeta_3 \right) + C_A n_f^2 \left(\frac{560290}{6561} + \frac{9152}{243} \zeta_3 - \frac{296}{27} \zeta_2 - \frac{424}{27} \zeta_2^2 \right) \\
& + C_A C_F n_f \left(-\frac{623255}{486} + \frac{1216}{9} \zeta_5 + \frac{35176}{81} \zeta_3 - \frac{925}{9} \zeta_2 + \frac{368}{3} \zeta_2 \zeta_3 - \frac{128}{45} \zeta_2^2 \right) \\
& + C_A^2 n_f \left(-\frac{7335209}{6561} + \frac{856}{9} \zeta_5 - \frac{2216}{81} \zeta_3 - \frac{37054}{729} \zeta_2 - 104 \zeta_2 \zeta_3 + \frac{10616}{45} \zeta_2^2 \right) \\
& + C_A^3 \left(\frac{35421539}{13122} + \frac{4444}{9} \zeta_5 - \frac{322280}{243} \zeta_3 - \frac{208}{9} \zeta_3^2 + \frac{510619}{729} \zeta_2 - \frac{308}{3} \zeta_2 \zeta_3 \right. \\
& \left. - \frac{118534}{135} \zeta_2^2 + \frac{75088}{945} \zeta_2^3 \right) \Big\}. \tag{4.21}
\end{aligned}$$

4.3 Mass factorisation kernel

The mass factorisation kernels are the solutions to the AP evolution equation which is controlled by the AP splitting functions $P_{aa'}(z_l, \mu_F^2)$ as given below

$$\mu_F^2 \frac{d}{d\mu_F^2} \Gamma_{ab}(z_l, \mu_F^2, \epsilon) = \frac{1}{2} \sum_{a'=q, \bar{q}, g} P_{aa'}(z_l, \mu_F^2) \otimes \Gamma_{a'b}(z_l, \mu_F^2, \epsilon), \quad a, b = q, \bar{q}, g, \tag{4.22}$$

where the perturbative expansion of the AP splitting functions read as,

$$P(z_l, \mu_F^2) = \sum_{i=1}^{\infty} a_s^i(\mu_F^2) P^{(i-1)}(z_l). \tag{4.23}$$

As discussed in the previous section, only the diagonal parts of splitting functions $P_{ab}(z, \mu_F^2)$ in $\Gamma_{ab}(z, \mu_F^2, \epsilon)$ need to be kept since the convolutions of two or more non-diagonal splitting functions give rise to terms which are of beyond NSV type. The diagonal $P_{gg}(z_l, \mu_F^2)$ are expanded around $z_l = 1$ and all those terms which do not contribute to SV+NSV are eliminated. The diagonal AP splitting functions near $z_l = 1$ take the following form:

$$\begin{aligned}
P_{gg}(z_l, a_s(\mu_F^2)) = 2 \Big[& B_g^A(a_s(\mu_F^2)) \delta(1 - z_l) + A_g^A(a_s(\mu_F^2)) \mathcal{D}_0(z_l) \\
& + C_g^A(a_s(\mu_F^2)) \log(1 - z_l) + D_g^A(a_s(\mu_F^2)) \Big] + \mathcal{O}((1 - z_l)), \tag{4.24}
\end{aligned}$$

where

$$C_g^A(a_s(\mu_F^2)) = \sum_{i=1}^{\infty} a_s^i(\mu_F^2) C_{g,i}^A, \quad D_g^A(a_s(\mu_F^2)) = \sum_{i=1}^{\infty} a_s^i(\mu_F^2) D_{g,i}^A. \tag{4.25}$$

The constants $C_{g,i}^A$ and $D_{g,i}^A$ can be obtained from the the splitting functions P_{gg} which are known to three loops in QCD [100, 101] (see [72, 100, 101, 106–112] for the lower order ones). We list $C_{g,i}^A$ and $D_{g,i}^A$ below

$$\begin{aligned}
C_{g,1}^A &= 0, \\
C_{g,2}^A &= 16C_A^2, \\
C_{g,3}^A &= C_A^2 n_f \left\{ -\frac{320}{9} \right\} + C_A^3 \left\{ \frac{2144}{9} - 64\zeta_2 \right\}, \\
D_{g,1}^A &= -4C_A, \\
D_{g,2}^A &= C_A n_f \left\{ \frac{40}{9} \right\} + C_A^2 \left\{ -\frac{268}{9} + 8\zeta_2 \right\}, \\
D_{g,3}^A &= C_A n_f^2 \left\{ \frac{16}{27} \right\} + C_A C_F n_f \left\{ \frac{110}{3} - 32\zeta_3 \right\} + C_A^2 n_f \left\{ \frac{908}{27} + \frac{112}{3}\zeta_3 - \frac{160}{9}\zeta_2 \right\} \\
&\quad + C_A^3 \left\{ -166 + \frac{56}{3}\zeta_3 + \frac{1072}{9}\zeta_2 - \frac{176}{5}\zeta_2^2 \right\}. \tag{4.26}
\end{aligned}$$

The RG equation in (4.22) can be solved by employing the perturbative expansion of the AP kernels

$$\Gamma_{gg}(z_l, \mu_F^2, \epsilon) = \delta(1-z_l) + \sum_{i=1}^{\infty} \hat{a}_s^i \left(\frac{\mu_F^2}{\mu^2} \right)^{i\frac{\epsilon}{2}} S_\epsilon^i \Gamma_{gg}^{(i)}(z_l, \epsilon). \tag{4.27}$$

The solutions of $\Gamma_{gg}^{(i)}$ in the \overline{MS} scheme are given by

$$\begin{aligned}
\Gamma_{gg}^{(1)}(z_l, \epsilon) &= \frac{1}{\epsilon} P_{gg}^{(0)}(z_l) \\
\Gamma_{gg}^{(2)}(z_l, \epsilon) &= \frac{1}{\epsilon^2} \left(\frac{1}{2} P_{gg}^{(0)}(z_l) \otimes P_{gg}^{(0)}(z_l) - \beta_0 P_{gg}^{(0)}(z_l) \right) + \frac{1}{\epsilon} \left(\frac{1}{2} P_{gg}^{(1)}(z_l) \right) \\
\Gamma_{gg}^{(3)}(z_l, \epsilon) &= \frac{1}{\epsilon^3} \left(\frac{4}{3} \beta_0^2 P_{gg}^{(0)}(z_l) - \beta_0 P_{gg}^{(0)}(z_l) \otimes P_{gg}^{(0)}(z_l) \right. \\
&\quad \left. + \frac{1}{6} P_{gg}^{(0)}(z_l) \otimes P_{gg}^{(0)}(z_l) \otimes P_{gg}^{(0)}(z_l) \right) + \frac{1}{\epsilon^2} \left(\frac{1}{2} P_{gg}^{(0)}(z_l) \otimes P_{gg}^{(1)}(z_l) \right. \\
&\quad \left. - \frac{1}{3} \beta_1 P_{gg}^{(0)}(z_l) - \frac{4}{3} \beta_0 P_{gg}^{(1)}(z_l) \right) + \frac{1}{\epsilon} \left(\frac{1}{3} P_{gg}^{(2)}(z_l) \right). \tag{4.28}
\end{aligned}$$

The most remarkable fact is that these quantities are universal, independent of the insertion of operators. Hence, for the process under consideration, we make use of the existing process independent results of the AP kernels and splitting functions.

4.4 Soft-collinear function

Exploiting the fact that the CF $\Delta_{d,g}^{A,SV+NSV}$ is finite, the infrared structure of $\mathcal{S}_{d,g}^A$ can be studied using the AP evolution equations of Γ_{gg} and the K+G differential equation of \hat{F}_g^P provided with the renormalisation group equation of Z_g^A . This is possible as we find that $\mathcal{S}_{d,g}^A$ also satisfies a K+G type differential equation:

$$q^2 \frac{d}{dq^2} \mathcal{S}_{d,g}^A = \frac{1}{2} \left[\overline{K}_{d,g}^A \left(\hat{a}_s, \frac{\mu_R^2}{\mu^2}, \epsilon, z_1, z_2 \right) + \overline{G}_{d,g}^A \left(\hat{a}_s, \frac{q^2}{\mu_R^2}, \frac{\mu_R^2}{\mu^2}, \epsilon, z_1, z_2 \right) \right] \otimes \mathcal{S}_{d,g}^A, \tag{4.29}$$

where the infrared singular part is contained in $\overline{K}_{d,g}^A$ in terms of universal anomalous dimensions while the finite $\overline{G}_{d,g}^A$ is controlled by certain process independent but initial state dependent functions and also certain process dependent pieces. Since the K+G equation (4.29) corresponding to $\mathcal{S}_{d,g}^A$ admits a solution of convoluted exponential form, we write

$$\mathcal{S}_{d,g}^A = \mathcal{C} \exp \left(2\Phi_{d,g}^A(\hat{a}_s, \mu^2, q^2, z_1, z_2, \epsilon) \right), \quad (4.30)$$

where the real emission contributions are encapsulated in the function $\Phi_{d,g}^A$ which is termed as the soft-collinear function. Furthermore, $\Phi_{d,g}^A$ being independent of μ_R^2 satisfies the RG equation, $\mu_R^2 \frac{d}{d\mu_R^2} \Phi_{d,g}^A = 0$ and consequently

$$\mu_R^2 \frac{d}{d\mu_R^2} \overline{K}_{d,g}^A = -\mu_R^2 \frac{d}{d\mu_R^2} \overline{G}_{d,g}^A = -\delta(1-z_1)\delta(1-z_2)a_s(\mu_R^2)\overline{A}_g^A. \quad (4.31)$$

The right hand side of the above equation is proportion to $\delta(1-z_1)\delta(1-z_2)$ as the most singular terms resulting from $\overline{K}_{d,g}^A$ should cancel with those from the form factor contribution which is proportional to only pure delta functions. To make the CF $\Delta_{d,g}^{A,SV+NSV}$ finite, the poles from $\Phi_{d,g}^A$ have to cancel with those coming from \hat{F}_g^A and Γ_{gg} . Hence the constants \overline{A}_g^A should satisfy $\overline{A}_g^A = -A_g^A$. The RGE (4.31) for $\overline{G}_{d,g}^A$ can be solved using the above mentioned relation to get

$$\begin{aligned} \overline{G}_{d,g}^A \left(\hat{a}_s, \frac{q^2}{\mu_R^2}, \frac{\mu_R^2}{\mu^2}, z_1, z_2, \epsilon \right) &= \overline{G}_{d,g}^A \left(a_s(\mu_R^2), \frac{q^2}{\mu_R^2}, z_1, z_2, \epsilon \right) \\ &= \overline{G}_{d,g}^A(a_s(q^2), 1, z_1, z_2, \epsilon) - \delta(1-z_1)\delta(1-z_2) \int_{\frac{q^2}{\mu_R^2}}^1 \frac{d\lambda^2}{\lambda^2} A_g^A(a_s(\lambda^2 \mu_R^2)). \end{aligned} \quad (4.32)$$

With these solutions, it is now straightforward to solve the differential equation (4.29) for obtaining the form of $\Phi_{d,g}^A$. For convenience, we decompose the soft-collinear function as $\Phi_{d,g}^A = \Phi_{d,g,SV}^A + \Phi_{d,g,NSV}^A$ in such a way that $\Phi_{d,g,SV}^A$ contains only the SV terms i.e all the distributions $\mathcal{D}_k(z_l)$ and $\delta(1-z_l)$ and $\Phi_{d,g,NSV}^A$ contains the NSV terms namely $\log^k(1-z_l), l=1,2, k=0, \dots$ in the limit $z_{1(2)} \rightarrow 1$. An all order solution for $\Phi_{d,g,SV}^A$ in powers of \hat{a}_s in dimensional regularisation is given in [53] and we reproduce it here for completeness:

$$\Phi_{d,g,SV}^A = \sum_{i=1}^{\infty} \hat{a}_s^i \left(\frac{q^2 \bar{z}_1 \bar{z}_2}{\mu^2} \right)^{i \frac{\epsilon}{2}} S_\epsilon^i \left[\frac{(i\epsilon)^2}{4\bar{z}_1 \bar{z}_2} \hat{\phi}_{d,g}^{A,(i)}(\epsilon) \right], \quad (4.33)$$

with

$$\hat{\phi}_{d,g}^{A,(i)}(\epsilon) = \frac{1}{i\epsilon} \left[\overline{K}_{d,g}^{A(i)}(\epsilon) + \overline{G}_{d,g,SV}^{A(i)}(\epsilon) \right]. \quad (4.34)$$

The constants $\overline{K}_{d,g}^{A,(i)}(\epsilon)$ are determined by expanding $\overline{K}_{d,g}^A$ in powers of \hat{a}_s as follows

$$\overline{K}_{d,g}^A \left(\hat{a}_s, \frac{\mu_R^2}{\mu^2}, z_1, z_2, \epsilon \right) = \delta(1-z_1)\delta(1-z_2) \sum_{i=1}^{\infty} \hat{a}_s^i \left(\frac{\mu_R^2}{\mu^2} \right)^{i\frac{\epsilon}{2}} S_\epsilon^i \overline{K}_{d,g}^{A,(i)}(\epsilon) \quad (4.35)$$

and solving the RGE (4.31) for $\overline{K}_{d,g}^A$. The constants $\overline{K}_{d,g}^{A,(i)}(\epsilon)$ are related to the constants $K_{d,g}^{A,(i)}(\epsilon)$ which appear in the form factor by $\overline{K}_{d,g}^{A,(i)}(\epsilon) = K_{d,g}^{A,(i)}(\epsilon)|_{A_g^A \rightarrow -A_g^A}$, due to the IR pole cancellation. $\overline{G}_{d,g,SV}^{A,(i)}(\epsilon)$ are related to the finite functions $\overline{G}_{d,g,SV}^A(a_s(q^2), 1, z_1, z_2, \epsilon)$. In terms of renormalized coupling constant, we find

$$\sum_{i=1}^{\infty} \hat{a}_s^i \left(\frac{q^2(1-z_1)(1-z_2)}{\mu^2} \right)^{i\frac{\epsilon}{2}} S_\epsilon^i \overline{G}_{d,g,SV}^{A,(i)}(\epsilon) = \sum_{i=1}^{\infty} a_s^i (q^2(1-z_1)(1-z_2)) \overline{G}_{d,g,i}^A(\epsilon). \quad (4.36)$$

Using $\overline{K}_{d,g}^{A,(i)}$ from Eq. 4.35 after putting the explicit values of A_g^A and $\overline{G}_{d,g,SV}^{A,(i)}$ from Eq. 4.36, we find that $\hat{\phi}_{d,g}^{A,(i)}(\epsilon)$ in $\Phi_{d,g,SV}^A$ up to third order in \hat{a}_s takes the following form

$$\begin{aligned} \hat{\phi}_{d,g}^{A,(1)}(\epsilon) &= \frac{1}{\epsilon^2} 8C_A + \frac{1}{\epsilon} \overline{\mathcal{G}}_{d,g,1}^A(\epsilon), \\ \hat{\phi}_{d,g}^{A,(2)}(\epsilon) &= \frac{1}{\epsilon^3} \left\{ C_{Anf} \left(\frac{8}{3} \right) + C_A^2 \left(-\frac{44}{3} \right) \right\} + \frac{1}{\epsilon^2} \left\{ n_f \left(\frac{2}{3} \overline{\mathcal{G}}_{d,g,1}^A(\epsilon) \right) + C_A \left(-\frac{11}{3} \overline{\mathcal{G}}_{d,g,1}^A(\epsilon) \right) \right. \\ &\quad \left. + C_{Anf} \left(-\frac{20}{9} \right) + C_A^2 \left(\frac{134}{9} - 4\zeta_2 \right) \right\} + \frac{1}{2\epsilon} \overline{\mathcal{G}}_{d,g,2}^A(\epsilon), \\ \hat{\phi}_{d,g}^{A,(3)}(\epsilon) &= \frac{1}{\epsilon^4} \left\{ C_{Anf}^2 \left(\frac{128}{81} \right) + C_A^2 n_f \left(-\frac{1408}{81} \right) + C_A^3 \left(\frac{3872}{81} \right) \right\} + \frac{1}{\epsilon^3} \left\{ n_f^2 \left(\frac{16}{27} \overline{\mathcal{G}}_{d,g,1}^A(\epsilon) \right) \right. \\ &\quad \left. + C_{Anf} \left(-\frac{176}{27} \overline{\mathcal{G}}_{d,g,1}^A(\epsilon) \right) + C_{Anf}^2 \left(-\frac{640}{243} \right) + C_A C_{Fnf} \left(\frac{16}{9} \right) + C_A^2 \left(\frac{484}{27} \overline{\mathcal{G}}_{d,g,1}^A(\epsilon) \right) \right. \\ &\quad \left. + C_A^2 n_f \left(\frac{8528}{243} - \frac{128}{27} \zeta_2 \right) + C_A^3 \left(-\frac{26032}{243} + \frac{704}{27} \zeta_2 \right) \right\} + \frac{1}{\epsilon^2} \left\{ n_f \left(\frac{8}{9} \overline{\mathcal{G}}_{d,g,2}^A(\epsilon) \right) \right. \\ &\quad \left. + C_{Fnf} \left(\frac{2}{3} \overline{\mathcal{G}}_{d,g,1}^A(\epsilon) \right) + C_A \left(-\frac{44}{9} \overline{\mathcal{G}}_{d,g,2}^A(\epsilon) \right) + C_{Anf} \left(\frac{10}{9} \overline{\mathcal{G}}_{d,g,1}^A(\epsilon) \right) + C_{Anf}^2 \left(-\frac{32}{243} \right) \right. \\ &\quad \left. + C_A C_{Fnf} \left(-\frac{220}{27} + \frac{64}{9} \zeta_3 \right) + C_A^2 \left(-\frac{34}{9} \overline{\mathcal{G}}_{d,g,1}^A(\epsilon) \right) + C_A^2 n_f \left(-\frac{1672}{243} - \frac{224}{27} \zeta_3 \right) \right. \\ &\quad \left. + \frac{320}{81} \zeta_2 \right\} + C_A^3 \left(\frac{980}{27} + \frac{176}{27} \zeta_3 - \frac{2144}{81} \zeta_2 + \frac{352}{45} \zeta_2^2 \right) \left. \right\} + \frac{1}{3\epsilon} \overline{\mathcal{G}}_{d,g,3}^A(\epsilon). \quad (4.37) \end{aligned}$$

In the above equations, $\overline{\mathcal{G}}_{d,g,i}^A(\epsilon)$ are parametrised as follows

$$\overline{\mathcal{G}}_{d,g,i}^A(\epsilon) = -f_{g,i}^A + \sum_{k=0}^{\infty} \epsilon^k \overline{\mathcal{G}}_{d,g,i}^{A,(k)}, \quad (4.38)$$

where

$$\overline{\mathcal{G}}_{d,g,1}^{A,(0)} = 0, \quad \overline{\mathcal{G}}_{d,g,2}^{A,(0)} = -2\beta_0 \overline{\mathcal{G}}_{d,g,1}^{A,(1)}, \quad \overline{\mathcal{G}}_{d,g,3}^{A,(0)} = -2\beta_1 \overline{\mathcal{G}}_{d,g,1}^{A,(1)} - 2\beta_0 (\overline{\mathcal{G}}_{d,g,2}^{A,(1)} + 2\beta_0 \overline{\mathcal{G}}_{d,g,1}^{A,(2)}). \quad (4.39)$$

The unknown constants $\overline{\mathcal{G}}_{d,g,i}^{A,(k)}$ will be determined in the next section.

Let us now study in detail the structure of $\Phi_{d,g,NSV}^A$ using the Eq.(4.29). Subtracting out the K+G equation for the SV part $\Phi_{d,g,SV}^A$ from Eq.(4.29), we find that $\Phi_{d,g,NSV}^A$ satisfies

$$q^2 \frac{d}{dq^2} \Phi_{d,g,NSV}^A(q^2, z_j, \epsilon) = \frac{1}{2} \left[G_{d,L}^{A,g} \left(\hat{a}_s, \frac{q^2}{\mu_R^2}, \frac{\mu_R^2}{\mu^2}, \epsilon, z_j \right) \right], \quad (4.40)$$

where $G_{d,L}^{A,g} = \overline{G}_{d,g}^A - \overline{G}_{d,g,SV}^A$,

$$G_{d,L}^{A,g} \left(\hat{a}_s, \frac{q^2}{\mu_R^2}, \frac{\mu_R^2}{\mu^2}, z_j, \epsilon \right) = \sum_{i=1}^{\infty} a_s^i (q^2(1-z_j)^2) \mathcal{G}_{d,L,i}^{A,g}(\bar{z}, \epsilon). \quad (4.41)$$

Now integrating (4.40), we obtain the following structure for $\Phi_{d,g,NSV}^A$

$$\Phi_{d,g,NSV}^A = \sum_{i=1}^{\infty} \hat{a}_s^i \left(\frac{q^2 \bar{z}_1 \bar{z}_2}{\mu^2} \right)^{i \frac{\epsilon}{2}} S_\epsilon^i \left[\frac{i\epsilon}{4\bar{z}_1} \varphi_{d,g}^{A,(i)}(\bar{z}_2, \epsilon) + \frac{i\epsilon}{4\bar{z}_2} \varphi_{d,g}^{A,(i)}(\bar{z}_1, \epsilon) \right], \quad (4.42)$$

where $\varphi_{d,g}^{A,(i)}(\bar{z}_1, \epsilon)$ are found to be as follows

$$\begin{aligned} \varphi_{d,G}^{A,(1)}(\bar{z}_j, \epsilon) &= \frac{1}{\epsilon} \mathcal{G}_{d,L,1}^{A,g}(\bar{z}_j, \epsilon) \\ \varphi_{d,G}^{A,(2)}(\bar{z}_j, \epsilon) &= \frac{1}{\epsilon^2} \left\{ n_f \left(\frac{2}{3} \mathcal{G}_{d,L,1}^{A,g}(\bar{z}_j, \epsilon) \right) + C_A \left(-\frac{11}{3} \mathcal{G}_{d,L,1}^{A,g}(\bar{z}_j, \epsilon) \right) \right\} + \frac{1}{2\epsilon} \mathcal{G}_{d,L,2}^{A,g}(\bar{z}_j, \epsilon) \\ \varphi_{d,G}^{A,(3)}(\bar{z}_j, \epsilon) &= \frac{1}{\epsilon^3} \left\{ n_f^2 \left(\frac{16}{27} \mathcal{G}_{d,L,1}^{A,g}(\bar{z}_j, \epsilon) \right) + C_A n_f \left(-\frac{176}{27} \mathcal{G}_{d,L,1}^{A,g}(\bar{z}_j, \epsilon) \right) \right. \\ &\quad \left. + C_A^2 \left(\frac{484}{27} \mathcal{G}_{d,L,1}^{A,g}(\bar{z}_j, \epsilon) \right) \right\} + \frac{1}{\epsilon^2} \left\{ n_f \left(\frac{8}{9} \mathcal{G}_{d,L,2}^{A,g}(\bar{z}_j, \epsilon) \right) + C_F n_f \left(\frac{2}{3} \mathcal{G}_{d,L,1}^{A,g}(\bar{z}_j, \epsilon) \right) \right. \\ &\quad \left. + C_A \left(-\frac{44}{9} \mathcal{G}_{d,L,2}^{A,g}(\bar{z}_j, \epsilon) \right) + C_A n_f \left(\frac{10}{9} \mathcal{G}_{d,L,1}^{A,g}(\bar{z}_j, \epsilon) \right) + C_A^2 \left(-\frac{34}{9} \mathcal{G}_{d,L,1}^{A,g}(\bar{z}_j, \epsilon) \right) \right\} \\ &\quad + \frac{1}{3\epsilon} \mathcal{G}_{d,L,3}^{A,g}(\bar{z}_j, \epsilon). \end{aligned} \quad (4.43)$$

Here, $\mathcal{G}_{d,L,i}^{A,g}(\bar{z}, \epsilon)$ are expanded in powers of ϵ as

$$\mathcal{G}_{d,L,i}^{A,g}(\bar{z}_j, \epsilon) = 2L_{g,i}^A(a_s, \bar{z}_l) + \sum_{k=0}^{\infty} \epsilon^k \mathcal{G}_{d,L,i}^{A,g,(k)}(\bar{z}_j), \quad (4.44)$$

with

$$\begin{aligned} \mathcal{G}_{d,L,1}^{A,g,(0)}(\bar{z}_j) &= 0, \quad \mathcal{G}_{d,L,2}^{A,g,(0)}(\bar{z}_j) = -2\beta_0 \mathcal{G}_{d,L,1}^{A,g,(1)}(\bar{z}_j), \\ \mathcal{G}_{d,L,3}^{A,g,(0)}(\bar{z}_j) &= -2\beta_1 \mathcal{G}_{d,L,1}^{A,g,(1)}(\bar{z}_j) - 2\beta_0 (\mathcal{G}_{d,L,2}^{A,g,(1)}(\bar{z}_j) + 2\beta_0 \mathcal{G}_{d,L,1}^{A,g,(2)}(\bar{z}_j)). \end{aligned} \quad (4.45)$$

The anomalous dimensions $L_{g,i}^A$ can be determined by demanding finiteness of $\Delta_{d,g}^A$ and it turns out that it is half of NSV part of the AP splitting functions (see [1]), that is

$$L_{g,i}^A(a_s, \bar{z}_l) = C_{g,i}^A(a_s) \log(1-z_l) + D_{g,i}^A(a_s). \quad (4.46)$$

The coefficients $\mathcal{G}_{d,L,i}^{A,g,(j)}(\bar{z}_j)$ in the above equations are parametrised in terms of $\log^k(1 - z_j)$, $k = 0, 1, \dots$ and all the terms that vanish as $z_j \rightarrow 1$ are dropped

$$\mathcal{G}_{d,L,i}^{A,g,(j)}(\bar{z}_j) = \sum_{k=0}^{i+j-1} \mathcal{G}_{d,L,i}^{A,g,(j,k)} \log^k(1 - z_j). \quad (4.47)$$

The highest power of the $\log(1 - z_j)$ at every order depends on the order of the perturbation, namely the power of a_s and also the power of ϵ at each order in a_s . Hence the summation runs from 0 to $i + j - 1$.

Next, we obtain an the integral representation of $\Phi_{d,g,SV}^A$ which is given by

$$\begin{aligned} \Phi_{d,g,SV}^A &= \frac{1}{2} \delta(\bar{z}_2) \left(\frac{1}{\bar{z}_1} \left\{ \int_{\mu_F^2}^{q^2 \bar{z}_1} \frac{d\lambda^2}{\lambda^2} A_g^A(a_s(\lambda^2)) + \bar{G}_{d,g,SV}^A(a_s(q_1^2), \epsilon) \right\} \right)_+ \\ &+ q^2 \frac{d}{dq^2} \left[\left(\frac{1}{4\bar{z}_1 \bar{z}_2} \left\{ \int_{\mu_R^2}^{q^2 \bar{z}_1 \bar{z}_2} \frac{d\lambda^2}{\lambda^2} A_g^A(a_s(\lambda^2)) + \bar{G}_{d,g,SV}^A(a_s(q_{12}^2), \epsilon) \right\} \right)_+ \right] \\ &+ \frac{1}{2} \delta(\bar{z}_1) \delta(\bar{z}_2) \sum_{i=1}^{\infty} \hat{a}_s^i \left(\frac{q^2}{\mu^2} \right)^{i \frac{\epsilon}{2}} S_\epsilon^i \hat{\phi}_{d,g}^{A,(i)}(\epsilon) \\ &+ \frac{1}{2} \delta(\bar{z}_2) \left(\frac{1}{\bar{z}_1} \right)_+ \sum_{i=1}^{\infty} \hat{a}_s^i \left(\frac{\mu_F^2}{\mu^2} \right)^{i \frac{\epsilon}{2}} S_\epsilon^i K_g^{A,(i)}(\epsilon) + (z_1 \leftrightarrow z_2), \end{aligned} \quad (4.48)$$

where $q_l^2 = q^2(1 - z_l)$ and $q_{12}^2 = q^2 \bar{z}_1 \bar{z}_2$. The subscript $+$ indicates the standard plus distribution. Similarly, we find an integral representation of the NSV part, $\Phi_{d,g,NSV}^A$ which reads as

$$\begin{aligned} \Phi_{d,g,NSV}^A &= \frac{1}{2} \delta(\bar{z}_2) \left(\left\{ \int_{\mu_F^2}^{q^2 \bar{z}_1} \frac{d\lambda^2}{\lambda^2} L_g^A(a_s(\lambda^2), \bar{z}_1) + \varphi_{d,f,g}^A(a_s(q_2^2), \bar{z}_1, \epsilon) \right\} \right) \\ &+ q^2 \frac{d}{dq^2} \left[\left(\frac{1}{2\bar{z}_1} \left\{ \int_{\mu_F^2}^{q^2 \bar{z}_1 \bar{z}_2} \frac{d\lambda^2}{\lambda^2} L_g^A(a_s(\lambda^2), \bar{z}_1) + \varphi_{d,f,g}^A(a_s(q_{12}^2), \bar{z}_1, \epsilon) \right\} \right)_+ \right] \\ &+ \frac{1}{2} \delta(\bar{z}_2) \varphi_{d,s,g}^A(\bar{z}_1, \epsilon) + (z_1 \leftrightarrow z_2), \end{aligned} \quad (4.49)$$

where,

$$\varphi_{d,a,g}^A(a_s(\lambda^2), \bar{z}_l) = \sum_{i=1}^{\infty} \hat{a}_s^i \left(\frac{\lambda^2}{\mu^2} \right)^{i \frac{\epsilon}{2}} S_\epsilon^i \varphi_{d,a,g}^{A,(i)}(z_l, \epsilon). \quad a = f, s \quad (4.50)$$

$\varphi_{d,s,g}^A$ is the singular part of the NSV solution. The finite part $\varphi_{d,f,g}^A$ is parametrized in the following way,

$$\begin{aligned} \varphi_{d,f,g}^A(a_s(\lambda^2), \bar{z}_l) &= \sum_{i=1}^{\infty} \sum_{k=0}^{\infty} \hat{a}_s^i \left(\frac{\lambda^2}{\mu^2} \right)^{i \frac{\epsilon}{2}} S_\epsilon^i \varphi_{d,g}^{A,(i,k)}(\epsilon) \ln^k \bar{z}_l, \\ &= \sum_{i=1}^{\infty} \sum_{k=0}^i a_s^i(\lambda^2) \varphi_{d,g,i}^{A,(k)} \ln^k \bar{z}_l. \end{aligned} \quad (4.51)$$

The upper limit on the sum over k is controlled by the dimensionally regularised Feynman integrals that contribute to order a_s^i .

5 Matching with the inclusive

The unknown coefficients of both SV and NSV solutions of $\Phi_{d,g}^A$, namely $\overline{\mathcal{G}}_{d,g,i}^{A,(k)}$ and $\varphi_{d,g,i}^{A,(k)}$ can be determined using the fixed order predictions of $\Delta_{d,g}^A$, at every order in perturbation theory. However, it can also be determined alternatively from corresponding inclusive cross section using the relation,

$$\int_0^1 dx_1^0 \int_0^1 dx_2^0 (x_1^0 x_2^0)^{N-1} \frac{d\sigma^A}{dy} = \int_0^1 d\tau \tau^{N-1} \sigma^A, \quad (5.1)$$

where σ^A is the inclusive cross section. This relation in the large N limit gives

$$\sum_{i=1}^{\infty} \hat{a}_s^i \left(\frac{q^2}{\mu^2} \right)^{\frac{i\epsilon}{2}} S_\epsilon^i \left[t_1^i(\epsilon) \hat{\phi}_{d,g}^{A,(i)}(\epsilon) - t_2^i(\epsilon) \hat{\phi}_g^{A,(i)}(\epsilon) + \sum_{k=0}^{\infty} \left(t_3^{(i,k)}(\epsilon) \varphi_{d,g}^{A,(i,k)}(\epsilon) - t_4^{(i,k)}(\epsilon) \varphi_g^{A,(i,k)}(\epsilon) \right) \right] = 0, \quad (5.2)$$

where

$$t_1^i = \frac{i\epsilon(2-i\epsilon)}{4N^{i\epsilon}} \Gamma^2 \left(1 + i\frac{\epsilon}{2} \right), \quad t_2^i = \frac{i\epsilon(1-i\epsilon)}{2N^{i\epsilon}} \Gamma(1+i\epsilon),$$

$$t_3^{(i,k)} = \Gamma \left(1 + i\frac{\epsilon}{2} \right) \frac{\partial^k}{\partial \alpha^k} \left(\frac{\Gamma(1+\alpha)}{N^{\alpha+i\epsilon/2}} \right)_{\alpha=i\frac{\epsilon}{2}}, \quad t_4^{(i,k)} = \frac{\partial^k}{\partial \hat{\alpha}^k} \left(\frac{\Gamma(1+\hat{\alpha})}{N^{\hat{\alpha}}} \right)_{\hat{\alpha}=i\epsilon}. \quad (5.3)$$

Here we keep $\ln^k N$ as well as $\mathcal{O}(1/N)$ terms for the determination of the SV and NSV coefficients. The constants $\hat{\phi}_g^{A,(i)}$ and $\varphi_g^{A,(i,k)}$ are the inclusive counterparts to the SV and NSV coefficients $\hat{\phi}_{d,g}^{A,(i)}$ and $\varphi_{d,g}^{A,(i,k)}$ respectively which are known to third order in QCD for Drell-Yan, for Higgs production in gluon fusion and in bottom quark annihilation (for NSV see [79]).

Using the above relations in Eq. (5.2), the SV coefficients $\overline{\mathcal{G}}_{d,g,i}^{A,(k)}$ up to second order are found to be

$$\begin{aligned} \overline{\mathcal{G}}_{d,g,1}^{A,(1)} &= C_A \left(-\zeta_2 \right), \\ \overline{\mathcal{G}}_{d,g,1}^{A,(2)} &= C_A \left(\frac{1}{3} \zeta_3 \right), \\ \overline{\mathcal{G}}_{d,g,1}^{A,(3)} &= C_A \left(\frac{1}{80} \zeta_2^2 \right), \\ \overline{\mathcal{G}}_{d,g,2}^{A,(1)} &= C_A^2 \left(\frac{2428}{81} - \frac{67}{3} \zeta_2 - 4\zeta_2^2 - \frac{44}{3} \zeta_3 \right) \\ &\quad + C_{An_f} \left(-\frac{328}{81} + \frac{10}{3} \zeta_2 + \frac{8}{3} \zeta_3 \right). \end{aligned} \quad (5.4)$$

Note that the above SV coefficients are identical to the corresponding SV coefficients of scalar Higgs given in Eq.(35) of [53]. This universality nature of SV coefficients $\overline{\mathcal{G}}_{d,g,i}^{A,(k)}$ is expected to hold to all orders in perturbation theory because of the fact that it originates

entirely from the soft part of the differential cross section. Further, this property has been explicitly verified till third order in QCD perturbation theory [34] for the case of inclusive cross section. The explicit expressions for NSV coefficients $\varphi_{d,g,i}^{A(k)}$ for the pseudo-scalar production in gluon fusion can be obtained from the corresponding results for inclusive coefficients $\varphi_{g,i}^{A(k)}$ given in [85]. The results up to second order are provided below

$$\begin{aligned}
\varphi_{d,g,1}^{A,(0)} &= 2C_A, \\
\varphi_{d,g,1}^{A,(1)} &= 0, \\
\varphi_{d,g,2}^{A,(0)} &= C_{Anf} \left(-\frac{136}{27} + \frac{8}{3}\zeta_2 \right) + C_A^2 \left(\frac{904}{27} - 28\zeta_3 - \frac{104}{3}\zeta_2 \right), \\
\varphi_{d,g,2}^{A,(1)} &= C_{Anf} \left(-\frac{2}{3} \right) + C_A^2 \left(\frac{2}{3} \right), \\
\varphi_{d,g,2}^{A,(2)} &= -4C_A^2.
\end{aligned} \tag{5.5}$$

We notice that the NSV coefficients $\varphi_{d,g,i}^{A(k)}$ of the pseudo-scalar Higgs are also identical to the corresponding NSV coefficients of scalar Higgs up to second order in a_s [1, 84].

6 Results of the SV and NSV rapidity distributions

In this section we present the analytic results of the SV and NSV rapidity distributions, $\Delta_{d,g}^{A,SV}$ and $\Delta_{d,g}^{A,NSV}$ respectively, at the partonic level to N³LO in QCD. By expanding the formula in Eq. (4.4) in powers of a_s and substituting the explicit expressions for all the anomalous dimensions, also the SV and NSV coefficients, we find, at a_s order,

$$\Delta_{d,g,1}^{A,NSV} = \mathbf{L}_{\mathbf{z}_1} \left\{ C_A(-4\bar{\delta}) \right\} + \bar{\mathcal{D}}_0 \left\{ C_A(-4) \right\} + C_A \left\{ 2\bar{\delta} \right\} + (z_1 \leftrightarrow z_2), \tag{6.1}$$

and at a_s^2 order

$$\begin{aligned}
\Delta_{d,g,2}^{A,NSV} &= \mathbf{L}_{\mathbf{z}_1}^3 \left\{ C_A^2(-8\bar{\delta}) \right\} + \mathbf{L}_{\mathbf{z}_1}^2 \left\{ C_A^2(-24\bar{\mathcal{D}}_0) + \bar{\delta} \left[C_{Anf} \left(-\frac{4}{3} \right) + C_A^2 \left(\frac{94}{3} \right) \right] \right\} \\
&+ \mathbf{L}_{\mathbf{z}_1} \left\{ \bar{\mathcal{D}}_0 \left[C_{Anf} \left(-\frac{8}{3} \right) + C_A^2 \left(\frac{164}{3} \right) \right] + C_A^2(-48\bar{\mathcal{D}}_1) \right. \\
&+ \bar{\delta} \left[C_{Anf} \left(\frac{46}{9} \right) + C_A^2 \left(-\frac{616}{9} - 8\zeta_2 \right) \right] \left. \right\} + \bar{\mathcal{D}}_0 \left\{ C_{Anf} \left(\frac{52}{9} \right) \right. \\
&+ C_A^2 \left(-\frac{622}{9} - 8\zeta_2 \right) \left. \right\} + \bar{\mathcal{D}}_1 \left\{ C_{Anf} \left(-\frac{8}{3} \right) + C_A^2 \left(\frac{116}{3} \right) \right\} + \bar{\mathcal{D}}_2 \left\{ -24C_A^2 \right\} \\
&+ \bar{\delta} \left\{ C_{Anf} \left(-\frac{136}{27} + \frac{8}{3}\zeta_2 \right) + C_A^2 \left(\frac{1336}{27} - 60\zeta_3 - \frac{80}{3}\zeta_2 \right) \right\} + (z_1 \leftrightarrow z_2). \tag{6.2}
\end{aligned}$$

In the above expressions, $L_{\mathbf{z}_1} = \ln(\bar{z}_1)$, $\bar{\delta} = \delta(\bar{z}_2)$, $\bar{\mathcal{D}}_j = \left(\frac{\ln^j(\bar{z}_2)}{\bar{z}_2} \right)_+$ and $\zeta_2 = 1.6449 \dots$ and $\zeta_3 = 1.20205 \dots$.

Next at a_s^3 , the CF requires the third order NSV coefficients $\varphi_{d,g,3}^{A,(k)}$ with $k = 0, 1, 2, 3$. Since the full N³LO results for both inclusive and rapidity distribution of pseudo-scalar Higgs are not available, we could not extract these NSV coefficients either directly from the rapidity results or by matching with the inclusive results. However, we apply the same ratio method discussed in sub-section 3.1 on the SV+NSV results of scalar Higgs rapidity distribution computed in [1] to obtain the third order CF of pseudo-scalar Higgs at SV+NSV accuracy. At a_s^3 , we find

$$\begin{aligned}
\Delta_{d,g,3}^{A,NSV} = & \mathbf{L}_{\mathbf{z}_1}^5 \left\{ C_A^3(-8\bar{\delta}) \right\} + \mathbf{L}_{\mathbf{z}_1}^4 \left\{ C_A^3(-40\bar{\mathcal{D}}_0) + \bar{\delta} \left[C_A^3\left(\frac{616}{9}\right) + n_f C_A^2\left(-\frac{40}{9}\right) \right] \right\} \\
& + \mathbf{L}_{\mathbf{z}_1}^3 \left\{ \bar{\mathcal{D}}_0 \left[C_A^3\left(\frac{2320}{9}\right) + n_f C_A^2\left(-\frac{160}{9}\right) \right] - C_A^3(160\bar{\mathcal{D}}_1) + \bar{\delta} \left[C_A^3\left(-\frac{2560}{9}\right) \right. \right. \\
& + 64\zeta_2) + n_f C_A^2\left(\frac{1036}{27}\right) + n_f^2 C_A\left(-\frac{16}{27}\right) \left. \left. \right] \right\} + \mathbf{L}_{\mathbf{z}_1}^2 \left\{ \bar{\mathcal{D}}_0 \left[C_A^3\left(-\frac{7516}{9} + 192\zeta_2\right) \right. \right. \\
& + n_f C_A^2\left(\frac{1016}{9}\right) + n_f^2 C_A\left(-\frac{16}{9}\right) \left. \left. \right] + \bar{\mathcal{D}}_1 \left[C_A^3\left(\frac{2128}{3}\right) + n_f C_A^2\left(-\frac{160}{3}\right) \right] \right. \\
& - C_A^3(240\bar{\mathcal{D}}_2) + \bar{\delta} \left[C_A^3\left(\frac{24982}{27} - 488\zeta_3 - 400\zeta_2\right) + n_f C_A^2\left(-\frac{3668}{27} + 38\zeta_2\right) \right. \\
& \left. \left. - 4 C_A C_F n_f + n_f^2 C_A\left(\frac{88}{27}\right) \right] \right\} + \mathbf{L}_{\mathbf{z}_1} \left\{ \bar{\mathcal{D}}_0 \left[C_A^3\left(\frac{44800}{27} - 976\zeta_3 - \frac{2288}{3}\zeta_2\right) \right. \right. \\
& + n_f C_A^2\left(-\frac{6860}{27} + \frac{224}{3}\zeta_2\right) - 8 C_A C_F n_f + n_f^2 C_A\left(\frac{184}{27}\right) \left. \left. \right] \right. \\
& + \bar{\mathcal{D}}_1 \left[C_A^3\left(-\frac{14528}{9} + 384\zeta_2\right) + n_f C_A^2\left(\frac{1960}{9}\right) + n_f^2 C_A\left(-\frac{32}{9}\right) \right] \\
& + \bar{\mathcal{D}}_2 \left[C_A^3\left(\frac{1888}{3}\right) + n_f C_A^2\left(-\frac{160}{3}\right) \right] + C_A^3(-160\bar{\mathcal{D}}_3) + \bar{\delta} \left[C_A^3\left(-\frac{145670}{81}\right) \right. \\
& + \frac{4936}{3}\zeta_3 + 336\zeta_2 + \frac{64}{5}\zeta_2^2) + n_f C_A^2\left(\frac{8528}{27} - 40\zeta_3 - \frac{920}{9}\zeta_2\right) \\
& \left. \left. + C_A C_F n_f \left(258 - 48 \ln\left(\frac{\mu_R^2}{m_t^2}\right) - 96\zeta_3 - \frac{8}{3}\zeta_2\right) + n_f^2 C_A\left(-\frac{328}{81} + \frac{32}{9}\zeta_2\right) \right] \right\} \\
& + \bar{\mathcal{D}}_0 \left[C_A^3\left(-\frac{127114}{81} + 1400\zeta_3 + \frac{2200}{9}\zeta_2 + \frac{64}{5}\zeta_2^2\right) + n_f C_A^2\left(\frac{24488}{81} - 32\zeta_3 \right. \right. \\
& \left. \left. - \frac{232}{3}\zeta_2\right) + C_A C_F n_f \left(254 - 48 \ln\left(\frac{\mu_R^2}{m_t^2}\right) - 96\zeta_3\right) + n_f^2 C_A\left(-\frac{496}{81} + \frac{32}{9}\zeta_2\right) \right] \\
& + \bar{\mathcal{D}}_1 \left[C_A^3\left(\frac{35044}{27} - 976\zeta_3 - \frac{2384}{3}\zeta_2\right) + n_f C_A^2\left(-\frac{6056}{27} + \frac{224}{3}\zeta_2\right) - 8 C_A C_F n_f \right. \\
& \left. + n_f^2 C_A\left(\frac{208}{27}\right) \right] + \bar{\mathcal{D}}_2 \left[C_A^3\left(-\frac{6748}{9} + 192\zeta_2\right) + n_f C_A^2\left(\frac{896}{9}\right) + n_f^2 C_A\left(-\frac{16}{9}\right) \right] \\
& + \bar{\mathcal{D}}_3 \left[C_A^3\left(\frac{1600}{9}\right) + n_f C_A^2\left(-\frac{160}{9}\right) + C_A^3(-40\bar{\mathcal{D}}_4) \right] + \bar{\delta} \left[C_A^3\left(\frac{859052}{729} - 192\zeta_5 \right. \right.
\end{aligned}$$

$$\begin{aligned}
& -\frac{51068}{27}\zeta_3 - \frac{64400}{81}\zeta_2 + \frac{608}{3}\zeta_2\zeta_3 - 128\zeta_2^2) + n_f C_A^2 \left(-\frac{150088}{729} + \frac{488}{3}\zeta_3 \right. \\
& + \frac{12200}{81}\zeta_2 + \frac{88}{15}\zeta_2^2) + C_A C_F n_f \left(-\frac{5038}{27} + 24 \ln\left(\frac{\mu_R^2}{m_t^2}\right) + \frac{760}{9}\zeta_3 + \frac{16}{3}\zeta_2 + \frac{32}{5}\zeta_2^2 \right) \\
& \left. + n_f^2 C_A \left(-\frac{232}{729} + \frac{32}{27}\zeta_3 - \frac{176}{27}\zeta_2 \right) \right] + (z_1 \leftrightarrow z_2). \tag{6.3}
\end{aligned}$$

Now, using the above result of $\Delta_{d,g,3}^{A,NSV}$ at a_s^3 , we extract the NSV coefficients $\varphi_{d,g,3}^{A,(k)}$ with $k = 0, 1, 2, 3$ and they are given by

$$\begin{aligned}
\varphi_{d,g,3}^{A,(0)} &= C_A n_f^2 \left(-\frac{232}{729} + \frac{32}{27}\zeta_3 - \frac{176}{27}\zeta_2 \right) + C_A^2 n_f \left(-\frac{80860}{729} + \frac{704}{9}\zeta_3 + \frac{11960}{81}\zeta_2 - \frac{24}{5}\zeta_2^2 \right) \\
&+ C_A^3 \left(\frac{423704}{729} + 192\zeta_5 - \frac{18188}{27}\zeta_3 - \frac{55448}{81}\zeta_2 + \frac{176}{3}\zeta_2\zeta_3 + \frac{1384}{15}\zeta_2^2 \right) \\
&+ C_F C_A n_f \left(-\frac{2158}{27} + \frac{472}{9}\zeta_3 + \frac{16}{3}\zeta_2 + \frac{32}{5}\zeta_2^2 \right), \\
\varphi_{d,g,3}^{A,(1)} &= C_A n_f^2 \left(\frac{56}{27} \right) + C_A^2 n_f \left(\frac{1528}{81} - 8\zeta_3 - \frac{152}{9}\zeta_2 \right) + C_A^3 \left(-\frac{18988}{81} + \frac{448}{3}\zeta_3 + \frac{752}{9}\zeta_2 \right) \\
&+ C_F C_A n_f \left(4 - \frac{8}{3}\zeta_2 \right), \\
\varphi_{d,g,3}^{A,(2)} &= C_A n_f^2 \left(\frac{8}{27} \right) + C_A^2 n_f \left(\frac{164}{27} + \frac{2}{3}\zeta_2 \right) + C_A^3 \left(-\frac{1432}{27} + \frac{40}{3}\zeta_2 \right), \\
\varphi_{d,g,3}^{A,(3)} &= C_A^2 n_f \left(\frac{32}{27} \right) + C_A^3 \left(-\frac{176}{27} \right). \tag{6.4}
\end{aligned}$$

Here, we notice that the above NSV coefficients are same for both pseudo-scalar and scalar Higgs production via gluon fusion [1]. However, the universality of $\varphi_{d,g,3}^{A,(k)}$ at third order can be checked only when the explicit N³LO results are available for the pseudo-scalar Higgs boson production in gluon fusion. The results of SV rapidity distributions to N³LO can be found in Appendix D.

7 More on the \vec{z} space solution $\Phi_{d,g}^A$

In the following, we discuss in detail the characteristic structure of SV and NSV solutions given in 4.33 and 4.42, respectively. Both the SV and NSV parts of $\Phi_{d,g}^A$ satisfy the K+G equation and they contain singular as well as finite parts at every order. The pole part in the SV solution namely the soft and collinear divergences which are proportional to the distributions $\delta(1-z_l)$ and $\mathcal{D}_0(z_l)$ get cancelled against those resulting from the FFs entirely and the AP kernels partially. And the z dependent finite part correctly reproduces all the distributions in the SV part of CFs $\Delta_{d,g}^A$. The NSV part, $\Phi_{d,g,NSV}^A$, which comprises of terms like $\mathcal{D}_i(z_l) \ln^k(1-z_j)$ and $\delta(1-z_l) \ln^k(1-z_j)$ with $(l, j = 1, 2)$, $(i, k = 0, 1, \dots)$ removes the remaining collinear divergences of the AP kernels. The finite part of it along with SV counterpart give rises to next to SV terms to CFs $\Delta_{d,g}^A$. Note that the SV part $\Phi_{d,g}^A$ plays a vital role in producing the next to SV terms for the CFs $\Delta_{d,g}^A$ at every order, when

the exponential is expanded in powers of a_s . This is due to the fact that the convolutions of two or more distributions contribute to certain next to SV logarithms in addition to the distributions.

Let us now focus on a peculiar feature that the NSV solution exhibits. Unlike in the case of SV solution, the NSV solution has the explicit z dependency due to two pieces. One of them is from the ansatz $(1 - z_l)^{i\epsilon/2}(1 - z_j)^{i\epsilon/2}/(1 - z_l)$ and the other one is from the coefficient $\varphi_{d,g}^{A,(i)}(z_j, \epsilon)$. This enables us to construct a class of solutions, a minimal class, to the K+G equation, satisfying the correct divergent structure as well as the dependence on $\ln^k(1 - z_j)$ with $(l, j = 1, 2)$, $(i, k = 0, 1, \dots)$ [79] as given below

$$\Phi_{d,g,NSV}^{A,j} = \sum_{i=1}^{\infty} \hat{a}_s^i \left(\frac{q^2 \bar{z}_1^{\alpha_1} \bar{z}_2^{\alpha_2}}{\mu^2} \right)^{i\frac{\epsilon}{2}} S_\epsilon^i \left[\frac{i\epsilon}{4\bar{z}_1} \varphi_{d,g,\alpha_2}^{A,(i)}(\bar{z}_2, \epsilon) \right] + (\bar{z}_1 \leftrightarrow \bar{z}_2)|_{(\alpha_1 \rightarrow \beta_1, \alpha_2 \rightarrow \beta_2)}, \quad (7.1)$$

with $j = (\alpha_1, \alpha_2, \beta_1, \beta_2)$ and $\bar{z}_l = (1 - z_l)$ for $l = 1, 2$. It is to be noted that $\alpha_1 = \beta_1 = 1$ for obtaining a finite $\Delta_{d,g}^A$, whereas α_2 and β_2 can be arbitrary. The predictions from the solutions $\Phi_{d,g,NSV}^{A,j}$ are found to be independent of the choice of α_2 and β_2 owing to the explicit z -dependence of the coefficients $\varphi_{d,g,j}^{A,(i)}(z_l, \epsilon)$ with $j = \alpha_2$ for $l = 2$ and $j = \beta_2$ for $l = 1$ at every order in \hat{a}_s and in ϵ . It is straightforward to show that any variation of α_2 and β_2 in the factors $(1 - z_2)^{i\alpha_2\epsilon/2}$ and $(1 - z_1)^{i\beta_2\epsilon/2}$ can always be compensated by suitably adjusting the z independent coefficients of $\ln(1 - z_1)$ and $\ln(1 - z_2)$ terms in $\varphi_{d,g,\beta_2}^{A,(i)}(z_1, \epsilon)$ and $\varphi_{d,g,\alpha_2}^{A,(i)}(z_2, \epsilon)$, respectively at every order in \hat{a}_s . Here, the logarithmic structure of $\varphi_{d,f,g}^{A,j}$ plays a crucial role. Under this scale transformation, the expression given in (4.51) takes the following form

$$\varphi_{d,f,g}^{A,j}(a_s(q^2 \bar{z}_l^j), \bar{z}_l) = \sum_{i=1}^{\infty} \sum_{k=0}^i a_s^i (q^2 \bar{z}_l^j) \varphi_{d,g,j,i}^{A,(k)} \ln^k \bar{z}_l. \quad (7.2)$$

The fact that the predictions are insensitive to j relate the coefficients $\varphi_{d,g,j,i}^{A,(k)}$ and $\varphi_{d,g,i}^{A,(k)}$, the solution corresponding to $j = 1$, as given below

$$\begin{aligned} \varphi_{d,g,j,1}^{A,(0)} &= \varphi_{d,g,1}^{A,(0)}, \quad \varphi_{d,g,j,1}^{A,(1)} = -D_1^A \bar{j} + \varphi_{d,g,1}^{A,(1)}, \quad \varphi_{d,g,j,2}^{A,(0)} = \varphi_{d,g,2}^{A,(0)}, \\ \varphi_{d,g,j,2}^{A,(1)} &= -\bar{j} \left(D_2^A - \beta_0 \varphi_{d,g,1}^{A,(0)} \right) + \varphi_{d,g,2}^{A,(1)}, \\ \varphi_{d,g,j,2}^{A,(2)} &= -\frac{1}{2} \bar{j}^2 \beta_0 D_1^A - \bar{j} \left(C_2^A - \beta_0 \varphi_{d,g,1}^{A,(1)} \right) + \varphi_{d,g,2}^{A,(2)} \\ \varphi_{d,g,j,3}^{A,(0)} &= \varphi_{d,g,3}^{A,(0)}, \quad \varphi_{d,g,j,3}^{A,(1)} = -\bar{j} \left(D_3^A - \beta_1 \varphi_{d,g,1}^{A,(0)} - 2\beta_0 \varphi_{d,g,2}^{A,(0)} \right) + \varphi_{d,g,3}^{A,(1)} \\ \varphi_{d,g,j,3}^{A,(2)} &= -\bar{j}^2 \left(\frac{1}{2} \beta_1 D_1^A + \beta_0 D_2^A - \beta_0^2 \varphi_{d,g,1}^{A,(0)} \right) - \bar{j} \left(C_3^A \bar{j} - \beta_1 \varphi_{d,g,1}^{A,(1)} - 2\beta_0 \varphi_{d,g,2}^{A,(1)} \right) + \varphi_{d,g,3}^{A,(2)} \\ \varphi_{d,g,j,3}^{A,(3)} &= \beta_0^2 \left(-\frac{1}{3} D_1^A \bar{j}^3 + \bar{j}^2 \varphi_{d,g,1}^{A,(1)} \right) + \beta_0 \bar{j} \left(-C_2^A \bar{j} + 2\varphi_{d,g,2}^{A,(2)} \right) + \varphi_{d,g,3}^{A,(3)} \\ \varphi_{d,g,j,4}^{A,(0)} &= \varphi_{d,g,4}^{A,(0)}, \quad \varphi_{d,g,j,4}^{A,(1)} = -D_4^A \bar{j} + \beta_2 \bar{j} \varphi_{d,g,1}^{A,(0)} + 2\beta_1 \bar{j} \varphi_{d,g,2}^{A,(0)} + 3\beta_0 \bar{j} \varphi_{d,g,3}^{A,(0)} + \varphi_{d,g,4}^{A,(1)} \\ \varphi_{d,g,j,4}^{A,(2)} &= -C_4^A \bar{j} - \frac{1}{2} \beta_2 D_1^A \bar{j}^2 - \beta_1 D_2^A \bar{j}^2 - \frac{3}{2} \beta_0 D_3^A \bar{j}^2 + \frac{5}{2} \beta_0 \beta_1 \bar{j}^2 \varphi_{d,g,1}^{A,(0)} + \beta_2 \bar{j} \varphi_{d,g,1}^{A,(1)} + 3\beta_0 \bar{j}^2 \varphi_{d,g,2}^{A,(0)} \end{aligned}$$

$$\begin{aligned}
& +2\beta_1\bar{j}\varphi_{d,g,2}^{A,(1)} + 3\beta_0\bar{j}\varphi_{d,g,3}^{A,(1)} + \varphi_{d,g,4}^{A,(2)} \\
\varphi_{d,g,j,4}^{A,(3)} &= \beta_0^3\bar{j}^3\varphi_{d,g,1}^{A,(0)} + \beta_0^2\bar{j}^2\left(-D_2^{A\bar{j}} + 3\varphi_{d,g,2}^{A,(1)}\right) - \frac{1}{6}\beta_1\bar{j}\left(6C_2^{A\bar{j}} + 5\beta_0\bar{j}\left(D_1^{A\bar{j}} - 3\varphi_{d,g,1}^{A,(1)}\right)\right. \\
& \left.-12\varphi_{d,g,2}^{A,(2)}\right) - \frac{3}{2}\beta_0\bar{j}\left(C_3^{A\bar{j}} - 2\varphi_{d,g,3}^{A,(2)}\right) + \varphi_{d,g,4}^{A,(3)} \\
\varphi_{d,g,j,4}^{A,(4)} &= \beta_0^3\left(-\frac{1}{4}D_1^{A\bar{j}^4} + \bar{j}^3\varphi_{d,g,1}^{A,(1)}\right) + \beta_0^2\bar{j}^2\left(-C_2^{A\bar{j}} + 3\varphi_{d,g,2}^{A,(2)}\right) + 3\beta_0\bar{j}\varphi_{d,g,3}^{A,(3)} + \varphi_{d,g,4}^{A,(4)}, \quad (7.3)
\end{aligned}$$

with j being α_2 and β_2 for the coefficients of $\ln(1-z_2)$ and $\ln(1-z_1)$ respectively. In the above equations, $\bar{j} = (\alpha_2 - 1)$ and $(\beta_2 - 1)$ for $j = \alpha_2$ and β_2 respectively. The above relations are the transformations for $\varphi_{d,g,j,i}^{A,(k)}$ that are required to compensate the contributions resulting from the change in the exponents of $(1-z_1)$ and $(1-z_2)$ from $(i\epsilon)/2$ to $(ij\epsilon)/2$. The function $\Phi_{d,g,NSV}^{A,j}$ being insensitive to the choice of the scales α_2 and β_2 indicates its invariance under certain gauge like transformations on both $(1-z_l)^{i\epsilon/2}$ and $\varphi_{d,f,g}^{A,j}(z_l, \epsilon)$. Due to this invariance, these transformations neither alter the divergent structure nor the finite parts of $\Phi_{d,g,NSV}^A$. However, we choose to work with $\alpha_2 = \beta_2 = 1$ in the NSV solution to have more resemblance with its SV counterpart. In summary, we find a minimal class of solutions to the K+G equation without affecting neither the all order structure nor the predictions for $\Delta_{d,g}^A$. We will show later that this choice will allow us to study resummation in two-dimensional Mellin space for SV as well as NSV parts with single $\mathcal{O}(1)$ term denoted by $\omega = a_s\beta_0 \ln(N_1N_2)$.

8 Resummation in the Mellin \vec{N} space

This section is devoted to the study of all order perturbative structure of $\Delta_{d,g}^A$ in the Mellin space. To find the structure of $\Delta_{d,g}^A$ in the Mellin space, we use the integral representations of both $\Phi_{d,g,SV}^A$ and $\Phi_{d,g,NSV}^A$ given in (4.48) and (4.49) respectively. As a result, $\Psi_{d,g}^A$ in (4.4) takes the following form

$$\begin{aligned}
\Psi_{d,g}^A(q^2, \mu_F^2, z_1, z_2) &= \frac{\delta(\bar{z}_1)}{2} \left(\int_{\mu_F^2}^{q^2\bar{z}_2} \frac{d\lambda^2}{\lambda^2} \mathcal{P}_{gg}(a_s(\lambda^2), \bar{z}_2) + \mathcal{Q}_{d,g}^A(a_s(q_2^2), \bar{z}_2) \right)_+ \\
&+ \frac{1}{4} \left(\frac{1}{\bar{z}_1} \left\{ \mathcal{P}_{gg}(a_s(q_{12}^2), \bar{z}_2) + 2L_g^A(a_s(q_{12}^2), \bar{z}_2) \right. \right. \\
&+ \left. \left. q^2 \frac{d}{dq^2} (\mathcal{Q}_{d,g}^A(a_s(q_2^2), \bar{z}_2) + 2\varphi_{d,f,g}^A(a_s(q_2^2), \bar{z}_2)) \right\} \right)_+ \\
&+ \frac{1}{2} \delta(\bar{z}_1) \delta(\bar{z}_2) \ln(g_{d,g,0}^A(a_s(\mu_F^2))) + \bar{z}_1 \leftrightarrow \bar{z}_2, \quad (8.1)
\end{aligned}$$

where $\mathcal{P}_{gg}(a_s, \bar{z}_l) = P_{gg}(a_s, \bar{z}_l) - 2B_g^A(a_s)\delta(\bar{z}_l)$, $q_l^2 = q^2(1-z_l)$ and $q_{12}^2 = q^2\bar{z}_1\bar{z}_2$. The subscript $+$ indicates standard plus distribution. The function $\mathcal{Q}_{d,g}^P$ in (8.1) is given as

$$\mathcal{Q}_{d,g}^A(a_s, \bar{z}_l) = \frac{2}{\bar{z}_l} \mathbf{D}_{d,g}^A(a_s) + 2\varphi_{d,f,g}^A(a_s, \bar{z}_l). \quad (8.2)$$

The SV coefficient $\mathbf{D}_{d,g}^A$ are given in the Appendix A. The constant $g_{d,g,0}^A$ in (8.1) results from finite part of the virtual contributions and pure $\delta(\bar{z}_l)$ terms of $\Phi_{d,g}^A$.

Now we take the double Mellin transform of $\Delta_{d,g}^A$ in \vec{N} space as

$$\begin{aligned}\Delta_{d,g,\vec{N}}^A(q^2, \mu_R^2, \mu_F^2) &= \int_0^1 dz_1 z_1^{N_1-1} \int_0^1 dz_2 z_2^{N_2-1} \Delta_{d,g}^A(z_1, z_2)(q^2, \mu_R^2, \mu_F^2) \\ &= \tilde{g}_{d,g,0}^A(q^2, \mu_R^2, \mu_F^2) \exp\left(\Psi_{d,g,\vec{N}}^A(q^2, \mu_F^2)\right).\end{aligned}\quad (8.3)$$

The N -independent constant $\tilde{g}_{d,g,0}^A$ is given in Appendix E. The resummed result for $\Psi_{d,g,\vec{N}}^A$ takes the following form

$$\begin{aligned}\Psi_{d,g,\vec{N}}^A &= \left(g_{d,g,1}^A(\omega) + \frac{1}{N_1} \bar{g}_{d,g,1}^A(\omega)\right) \ln N_1 + \sum_{i=0}^{\infty} a_s^i \left(\frac{1}{2} g_{d,g,i+2}^A(\omega) + \frac{1}{N_1} \bar{g}_{d,g,i+2}^A(\omega)\right) \\ &+ \frac{1}{N_1} \left(h_{d,g,0}^A(\omega, N_1) + \sum_{i=1}^{\infty} a_s^i h_{d,g,i}^A(\omega, \omega_1, N_1)\right) + (N_1 \leftrightarrow N_2, \omega_1 \leftrightarrow \omega_2),\end{aligned}\quad (8.4)$$

with

$$\begin{aligned}h_{d,g,0}^A(\omega, N_l) &= h_{d,g,00}^A(\omega) + h_{d,g,01}^A(\omega) \ln N_l, \\ h_{d,g,i}^A(\omega, \omega_l, N_l) &= \sum_{k=0}^{i-1} h_{d,g,ik}^A(\omega) \ln^k N_l + \tilde{h}_{d,g,ii}^A(\omega, \omega_l) \ln^k N_l.\end{aligned}\quad (8.5)$$

In the above expressions, $\omega = a_s \beta_0 \ln N_1 N_2$ and $\omega_l = a_s \beta_0 \ln N_l$ for $l = 1, 2$. Here, $g_{d,g,i}^A$ are the resummation constants resulting from the SV contributions and $\bar{g}_{d,g,i}^A$ result entirely from A_g^A, B_g^A coefficients of P_{gg} and from the function $\mathbf{D}_{d,g}^A$ in (8.2). The function $\bar{g}_{d,g,1}^A$ is found to be identically zero and we find that none of the coefficients $\bar{g}_{d,g,i}^A$ contains explicit $\ln N_l$. The functions $h_{d,g,i}^A$ comprise of C_g^A and D_g^A which are present in P_{gg} as well as the pure NSV coefficients present in $\varphi_{d,f,g}^A$. We find that coefficient of $h_{d,g,01}^A$ is proportional to $C_{g,1}^A$ which is identically zero. Hence, at order a_s^0 , there is no $\frac{\ln N_l}{N_l}$ term. The SV resummation constant $g_{d,g,i}^A$ has been discussed in great detail in references [54, 113, 114] and the NSV resummation coefficients $\bar{g}_{d,g,i}^A$, $h_{d,g,ij}^A$ and $\tilde{h}_{d,g,ii}^A$ are provided in Appendix F and G. Our next aim is to include these resummed contributions consistently in the fixed order predictions to understand the phenomenological relevance of resumming the NSV contributions for the case of pseudo-scalar Higgs production in gluon fusion channel.

9 Numerical analysis

In this section, we study the impact of resummed soft-virtual and next-to-soft virtual (SV+NSV) contributions for the rapidity distribution of the pseudo-scalar Higgs production in gluon fusion channel at the LHC to NNLO_A+ $\overline{\text{NNLL}}$ accuracy. We use the MMHT2014(68cl) PDF set [115] and the corresponding strong coupling a_s through the Les Houches Accord PDF (LHAPDF) interface [116] at each order in perturbation theory with $n_f = 5$ active massless quark flavours throughout. Our predictions are based on Higgs effective field theory where the top quarks are integrated out at higher orders. Nevertheless,

we retain the top quark mass dependence at LO. The term $C_J^{(2)}$ in the Wilson coefficient C_J in (2.3) is taken to be zero in our analysis because it is not available in the literature yet. For simplicity, we have set $\cot \beta = 1$ in our numerical analysis. Results for other values of $\cot \beta$ can be easily obtained by rescaling the cross sections with $\cot^2 \beta$. For the fixed order rapidity distribution of the pseudo-scalar Higgs, we use the publicly available code FEHiP [94] of the scalar Higgs by taking into account the ratio factor discussed in section 3.1. The resummed contribution is obtained from $\Delta_{d,g,\vec{N}}^A$ in (8.3) after performing Mellin inversion which is done using an in-house FORTRAN based code. The resummed results are matched to the fixed order result in order to avoid any double counting of threshold logarithms as

$$\frac{d\sigma^{A,\text{match}}}{dY} = \frac{d\sigma^{A,(\text{SV}+\text{NSV})}}{dY} \Big|_{\text{resum}} - \frac{d\sigma^{A,(\text{SV}+\text{NSV})}}{dY} \Big|_{\text{FO}} + \frac{d\sigma^{A,\text{FO}}}{dY}. \quad (9.1)$$

We do the analysis for centre of mass energy $\sqrt{S} = 13$ TeV with the pseudo-scalar Higgs mass $m_A = 125$ GeV and $m_A = 700$ GeV, top quark pole mass $m_t = 173.3$ GeV and the Fermi constant $G_F = 4541.63$ pb. The numerical values for the aforementioned parameters are taken from the Particle Data Group 2020 [117]. To distinguish between the SV and SV+NSV resummed results, the NSV included resummed results have been denoted by $\overline{\text{N}}^n\overline{\text{LL}}$ for the n^{th} level logarithmic accuracy.

K-factor analysis: We begin our analysis by studying the higher order effects which are quantified through the K-factors as

$$K = \frac{\frac{d\sigma}{dY}(\mu_R = \mu_F = m_A)}{\frac{d\sigma^{\text{LO}}}{dY}(\mu_R = \mu_F = m_A)}. \quad (9.2)$$

We fix the central scale at $\mu_R = \mu_F = m_A$ throughout our analysis. In Table 1, we present the K-factor values of fixed order and resummed predictions at $m_A = 125$ GeV for benchmark rapidity values. We observe that the NLO result at the central scale is enhanced by 83.9% with respect to the LO one around the central rapidity region. However, the enhancement of the approximate NNLO (NNLO_A) result at the central scale is 27.9% in comparison to the NLO result. For the SV+NSV resummed results, we notice an enhancement of 60% and 36.2% when $\overline{\text{LL}}$ and $\overline{\text{NLL}}$ are added to LO and NLO respectively at the central rapidity region. The rapidity distribution increases by 14.76% when we include $\overline{\text{NNLL}}$ to NNLO_A . Further, at the central scale, the resummed rapidity distribution at $\text{NLO}+\overline{\text{NLL}}$ (25.6 pb) mimics that at NNLO_A (24 pb) around the central rapidity region. We also study the K-factor values for the high mass region i.e $m_A = 700$ GeV as given in Table 2. For the fixed order results, there is a large increment of 120% when we go from LO to NLO. Interestingly the higher order effects at NNLO_A give rise to only 12.6% correction to NLO around the central rapidity region. We find that there is an enhancement of 53.3% and 24.97% by the inclusion of $\overline{\text{LL}}$ and $\overline{\text{NLL}}$ resummed results

y	$K_{\text{LO}+\overline{\text{LL}}}$	K_{NLO}	$K_{\text{NLO}+\overline{\text{NLL}}}$	K_{NNLO_A}	$K_{\text{NNLO}_A+\overline{\text{NNLL}}}$
0-0.4	1.602	1.839	2.505	2.352	2.699
0.4-0.8	1.681	1.806	2.469	2.297	2.644
0.8-1.2	1.703	1.792	2.472	2.285	2.643
1.2-1.6	1.713	1.746	2.433	2.248	2.613
1.6-2.0	1.748	1.688	2.397	2.151	2.533

Table 1: K-factor values of fixed order and resummed results at the central scale $\mu_R = \mu_F = m_A$ for $m_A = 125$ GeV.

y	$K_{\text{LO}+\overline{\text{LL}}}$	K_{NLO}	$K_{\text{NLO}+\overline{\text{NLL}}}$	K_{NNLO_A}	$K_{\text{NNLO}_A+\overline{\text{NNLL}}}$
0-0.4	1.533	2.200	2.749	2.478	2.763
0.4-0.8	1.547	2.199	2.755	2.414	2.703
0.8-1.2	1.579	2.200	2.769	2.315	2.613
1.2-1.6	1.653	2.212	2.819	2.266	2.592
1.6-2.0	1.797	2.238	2.947	2.370	2.781

Table 2: K-factor values of fixed order and resummed results at the central scale $\mu_R = \mu_F = m_A$ for $m_A = 700$ GeV.

at LO and NLO respectively around the central rapidity region. At NNLO_A , the rapidity distribution increases by 11.48% when we include $\overline{\text{NNLL}}$. From Tables 1 and 2, it can be observed that resummed predictions not only bring in considerable enhancement in the fixed order results, but also improve the perturbative convergence till $\text{NNLO}_A + \overline{\text{NNLL}}$ accuracy.

7-point scale variation: Next, we study the theoretical uncertainties due to the unphysical renormalization (μ_R) and factorization (μ_F) scales in our results using the standard canonical 7-point variation approach. Here, $\mu = \{\mu_F, \mu_R\}$ is varied in the range $\frac{1}{2} \leq \frac{\mu}{m_A} \leq 2$, keeping the ratio μ_R/μ_F not larger than 2 and smaller than 1/2. In figure 1, we depict the bin-integrated rapidity distribution of the pseudo-scalar Higgs boson for the fixed order results in the left panel and the resummed results in the right panel around the central scale $\mu_R = \mu_F = m_A$ for $m_A = 125$ GeV(top) and $m_A = 700$ GeV(bottom). We have provided the fixed order as well as SV+NSV resummed results for benchmark

rapidity values at the central scale $\mu_R = \mu_F = m_A$ for $m_A = 125$ GeV and $m_A = 700$ GeV in Table 3 and 4 respectively at various perturbative orders. These tables also contain the maximum increments and decrements from the corresponding central scale values obtained by varying $\{\mu_R, \mu_F\}$ in the range $\{1/2, 2\}m_A$.

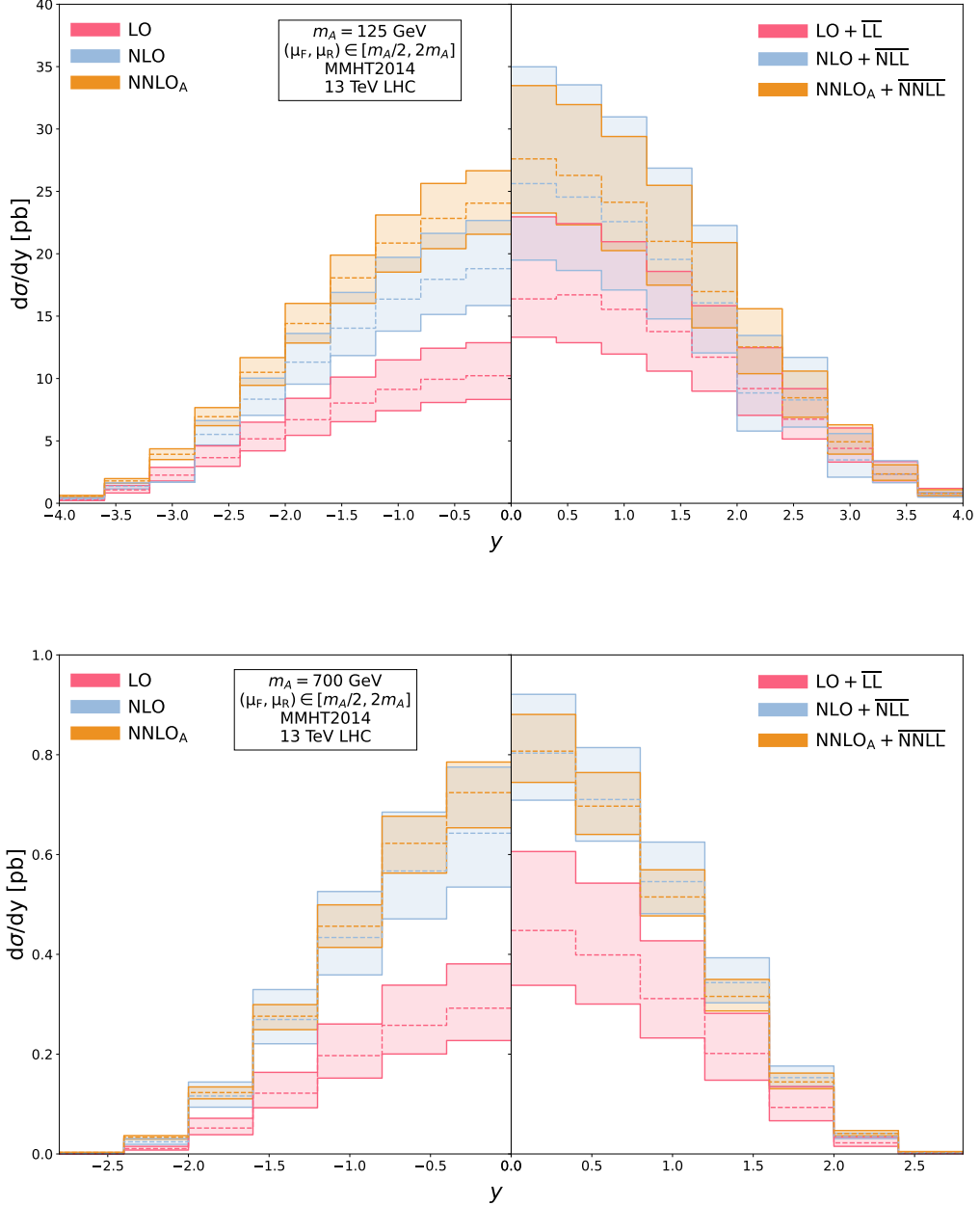


Figure 1: Comparison of 7-point scale variation between fixed order and SV+NSV resummed results for $m_A = 125$ (top) and $m_A = 700$ (bottom) GeV. The dashed lines refer to the corresponding central scale values at each order.

y	LO	LO+ $\overline{\text{LL}}$	NLO	NLO+ $\overline{\text{NLL}}$	NNLO _A	NNLO _A + $\overline{\text{NNLL}}$
0-0.4	10.225 ^{+2.645} _{-1.902}	16.379 ^{+6.580} _{-3.064}	18.805 ^{+3.862} _{-2.953}	25.623 ^{+9.360} _{-6.130}	24.054 ^{+2.599} _{-2.490}	27.605 ^{+5.873} _{-4.340}
0.4-0.8	9.938 ^{+2.490} _{-1.860}	16.704 ^{+5.7120} _{-3.833}	17.951 ^{+3.682} _{-2.815}	24.543 ^{+8.994} _{-5.883}	22.836 ^{+2.798} _{-2.428}	26.281 ^{+5.675} _{-3.959}
0.8-1.2	9.128 ^{+2.363} _{-1.707}	15.54 ^{+5.424} _{-3.581}	16.362 ^{+3.350} _{-2.563}	22.572 ^{+8.396} _{-5.474}	20.856 ^{+2.251} _{-2.327}	24.126 ^{+5.273} _{-3.873}
1.2-1.6	8.033 ^{+2.080} _{-1.495}	13.763 ^{+4.820} _{-3.171}	14.034 ^{+2.863} _{-2.193}	19.546 ^{+7.315} _{-4.765}	18.067 ^{+1.825} _{-2.037}	20.992 ^{+4.491} _{-3.508}
1.6-2.0	6.698 ^{+1.714} _{-1.252}	11.711 ^{+4.123} _{-2.723}	11.311 ^{+2.299} _{-1.762}	16.061 ^{+6.203} _{-4.008}	14.412 ^{+1.607} _{-1.566}	16.968 ^{+3.926} _{-2.906}

Table 3: Values of resummed rapidity distribution at various orders in comparison to the fixed order results in pb at the central scale $\mu_R = \mu_F = m_A = 125$ GeV for 13 TeV LHC.

y	LO	LO+ $\overline{\text{LL}}$	NLO	NLO+ $\overline{\text{NLL}}$	NNLO _A	NNLO _A + $\overline{\text{NNLL}}$
0-0.4	0.292 ^{+0.088} _{-0.065}	0.123 ^{+0.158} _{-0.1098}	0.643 ^{+0.0132} _{-0.1078}	0.803 ^{+0.1178} _{-0.0943}	0.724 ^{+0.0613} _{-0.07045}	0.807 ^{+0.0735} _{-0.0625}
0.4-0.8	0.257 ^{+0.0804} _{-0.0574}	0.399 ^{+0.14379} _{-0.09845}	0.567 ^{+0.1179} _{-0.0959}	0.710 ^{+0.1040} _{-0.0834}	0.622 ^{+0.0543} _{-0.0596}	0.697 ^{+0.06733} _{-0.0566}
0.8-1.2	0.197 ^{+0.0633} _{-0.0450}	0.311 ^{+0.1158} _{-0.0788}	0.434 ^{+0.0922} _{-0.0749}	0.546 ^{+0.07919} _{-0.0641}	0.456 ^{+0.0428} _{-0.0424}	0.515 ^{+0.0543} _{-0.0379}
1.2-1.6	0.122 ^{+0.0417} _{-0.0291}	0.201 ^{+0.0803} _{-0.0535}	0.434 ^{+0.06} _{-0.0486}	0.343 ^{+0.0497} _{-0.0405}	0.276 ^{+0.02322} _{-0.02688}	0.316 ^{+0.03399} _{-0.0291}
1.6-2.0	0.052 ^{+0.0195} _{-0.0132}	0.093 ^{+0.0416} _{-0.0267}	0.116 ^{+0.0279} _{-0.0224}	0.153 ^{+0.0232} _{-0.0181}	0.123 ^{+0.01131} _{-0.0125}	0.144 ^{+0.0177} _{-0.01365}

Table 4: Values of resummed rapidity distribution at various orders in comparison to the fixed order results in pb at the central scale $\mu_R = \mu_F = m_A = 700$ GeV for 13 TeV LHC.

Let us first look at the plot with $m_A = 125$ GeV in figure 1. This plot shows that the addition of SV+NSV resummed results to the fixed order ones increases the rapidity distribution at each order up to NNLO_A in perturbation theory. However, the percentage enhancement in the rapidity distribution decreases from 60% at LO to 14.76% at NNLO_A by the inclusion of $\overline{\text{LL}}$ and $\overline{\text{NNLL}}$ respectively at the central rapidity region. This indicates better perturbative convergence of the truncated series at higher orders due to the addition of the resummed predictions. We now compare the 7-point uncertainties of fixed order and SV+NSV resummed results due to μ_R and μ_F scales. We find that the combined uncertainty due to μ_R and μ_F scales lies in the range (+25.87%, -18.60%) at LO while at NNLO_A, it gets substantially reduced to (+10.80%, -10.35%) around the central

rapidity region. We see that the bands of resummed predictions till NNLO_A + $\overline{\text{NNLL}}$ are wider than that of the corresponding fixed order results throughout the rapidity spectrum for $m_A = 125$ GeV. Numerically, the combined uncertainty due to these unphysical scales lies between (+40.17%, -18.71%) at LO + $\overline{\text{LL}}$, (+36.53%, -23.92%) at NLO + $\overline{\text{NLL}}$ and (+21.27%, -15.72%) at NNLO_A + $\overline{\text{NNLL}}$ order around $y = 0$. This shows that there is a systematic decrease in the uncertainty when we go to higher logarithmic accuracy for SV+NSV resummed results. The plot for $m_A = 700$ GeV in figure 1 shows a similar trend of enhancement in the rapidity distribution by the addition of SV+NSV resummed results as was depicted above. The 7-point uncertainty values show that at lower orders, the resummed results show significantly more μ_R and μ_F variation as compared to the fixed order ones similar to the case of $m_A = 125$ GeV. However, at NNLO_A + $\overline{\text{NNLL}}$ accuracy, the combined uncertainty of the resummed result lies in the range (+9.11%, -7.74%) which is comparable to the uncertainty of (+8.47%, -9.73%) for the fixed order prediction at NNLO_A around central rapidity region. Thus, the SV+NSV resummed results become more relevant for higher values of pseudo-scalar Higgs boson mass. The above analysis suggests the need to understand the behavior of the resummed results w.r.t μ_R and μ_F scale variations in a better way. Hence, we study the impact of each scale individually by keeping the other fixed.

Uncertainties due to μ_R and μ_F scales individually: We now, discuss the effect of the factorization scale μ_F individually by keeping the renormalization scale μ_R fixed. Figure 2 shows the bin-integrated rapidity distributions for the fixed order(left panel) as well as the SV+NSV resummed results(right panel) at various perturbative orders for $m_A = 125$ GeV (top) and $m_A = 700$ GeV (bottom) keeping the renormalization scale fixed at $\mu_R = m_A$. The factorization scale is varied in the range $\{1/2, 1\}m_A$ around the central scale $\mu_F = \mu_R = m_A$ to get the uncertainty bands. The fixed order results show negligible dependence on the μ_F scale both at $m_A = 125$ GeV and $m_A = 700$ GeV. On the other hand, the resummed predictions show substantial dependence w.r.t the μ_F scale especially at $m_A = 125$ GeV. The uncertainty lies in the range (+36.53 %, - 23.92%) at NLO + $\overline{\text{NLL}}$ accuracy which comes down to (+ 21.27%, - 15.72%) at NNLO_A + $\overline{\text{NNLL}}$ accuracy around central rapidity region for $m_A = 125$ GeV. When we compare these μ_F scale uncertainty values with those at $m_A = 700$ GeV, we find that it vary in the range (+ 14.66 %, - 9.88%) and (+9.11 %, - 7.75%) at NLO + $\overline{\text{NLL}}$ and NNLO_A + $\overline{\text{NNLL}}$ order respectively around $y = 0$. Hence, as suggested by the 7-point scale variation analysis, the uncertainty decreases considerably at the higher value of the pseudo-scalar Higgs Boson mass. The uncertainty due to the factorisation scale decreases at higher orders for both the cases of m_A . Also, the higher order uncertainty bands lie within the lower order ones. These two observations hint towards improved reliability of the perturbative results and better perturbative convergence at higher orders.

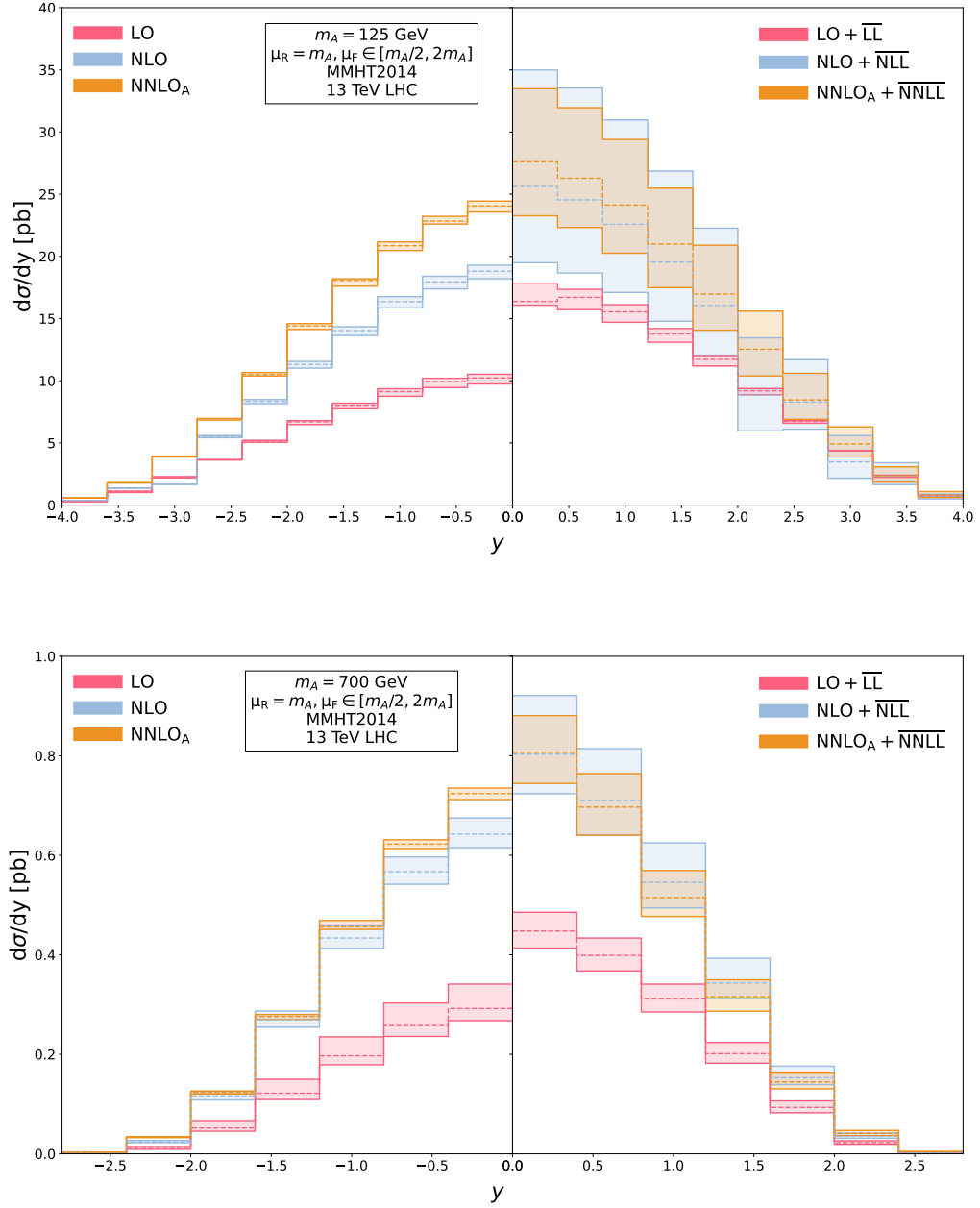


Figure 2: Comparison of μ_F scale variation between fixed order and SV+NSV resummed results for $m_A = 125$ (top) and $m_A = 700$ (bottom) GeV. The dashed lines refer to the corresponding central scale values at each order.

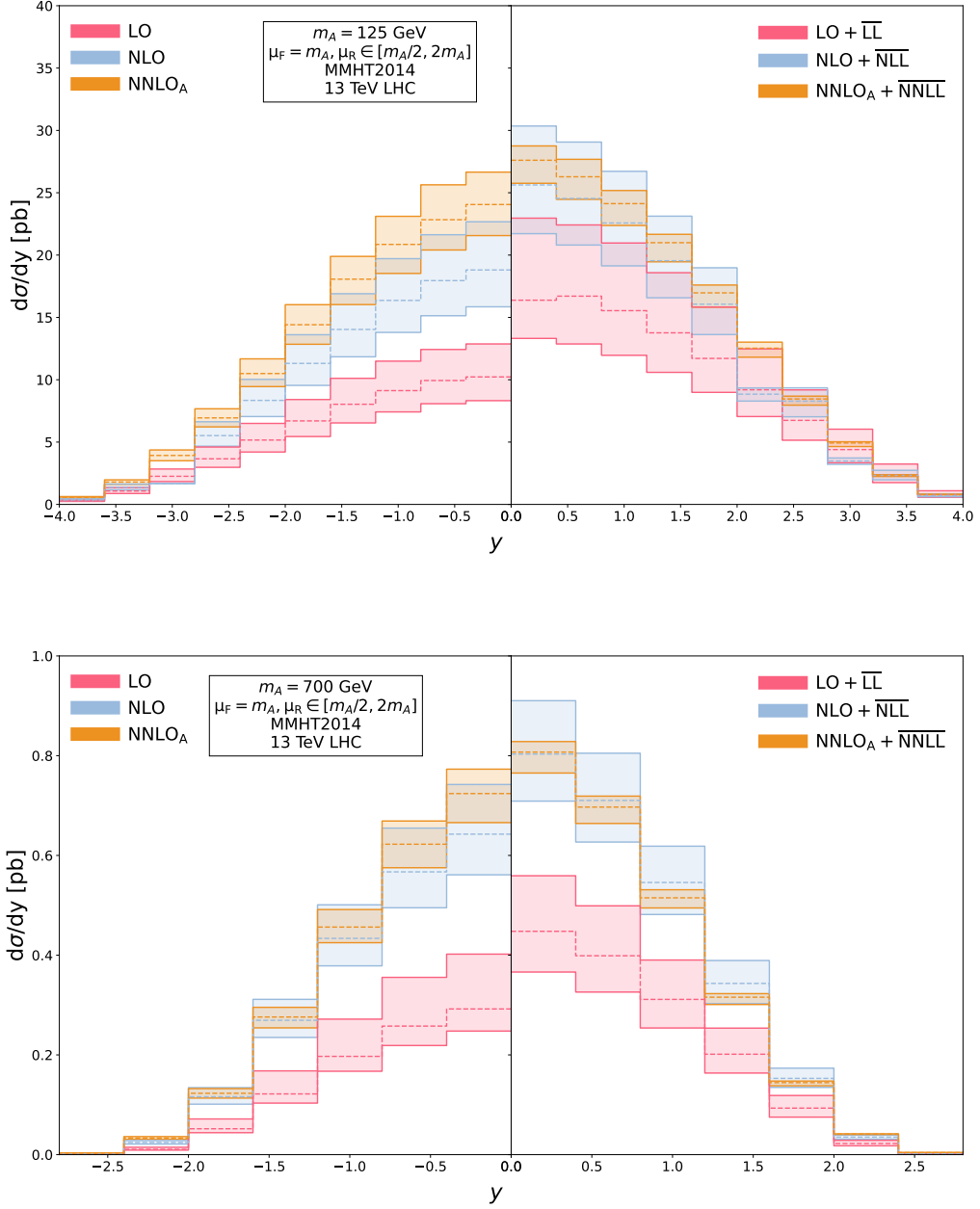


Figure 3: Comparison of μ_R scale variation between fixed order and SV+NSV resummed results for $m_A = 125$ (top) and $m_A = 700$ (bottom) GeV. The dashed lines refer to the corresponding central scale values at each order.

Next, we study the variation in the fixed order and SV+NSV resummed results w.r.t the renormalisation scale by keeping the factorisation scale fixed at $\mu_F = m_A$. The uncertainty bands are obtained by varying μ_R in the range $\{1/2, 1\}m_A$ around the central scale $\mu_F =$

$\mu_R = m_A$. In figure 3, we observe that from the NLO level, the μ_R scale uncertainty of the fixed order results decreases by the addition of resummed predictions for $m_A = 125$ GeV as well as $m_A = 700$ GeV. The numerical values of the μ_R uncertainties lie between (+18.45%, -15.24%) and (+4.16%, -6.69%) at NLO + $\overline{\text{NLL}}$ and NNLO_A + $\overline{\text{NNLL}}$ order respectively which is a considerable reduction from (+20.54%, -15.70%) and (+10.80%, -10.35%) at NLO and NNLO_A accuracy respectively around $y = 0$ for $m_A = 125$ GeV. Similarly, for the case of $m_A = 700$ GeV, they lie in the range (+13.33 %, - 11.74%) and (+ 2.62%, - 5.19%) at NLO + $\overline{\text{NLL}}$ and NNLO_A + $\overline{\text{NNLL}}$ respectively whereas they vary between (+15.48 %, - 12.69%) and (+6.76 %, - 8.04%) for NLO and NNLO_A order respectively around central rapidity region. From the above percentages, we also find that the uncertainty decreases as we go to higher orders for both cases of pseudo-scalar Higgs boson masses. In addition, the uncertainty bands of resummed results at higher orders are well within the lower orders from NLO level onwards.

Here, we performed a comparative study between the fixed order results and the SV+NSV resummed predictions for the rapidity distribution of pseudo-scalar Higgs boson in gluon fusion process. This has been done through the K-factor analysis, 7-point variation approach, and finally by studying the variation of μ_F and μ_R scales individually. We did the analysis for two different cases of pseudo-scalar Higgs boson masses $m_A = 125, 700$ GeV. The K-factor analysis showed that the inclusion of SV+NSV resummed predictions resulted in the enhancement of the fixed order results at every order in perturbation theory up to NNLO_A accuracy for both the cases of m_A . Also, we observed that the percentage enhancement by adding the resummed results decreases as we go from LO to NNLO_A accuracy. This shows that the resummed results are more reliable and have a better perturbative convergence. The study of factorisation scale variation showed that the addition of the resummed results especially at $m_A = 125$ GeV significantly increased the uncertainty of the fixed order results, which otherwise was almost independent of the μ_F scale variation. However, the dependence of the resummed results on the μ_F scale decreases considerably for the case of $m_A = 700$ GeV. The renormalisation scale dependence, on the other hand, gets improved by the inclusion of resummed predictions. In order to understand this behavior of SV+NSV resummed results in a better way, we compare them with the well established SV resummed results at various orders in the next section.

SV+NSV vs SV resummed predictions: In previous sections, we presented the observations on the behavior of SV+NSV resummed corrections by comparing them with the fixed-order results at various perturbative orders. Here, we try to understand the reasons behind those observations by comparing the full SV+NSV resummed predictions with the well-established SV resummed results which would help us to infer the behavior of resummed NSV logarithms in particular.

We begin our analysis with the K-factor values of SV and SV+NSV resummed results. We provide the K-factor values of SV and SV+NSV resummed results at various perturbative orders for benchmark rapidity values for $m_A = 125, 700$ GeV in Tables 5 and 6. Looking at the values in Tables 5 and 6, we find that the addition of resummed NSV logarithms enhances the SV resummed predictions for the rapidity distribution at each

y	$K_{\text{LO+LL}}$	$K_{\text{LO+LL}}$	$K_{\text{NLO+NLL}}$	$K_{\text{NLO+NLL}}$	$K_{\text{NNLO}_A+\text{NNLL}}$	$K_{\text{NNLO}_A+\text{NNLL}}$
0-0.4	1.411	1.602	2.159	2.505	2.502	2.699
0.4-0.8	1.410	1.681	2.126	2.469	2.447	2.644
0.8-1.2	1.428	1.703	2.125	2.472	2.441	2.643
1.2-1.6	1.437	1.713	2.086	2.433	2.409	2.613
1.6-2.0	1.466	1.748	2.047	2.397	2.324	2.533

Table 5: K-factor values of SV and SV+NSV resummed results at the central scale $\mu_R = \mu_F = m_A = 125$ GeV.

y	$K_{\text{LO+LL}}$	$K_{\text{LO+LL}}$	$K_{\text{NLO+NLL}}$	$K_{\text{NLO+NLL}}$	$K_{\text{NNLO}_A+\text{NNLL}}$	$K_{\text{NNLO}_A+\text{NNLL}}$
0-0.4	1.375	1.533	2.530	2.749	2.630	2.763
0.4-0.8	1.388	1.547	2.536	2.755	2.571	2.703
0.8-1.2	1.416	1.579	2.550	2.769	2.479	2.613
1.2-1.6	1.480	1.653	2.596	2.819	2.451	2.593
1.6-2.0	1.6035	1.797	2.703	2.947	2.612	2.781

Table 6: K-factor values of SV and SV+NSV resummed results at the central scale $\mu_R = \mu_F = m_A = 700$ GeV.

order in perturbation theory for both the values of m_A . For instance, there is an enhancement of 16.03% and 7.87% by the inclusion of resummed NSV logarithms at $\text{NLO}+\overline{\text{NLL}}$ and $\text{NNLO}_A + \overline{\text{NNLL}}$ respectively for $m_A = 125$ GeV. Similarly, for $m_A = 700$ GeV, the rapidity distribution increases by 8.66% and 5.06% when we go from $\text{NLO}+\text{NLL}$ and $\text{NNLO}_A+\text{NNLL}$ to $\text{NLO}+\overline{\text{NLL}}$ and $\text{NNLO}_A+\overline{\text{NNLL}}$ respectively. We also observe that the percentage enhancement in the rapidity distribution due to the resummed NSV logarithms decreases as we go from $\text{NLO}+\overline{\text{NLL}}$ to $\text{NNLO}_A+\overline{\text{NNLL}}$. This suggests better perturbative convergence of the SV+NSV resummed result which was already noticed while comparing it with the fixed order results.

Next, we study the uncertainties of the resummed NSV logarithms w.r.t the μ_R and μ_F scale variations. We first present the plots for canonical 7-point scale variation of the bin-integrated rapidity distribution in figure 4 for the pseudo-scalar Higgs boson mass,

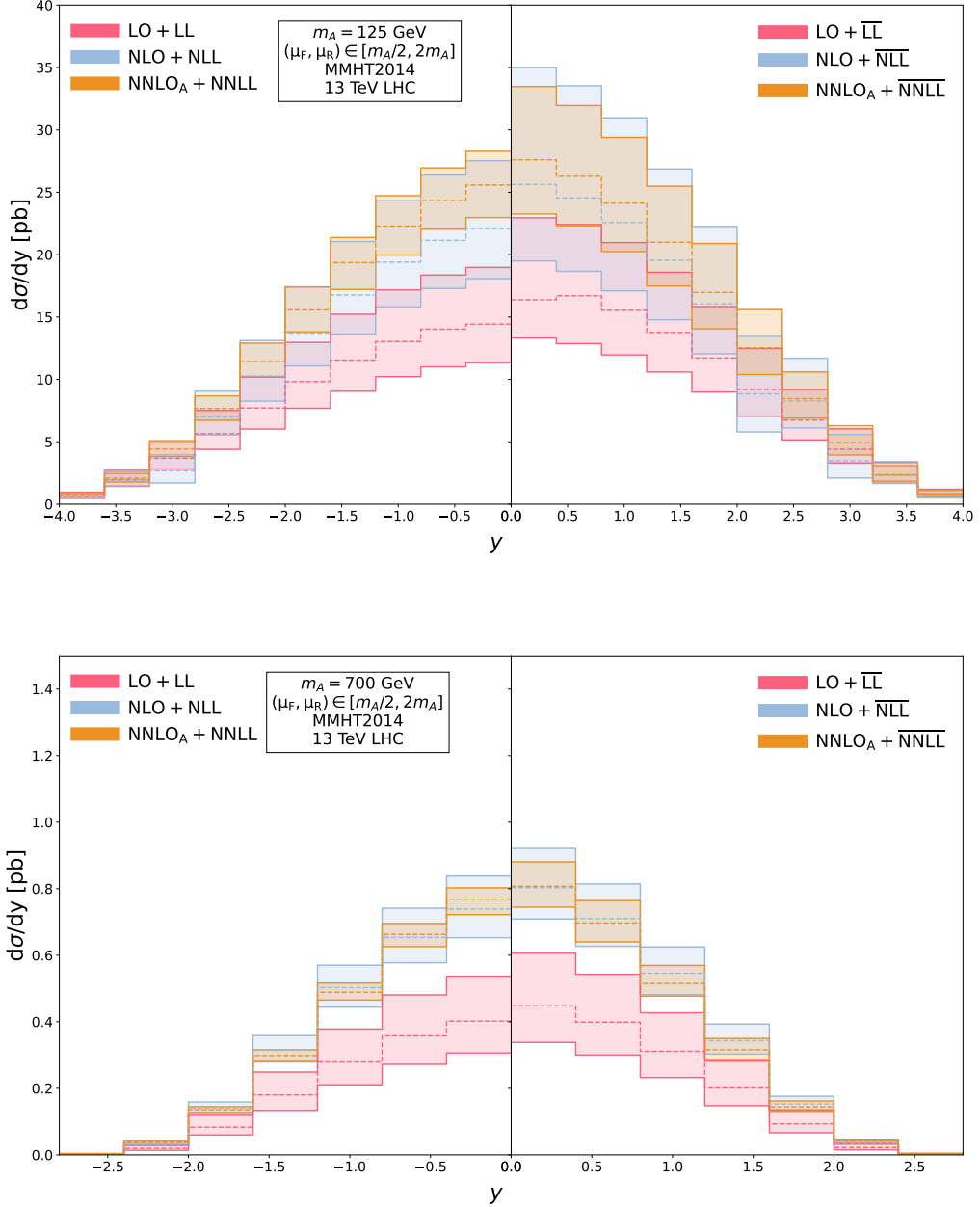


Figure 4: Comparison of 7-point scale variation between SV and SV+NSV resummed results for $m_A = 125$ (top) and 700 (bottom) GeV. The dashed lines refer to the corresponding central scale values at each order.

$m_A = 125, 700$ GeV in the top and bottom panels respectively. The scales $\mu = \{\mu_F, \mu_R\}$ are varied in the range $\frac{1}{2} \leq \frac{\mu}{m_A} \leq 2$, keeping the ratio μ_R/μ_F not larger than 2 and smaller than $1/2$ around the central scale $\mu_R = \mu_F = m_A$.

We also provide Tables 7 and 8 with the numerical values of the SV and SV+NSV

y	LO+LL	LO+ $\overline{\text{LL}}$	NLO+NLL	NLO+ $\overline{\text{NLL}}$	NNLO _A +NNLL	NNLO _A + $\overline{\text{NNLL}}$
0-0.4	14.430 ^{+4.547} _{-3.090}	16.379 ^{+6.580} _{-3.064}	22.086 ^{+5.446} _{-4.008}	25.623 ^{+9.360} _{-6.130}	25.583 ^{+2.696} _{-2.609}	27.605 ^{+5.873} _{-4.340}
0.4-0.8	14.022 ^{+4.339} _{-3.015}	16.704 ^{+5.712} _{-3.833}	21.137 ^{+5.237} _{-3.846}	24.543 ^{+8.994} _{-5.883}	24.326 ^{+2.621} _{-2.292}	26.281 ^{+5.675} _{-3.959}
0.8-1.2	13.035 ^{+4.135} _{-2.814}	15.54 ^{+5.424} _{-3.581}	19.402 ^{+4.919} _{-3.587}	22.572 ^{+8.396} _{-5.474}	22.287 ^{+2.434} _{-2.322}	24.126 ^{+5.273} _{-3.873}
1.2-1.6	11.546 ^{+3.677} _{-2.491}	13.763 ^{+4.820} _{-3.171}	16.759 ^{+4.291} _{-3.120}	19.546 ^{+7.315} _{-4.765}	19.3604 ^{+2.012} _{-2.148}	20.992 ^{+4.491} _{-3.508}
1.6-2.0	9.823 ^{+3.140} _{-2.140}	11.711 ^{+4.123} _{-2.723}	13.715 ^{+3.681} _{-2.636}	16.061 ^{+6.203} _{-4.008}	15.571 ^{+1.843} _{-1.764}	16.968 ^{+3.926} _{-2.906}

Table 7: Values of SV+NSV resummed rapidity distribution at various orders in comparison to the SV resummed results in pb at the central scale $\mu_R = \mu_F = m_A = 125$ GeV for 13 TeV LHC.

y	LO+LL	LO+ $\overline{\text{LL}}$	NLO+NLL	NLO+ $\overline{\text{NLL}}$	NNLO _A +NNLL	NNLO _A + $\overline{\text{NNLL}}$
0-0.4	0.4018 ^{+0.135} _{-0.094}	0.123 ^{+0.158} _{-0.1098}	0.7391 ^{+0.0990} _{-0.0863}	0.803 ^{+0.1178} _{-0.0943}	0.7685 ^{+0.0340} _{-0.0466}	0.807 ^{+0.0735} _{-0.0625}
0.4-0.8	0.3577 ^{+0.123} _{-0.0855}	0.399 ^{+0.14379} _{-0.09845}	0.6538 ^{+0.0875} _{-0.0763}	0.710 ^{+0.1040} _{-0.0834}	0.6628 ^{+0.0325} _{-0.0368}	0.697 ^{+0.06733} _{-0.0566}
0.8-1.2	0.2791 ^{+0.099} _{-0.0685}	0.311 ^{+0.1158} _{-0.0788}	0.5026 ^{+0.0672} _{-0.0586}	0.546 ^{+0.07919} _{-0.0641}	0.4886 ^{+0.0276} _{-0.0233}	0.515 ^{+0.0543} _{-0.0379}
1.2-1.6	0.1803 ^{+0.0686} _{-0.0465}	0.201 ^{+0.0803} _{-0.0535}	0.3162 ^{+0.0423} _{-0.0369}	0.343 ^{+0.0497} _{-0.0405}	0.2985 ^{+0.0167} _{-0.0178}	0.316 ^{+0.03399} _{-0.0291}
1.6-2.0	0.0831 ^{+0.0355} _{-0.0231}	0.093 ^{+0.0416} _{-0.0267}	0.1403 ^{+0.0186} _{-0.0164}	0.153 ^{+0.0232} _{-0.0181}	0.1355 ^{+0.009} _{-0.008}	0.144 ^{+0.0177} _{-0.01365}

Table 8: Values of SV+NSV resummed rapidity distribution at various orders in comparison to the SV resummed results in pb at the central scale $\mu_R = \mu_F = m_A = 700$ GeV for 13 TeV LHC.

resummed rapidity distributions at the central scale for benchmark rapidity values for $m_A = 125, 700$ GeV respectively. These tables also contain the corresponding maximum increments and decrements in the rapidity distribution from the central scale values. From figure 4, we observe that the inclusion of resummed NSV logarithms to the SV resummed predictions increases the 7-point scale uncertainty tremendously at $m_A = 125$ GeV for each perturbative order till NNLO_A. Quantitatively, the uncertainty lies between

(+24.66%, -18.15%) and (+10.54%, -10.2%) for NLO+NLL and NNLO_A+NNLL respectively around $y = 0$. When we include the resummed NSV logarithms to these predictions, the uncertainty increases to (+36.53%, -23.92%) and (+21.28%, -15.72%) at NLO + $\overline{\text{NLL}}$ and NNLO_A + $\overline{\text{NNLL}}$ respectively. However, for $m_A = 700$ GeV, the increase in the 7-point uncertainty due to the addition of resummed NSV logarithms is not very large. For instance, the uncertainty varies between (+14.67%, -11.74%) and (+9.11%, -7.74%) for NLO + $\overline{\text{NLL}}$ and NNLO_A + $\overline{\text{NNLL}}$ respectively which is not significantly higher than (+13.40%, -11.68%) and (+4.42%, -6.06%) at NLO+NLL and NNLO+NLL respectively around central rapidity region. We also observe that the bands of SV+NSV resummed results at NNLO_A + $\overline{\text{NNLL}}$ are completely within the bands of NLO + $\overline{\text{NLL}}$ results for both the values of m_A . On the other hand, this is not the case with SV resummed results at $m_A = 125$ GeV. This suggests that the inclusion of resummed NSV logarithms improves the convergence of the perturbative result especially for $m_A = 125$ GeV.

Before moving forward to the comparison of SV and SV+NSV resummed predictions under the variation of μ_R and μ_F scales individually, we would like to make few comments which would help in the better understanding of our results. The resummed predictions that we compute numerically for the phenomenological analysis, when truncated to a particular logarithmic accuracy, contains not only the distributions and logarithms that we are resumming using the all-order structure but also certain spurious terms. These spurious terms arise from the “inexact” Mellin inversion of the N -space resummed result and are beyond the precision of the resummed quantity. For instance, the spurious terms developed in the SV resummation are at the NSV and beyond NSV accuracy and those developed through NSV resummation are beyond NSV accuracy in perturbative QCD. We have discussed the effect of these spurious terms in our numerical results in great detail for the case of inclusive cross-section and the rapidity distribution of the Higgs Boson production through gluon fusion in Refs.[82, 84]. The same behaviour is expected to be followed by the SV and SV+NSV resummed results of rapidity distribution of the pseudo-scalar Higgs Boson as well.

Now, let us do the comparison of SV and SV+NSV resummed predictions by varying the factorisation scale μ_F keeping μ_R fixed. In figure 5, we provide plots for bin-integrated rapidity distributions for the resummed SV(left panel) and resummed SV+NSV(right panel) corrections for $m_A = 125, 700$ GeV keeping $\mu_R = m_A$ in the top and bottom panels respectively. The uncertainty bands are obtained by varying the factorization scale in the range $\{1/2, 1\}m_A$ around the central scale $\mu_F = \mu_R = m_A$. The plots given in figure 5 show that the inclusion of resummed NSV corrections to the SV resummed results worsens the variation of the result w.r.t the μ_F scale for both $m_A = 125, 700$ GeV. This can be seen directly from the numerical value of the uncertainty which lies between (+36.53%, -23.92%) and (+21.27%, -15.72%) at NLO + $\overline{\text{NLL}}$ and NNLO_A + $\overline{\text{NNLL}}$ respectively around central rapidity region for $m_A = 125$ GeV. These values are significantly larger than the corresponding SV resummed uncertainties of (+24.66%, -18.15%) and (+10.54%, -10.19%) at NLO+NLL and NNLO_A+NNLL respectively. Likewise, for $m_A = 700$ GeV, the uncertainty lies between (+14.66%, -9.88%) and (+9.11%, -7.75%) for SV+NSV resummed results at NLO + $\overline{\text{NLL}}$ and NNLO_A + $\overline{\text{NNLL}}$ respectively whereas it varies between (+9.58%,

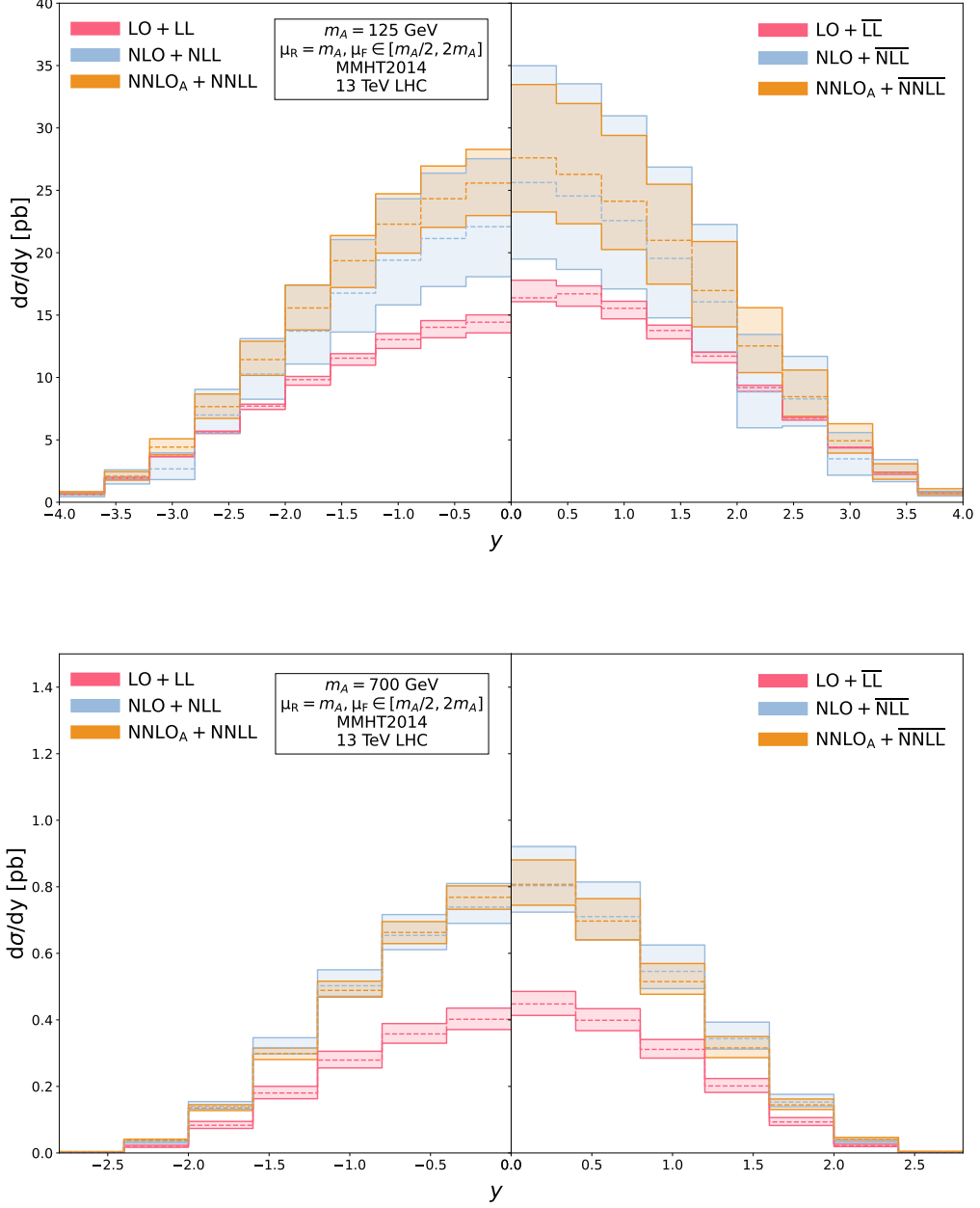


Figure 5: Comparison of μ_F scale variation between SV and SV+NSV resummed results with the scale $\mu_R = m_A$. The dashed lines refer to the corresponding central scale values at each order.

-6.63%) and (+4.43%, -4.71%) for SV resummed results at NLO+NLL and NNLO_A+NNLL respectively around $y = 0$. These values also suggest that the variation w.r.t the factorization scale decreases when we go from $m_A = 125$ GeV to $m_A = 700$ GeV for both SV and SV+NSV resummed predictions. We need to understand the reason behind this consider-

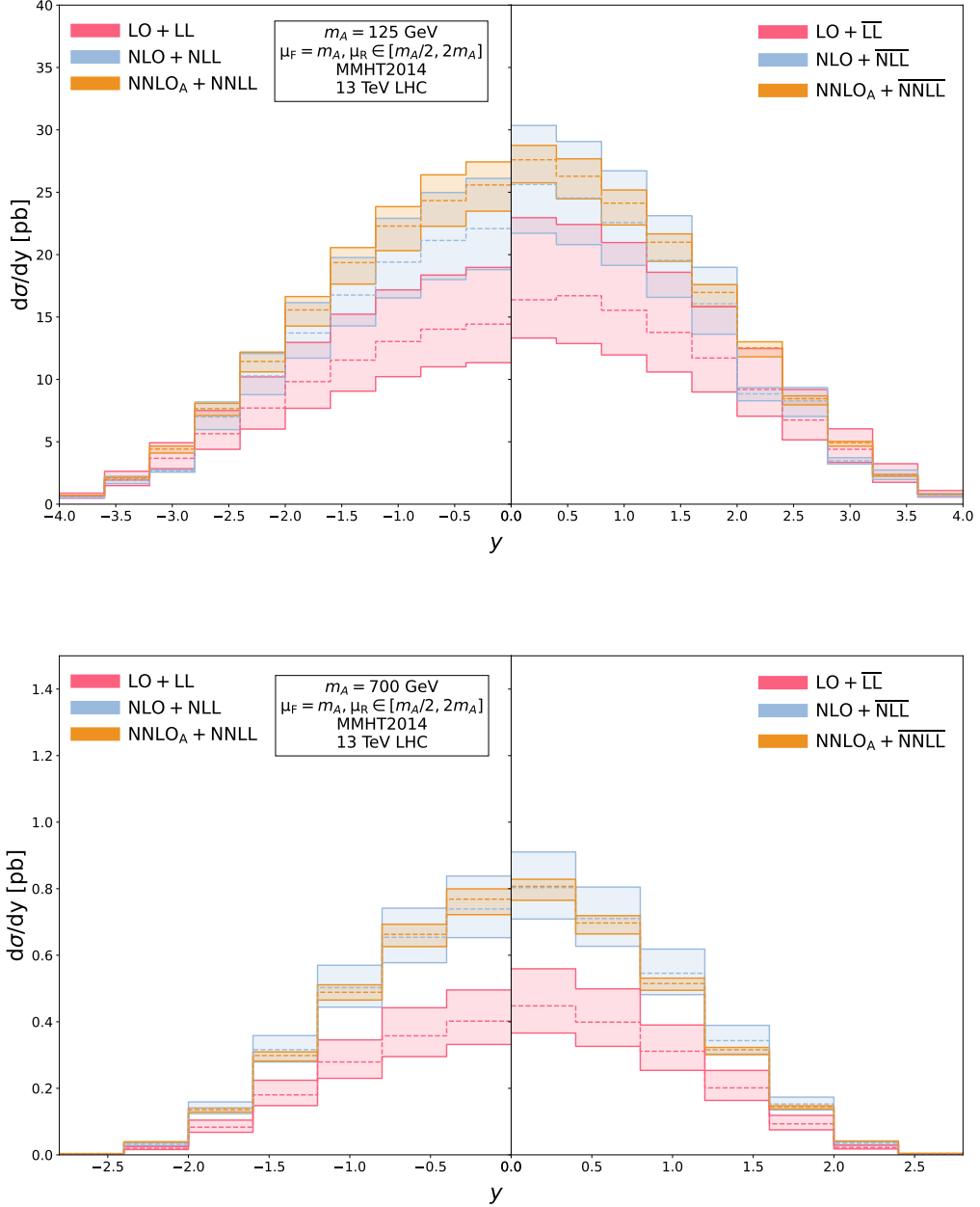


Figure 6: Comparison of μ_R scale variation between SV and SV+NSV resummed results with the scale $\mu_F = m_A$. The dashed lines refer to the corresponding central scale values at each order.

able μ_F scale variation of the resummed predictions. We stated in the paragraph above that our resummed results contain the spurious terms existing due to the "inexact" Mellin inversion. The detailed analysis done in the references [82] and [84] showed us that these spurious terms play an important role in the μ_F scale variation in our results. The study

demonstrated that the μ_F scale uncertainty arising due to the NSV logarithms gets compensated by the variation coming from the beyond NSV logarithms and this compensation increases with the increase in the order of perturbation theory.

First, we try to understand the behaviour of SV resummed results under μ_F variation. The μ_F scale variation seen in the SV resummed results comes mainly from the spurious beyond SV terms arising from the inexact Mellin inversion of the N -space SV resummed results. The plots in figure 5 also show us that the uncertainty decreases when we go from NLO+NLL to NNLO_A+NNLL. This confirms our analysis mentioned above that the compensation between μ_F uncertainty coming from spurious NSV and beyond NSV terms increases at higher orders thereby decreasing the overall scale dependency for the SV resummed result. Now, let us explore the reason for the huge dependency of SV+NSV resummed results on the factorization scale. For the case of SV resummed results, the spurious terms were the main source of μ_F uncertainty, however, for the SV+NSV resummed results, the NSV logarithms contribute significantly towards μ_F variation as well. This uncertainty due to the resummed NSV terms can be compensated by adding the resummed beyond NSV terms which is missing in our calculation. In this case, as well, we have the spurious beyond NSV terms, although now it acts as a compensating factor and cancels the uncertainty due to the resummed NSV logarithms. As a result, we observe that the μ_F variation decreases when we go from NLO + $\overline{\text{NLL}}$ to NNLO_A + $\overline{\text{NNLL}}$ accuracy. However, it can not compensate much and we need to resum the beyond NSV logarithms in order to completely cancel the uncertainty arising from the resummed NSV logarithms.

We next move on to compare the μ_R scale uncertainties of SV and SV+NSV resummed predictions. The plots given in figure 6 illustrate the variation of μ_R scale in the range $\{1/2, 1\}m_A$ around the central scale $\mu_F = \mu_R = m_A$ for the bin-integrated rapidity distributions of the resummed SV(left panel) and resummed SV+NSV(right panel) predictions keeping $\mu_F = m_A$ for $m_A = 125, 700$ GeV. The plots show that the inclusion of resummed NSV logarithms reduces the uncertainty due to the μ_R scale. The uncertainty varies between (+18.22%, -14.87%) and (+7.22%, -8.21%) for the SV resummed predictions at NLO+NLL and NNLO_A+NNLL around the central rapidity region for $m_A = 125$ GeV. The corresponding uncertainty bands for the SV+NSV resummed results lie in the range (+18.45%, -15.24%) and (+4.16%, -6.69%) for NLO + $\overline{\text{NLL}}$ and NNLO_A + $\overline{\text{NNLL}}$ respectively. Similar trends are observed for the case of $m_A = 700$ GeV where the μ_R scale variation lies in the range (+13.40%, -11.67%) and (+4.01%, -6.06%) for the SV resummed results at NLO+NLL and NNLO_A+NNLL respectively whereas for the SV+NSV resummed results, it lies between (+13.33%, -11.74%) and (+2.62%, -5.19%) at NLO+ $\overline{\text{NLL}}$ and NNLO_A + $\overline{\text{NNLL}}$ level respectively around the central rapidity region. We see from these numerical values that the uncertainty remains almost the same at the next-to-leading level for both SV and SV+NSV resummed results, but at the next-to-next-to-leading order, the μ_R scale uncertainty decreases by the addition of the resummed NSV logarithms to the SV resummed results. We know that the inclusion of higher order logarithmic corrections within a particular channel leads to a decrease in the sensitivity of the rapidity distribution w.r.t the renormalization scale. This suggests that the percentage contribution of the resummed NSV logarithms is higher at the NNLO_A + $\overline{\text{NNLL}}$ as compared to the NLO + $\overline{\text{NLL}}$

which results in the significant reduction in the μ_R uncertainty at this order.

To summarize the findings of this section, we observed that the resummed SV+NSV results are significantly dependent on the factorization scale and have large uncertainties related to this scale. In order to understand this, we compared our results with the fixed order as well as the SV resummed predictions. We found that the fixed order corrections have negligible dependence on μ_F scale whereas for the case of SV resummed results, the main source of μ_F variation is the spurious beyond SV terms arising from the "inexact" Mellin inversion of the N -space resummed results. When we add the resummed NSV logarithms, the μ_F uncertainty increases further. Our analysis showed that the reason for this large dependency of the SV+NSV resummed results is the absence of resummed beyond NSV terms which are supposed to cancel the μ_F variation of the NSV logarithms. This suggests that it is important to include resummed beyond NSV terms to get a more accurate and reliable prediction for the rapidity distribution of pseudo-scalar Higgs boson in gluon fusion process. We would also like to mention that we have used the same PDF set for both fixed order and resummed predictions. In order to understand the μ_F variation in a better way, resummed PDFs should be used if they are available. For the renormalization scale, we found that the SV+NSV resummed predictions are the least sensitive when we vary μ_R around the central scale value keeping μ_F fixed. Also, the μ_R scale uncertainty decreases when we go to higher orders in perturbation theory. Thus, as expected the μ_R scale variation decreases by the addition of higher order logarithmic contributions.

10 Discussions and Conclusions

We present the resummed rapidity distribution of pseudo-scalar Higgs Boson production via gluon fusion at LHC up to next-to-next-to-leading-logarithmic($\overline{\text{NNLL}}$) accuracy containing both resummed threshold SV contributions as well as next-to-SV ones. It has been matched to the fixed order predictions up to next-to-next-to-leading order(NNLO_A) accuracy. Beyond NLO, the fixed order rapidity distribution of the pseudo-scalar Higgs boson has been computed using the corresponding result for the scalar Higgs case by appropriately multiplying it with the ratio factor R_{AH} . This ratio method was first established in ref(37) by one of the authors for obtaining the inclusive cross-section of pseudo-scalar Higgs from that of the scalar Higgs boson. In [37], it was shown that the approximate result for the inclusive cross-section obtained in this way has an excellent agreement with the exact result and the difference is found only in terms of next-to-next-to soft distributions which are eventually suppressed in the threshold limit $z \rightarrow 1$. The same trend is expected to follow for the rapidity distribution as well. The resummed corrections have been obtained by using our formalism described in [1] where we restrict ourselves to the diagonal channel for the production of the pseudo-scalar Higgs.

We have performed a detailed numerical analysis of our computed results around the central scale values $\mu_R = \mu_F = m_A$ for benchmark rapidity values for two different cases of pseudo-scalar mass $m_A = 125, 700$ GeV. The K-factor values showed that there is a significant enhancement in the rapidity distribution by the addition of resummed SV+NSV corrections up to next-to-leading order. At NNLO_A , the inclusion of $\overline{\text{NNLL}}$ resummed

results increases the rapidity distribution however, the percentage enhancement drops substantially compared to that of lower order results. For instance, there is an enhancement of 53.3% and 24.97% by the inclusion of $\overline{\text{LL}}$ and $\overline{\text{NLL}}$ resummed results to LO and NLO respectively around the central rapidity region which comes down to an 11.48% increase when we include $\overline{\text{NNLL}}$ to NNLO_A accuracy at $m_A = 700$ GeV. This shows that the addition of resummed corrections improves the perturbative convergence of the result thereby making it more reliable. We further used canonical 7-point variation approach to show that the combined uncertainty due to μ_F and μ_R scales increases by the inclusion of SV+NSV resummed corrections to the fixed order results throughout the rapidity spectrum and for both the cases of pseudo-scalar Higgs masses. Although, the increase in the sensitivity to the unphysical scales decreases when we go to higher values of pseudo-scalar Higgs mass. For example, for $m_A = 700$ GeV, the 7-point scale uncertainty of the resummed result at NNLO_A + $\overline{\text{NNLL}}$ becomes comparable to that of the fixed order rapidity distribution at NNLO_A.

We studied the impact of the renormalisation and the factorisation scales individually on our result for the better understanding of their behaviour. We found that at higher orders, the uncertainty of our result is mainly driven by the factorisation scale. The inclusion of the resummed NSV logarithms to the well-established threshold SV resummed rapidity distribution increases the sensitivity of our result w.r.t the μ_F scale. The main reason behind this is the absence of resummed beyond NSV terms which is responsible for the cancellation of the uncertainty arising due to the resummed NSV logarithms. On the other hand, the uncertainty due to the μ_R scale decreases by the addition of the resummed NSV logarithms. This is expected because the addition of more corrections within the same partonic channel improves the μ_R scale uncertainties.

11 Acknowledgments

We would like to thank the computer administrative unit of IMSc for their help and support. S.T. is funded by the Deutsche Forschungsgemeinschaft (DFG, German Research Foundation) under grant 396021762 — TRR 257 “Particle Physics Phenomenology after the Higgs Discovery”.

A QCD β functions

$$\begin{aligned}
\beta_0 &= \frac{11}{3}C_A - \frac{2}{3}n_f, \\
\beta_1 &= \frac{34}{3}C_A^2 - 2n_fC_F - \frac{10}{3}n_fC_A, \\
\beta_2 &= \frac{2857}{54}C_A^3 - \frac{1415}{54}C_A^2n_f + \frac{79}{54}C_An_f^2 + \frac{11}{9}C_Fn_f^2 - \frac{205}{18}C_FC_An_f + C_F^2n_f \quad (\text{A.1})
\end{aligned}$$

B NLO Results

In this section, we present the analytical results of the NLO hadronic rapidity distribution for the production of the pseudo-scalar Higgs boson via gluon fusion as follows:

$$\begin{aligned}
\frac{d\sigma_{gg}^{A,(1)}}{dY} = & C_A \left[H_{gg}(x_1^0, x_2^0, \mu_F^2) \left\{ (4 + 6\zeta_2) + (2L_{QF}) \mathcal{K}(x_1^0, x_2^0) + \mathcal{K}^2(x_1^0, x_2^0) \right\} \right. \\
& + \int dx_1 \frac{H_{gg,1}(x_1, x_2^0, \mu_F^2)}{(x_1 - x_1^0)} (4\mathcal{K}_b^1) + \int dx_1 H_{gg}(x_1, x_2^0, \mu_F^2) \left\{ \left(-4 \frac{(x_1^0)^2}{x_1^3} + 4 \frac{x_1^0}{x_1^2} \right. \right. \\
& \left. \left. - \frac{8}{x_1} + \frac{4}{x_1^0} \right) \mathcal{K}_a^1 + \frac{4\mathcal{K}_c^1}{(x_1 - x_1^0)} \right\} + \int dx_1 \int dx_2 \frac{H_{gg,1}(x_1, x_2, \mu_F^2)}{(x_1 - x_1^0)} \left(-4 \frac{(x_1^0)^2}{x_1^3} \right. \\
& \left. + 4 \frac{x_1^0}{x_1^2} - \frac{8}{x_1} + \frac{4}{x_1^0} \right) + \int dx_1 \int dx_2 \frac{2 H_{gg,12}(x_1, x_2, \mu_F^2)}{(x_1 - x_1^0)(x_2 - x_2^0)} \\
& + \int dx_1 \int dx_2 \frac{H_{gg}(x_1, x_2, \mu_F^2)}{(x_1 + x_1^0)(x_2 + x_2^0)(x_1 x_2^0 + x_2 x_1^0)^4} \left\{ \frac{1}{x_1^3} \left(4 (x_1^0)^7 (x_2)^4 \right. \right. \\
& + 8 (x_1^0)^7 (x_2)^3 x_2^0 + 8 (x_1^0)^7 (x_2)^2 (x_2^0)^2 + 8 (x_1^0)^7 x_2 (x_2^0)^3 \Big) + \frac{1}{x_1^2} \left(16 (x_1^0)^6 (x_2)^3 x_2^0 \right. \\
& + 32 (x_1^0)^6 (x_2)^2 (x_2^0)^2 + 24 (x_1^0)^6 x_2 (x_2^0)^3 + 16 (x_1^0)^6 (x_2^0)^4 \Big) + \frac{1}{x_1} \left(4 (x_1^0)^5 (x_2)^4 \right. \\
& + 8 (x_1^0)^5 (x_2)^3 x_2^0 + 32 (x_1^0)^5 (x_2)^2 (x_2^0)^2 + 48 (x_1^0)^5 x_2 (x_2^0)^3 + 40 (x_1^0)^5 (x_2^0)^4 \Big) \\
& + \frac{1}{x_1 x_2} (12 (x_1^0 x_2^0)^5) + \frac{1}{x_1^0} \left(8 x_1^5 x_2 (x_2^0)^3 + 4 x_1^5 (x_2^0)^4 \right) \\
& + x_1^4 \left((16 x_2 x_2^0)^2 + 4 x_2 (x_2^0)^3 + 4 (x_2^0)^4 \right) \\
& + x_1^3 \left(12 x_2^3 x_1^0 x_2^0 + 8 x_1^0 x_2 (x_2^0)^3 + 28 x_1^0 (x_2^0)^4 \right) \\
& + x_1^2 \left(20 (x_2 x_1^0 x_2^0)^2 + 88 (x_1^0)^2 (x_2^0)^3 x_2 + 48 (x_1^0)^2 (x_2^0)^4 \right) + x_1 \left(68 (x_1^0 x_2^0)^3 x_2^0 \right) \\
& \left. + x_1 x_2 \left(64 (x_1^0 x_2^0)^3 \right) + 40 (x_1^0 x_2^0)^4 \right\} + (1 \leftrightarrow 2) . \tag{B.1}
\end{aligned}$$

For the qg and gq channels, we obtain

$$\begin{aligned}
\frac{d\sigma_{qg}^{A,(1)}}{dY} = & C_F \left[\int dx_1 H_{qg}(x_1, x_2^0, \mu_F^2) \left\{ \left(\frac{2x_1^0}{x_1^2} \right) + \left(-\frac{4}{x_1} + \frac{4}{x_1^0} + \frac{2x_1^0}{x_1^2} \right) K_a^1 \right\} \right. \\
& + \int dx_1 \int dx_2 \frac{H_{qg,2}(x_1, x_2, \mu_F^2)}{(x_2 - x_2^0)} \left\{ \frac{2x_1^0}{x_1^2} - \frac{4}{x_1} + \frac{4}{x_1^0} \right\} \\
& + \int dx_1 \int dx_2 \frac{H_{qg}(x_1, x_2, \mu_F^2)}{(x_1 + x_1^0)(x_2 + x_2^0)(x_1 x_2^0 + x_2 x_1^0)^4} \left\{ \frac{1}{x_1^2} \left(-2 (x_1^0)^5 x_2^3 \right. \right. \\
& \left. \left. - 4 (x_1^0)^5 x_2^2 x_2^0 - 4 (x_1^0)^5 x_2 (x_2^0)^2 \right) + \frac{1}{x_1} \left(2 (x_1^0)^4 x_2^3 - 2 (x_1^0)^4 x_2^2 x_2^0 - 4 (x_1^0)^4 x_2 (x_2^0)^2 \right) \right. \\
& \left. + \frac{1}{x_1^0} \left(8 x_1^4 x_2 (x_2^0)^2 + 4 x_1^4 (x_2^0)^3 \right) + \left(4 x_1^3 x_2^2 x_2^0 + 2 x_1^3 x_2 (x_2^0)^2 + 2 x_1^2 x_1^0 x_2^3 \right) \right.
\end{aligned}$$

$$\begin{aligned}
& -6x_1^2x_1^0x_2(x_2^0)^2 - x_1^2x_1^0(x_2^0)^3 + 3x_1(x_1^0)^2x_2(x_2^0)^2 + x_1(x_1^0)^2(x_2^0)^3 + 5(x_1^0)^3x_2^2x_2^0 \\
& + 7(x_1^0)^3x_2(x_2^0)^2 \Big) \Big] , \tag{B.2}
\end{aligned}$$

$$\frac{d\sigma_{q\bar{q}}^{A,(1)}}{dY} = \frac{d\sigma_{gq}^{A,(1)}}{dY} \Big|_{1 \leftrightarrow 2} . \tag{B.3}$$

For the $q\bar{q}$ -channel, we find

$$\begin{aligned}
\frac{d\sigma_{q\bar{q}}^{A,(1)}}{dY} = & \frac{(N^2 - 1)C_F}{N} \left[\int dx_1 dx_2 H_{q\bar{q}}(x_1, x_2, \mu_F^2) \left\{ \frac{1}{x_1^2} \left(4(x_1^0)^3(x_1^0x_2^0)^3x_2 \right. \right. \right. \\
& + 4(x_1^0x_2^0)^4(x_1^0)^2 \Big) + \frac{1}{x_1} \left(4(x_1^0)^5(x_2x_2^0)^2 + 8(x_1^0)^5x_2(x_2^0)^3 + 4(x_1^0)^5(x_2^0)^4 \right) \\
& + x_1^4 \left(4(x_2x_2^0)^4 + 4x_2(x_2^0)^3 \right) + x_1^3 \left(4x_1^0(x_2x_2^0)^2 + 8x_1^0x_2(x_2^0)^3 + x_1^0(x_2^0)^4 \right) \\
& + x_1^2 \left(-8(x_1^0x_2^0x_2)^2 + x_2(x_1^0)^2(x_2^0)^3 + (x_1^0x_2^0)^2(x_2^0)^2 \right) + x_1x_2 \left(-16(x_1^0x_2^0)^3 \right) \\
& \left. \left. \left. + x_1 \left(-12(x_1^0x_2^0)^3x_2^0 \right) - 8(x_1^0x_2^0)^4 \right\} \right] + (1 \leftrightarrow 2) . \tag{B.4}
\end{aligned}$$

In the above equations, we have introduced the following abbreviations

$$\begin{aligned}
H_{ab,12}(x_1, x_2, \mu_F^2) &= H_{ab}(x_1, x_2, \mu_F^2) - H_{ab}(x_1^0, x_2, \mu_F^2) - H_{ab}(x_1, x_2^0, \mu_F^2) \\
&+ H_{ab}(x_1^0, x_2^0, \mu_F^2) , \\
H_{ab,1}(x_1, z, \mu_F^2) &= H_{ab}(x_1, z, \mu_F^2) - H_{ab}(x_1^0, z, \mu_F^2) , \\
H_{ab,2}(z, x_2, \mu_F^2) &= H_{ab}(z, x_2, \mu_F^2) - H_{ab}(z, x_2^0, \mu_F^2) , \tag{B.5}
\end{aligned}$$

where

$$\begin{aligned}
H_{q\bar{q}}(x_1, x_2, \mu_F^2) &= f_q(x_1, \mu_F^2) f_{\bar{q}}(x_2, \mu_F^2) + f_{\bar{q}}(x_1, \mu_F^2) f_q(x_2, \mu_F^2) , \\
H_{gq}(x_1, x_2, \mu_F^2) &= f(x_1, \mu_F^2) \left(f_q(x_2, \mu_F^2) + f_{\bar{q}}(x_2, \mu_F^2) \right) , \\
H_{qg}(x_1, x_2, \mu_F^2) &= H_{gq}(x_2, x_1, \mu_F^2) , \\
H_{gg}(x_1, x_2, \mu_F^2) &= f_g(x_1, \mu_F^2) f_g(x_2, \mu_F^2) . \tag{B.6}
\end{aligned}$$

$$\begin{aligned}
\mathcal{K}_{a_1} &= \ln \left(\frac{2Q^2(1-x_2^0)(x_1-x_1^0)}{\mu_F^2(x_1+x_1^0)x_2^0} \right) , & \mathcal{K}_{b_1} &= \ln \left(\frac{Q^2(1-x_2^0)(x_1-x_1^0)}{\mu_F^2x_1^0x_2^0} \right) , \\
\mathcal{K}_{c_1} &= \ln \left(\frac{2x_1^0}{x_1+x_1^0} \right) , & \mathcal{K}(x_1^0, x_2^0) &= \ln \left(\frac{(1-x_1^0)(1-x_2^0)}{x_1^0x_2^0} \right) . \tag{B.7}
\end{aligned}$$

The \mathcal{K}_{a_2} , \mathcal{K}_{b_2} and \mathcal{K}_{c_2} can be obtained from \mathcal{K}_{a_1} , \mathcal{K}_{b_1} and \mathcal{K}_{c_1} by using $1 \leftrightarrow 2$ symmetry.

C Anomalous dimensions

$$\begin{aligned}
\gamma_{g,1}^A &= \frac{11}{3}C_A - \frac{2}{3}n_f, \\
\gamma_{g,2}^A &= \frac{34}{3}C_A^2 - 2n_fC_F - \frac{10}{3}n_fC_A, \\
\gamma_{g,3}^A &= \frac{2857}{54}C_A^3 - \frac{1415}{54}C_A^2n_f + \frac{79}{54}C_An_f^2 + \frac{11}{9}C_Fn_f^2 - \frac{205}{18}C_FC_An_f + C_F^2n_f. \quad (C.1)
\end{aligned}$$

$$\begin{aligned}
A_{g,1}^A &= 4C_A, \\
A_{g,2}^A &= 8C_A^2 \left\{ \frac{67}{18} - \zeta_2 \right\} + 8C_An_f \left\{ -\frac{5}{9} \right\}, \\
A_{g,3}^A &= 16C_A^3 \left\{ \frac{245}{24} - \frac{67}{9}\zeta_2 + \frac{11}{6}\zeta_3 + \frac{11}{5}\zeta_2^2 \right\} + 16C_AC_Fn_f \left\{ -\frac{55}{24} + 2\zeta_3 \right\} \\
&\quad + 16C_A^2n_f \left\{ -\frac{209}{108} + \frac{10}{9}\zeta_2 - \frac{7}{3}\zeta_3 \right\} + 16C_An_f^2 \left\{ -\frac{1}{27} \right\}. \quad (C.2)
\end{aligned}$$

$$\begin{aligned}
B_{g,1}^A &= n_f \left\{ -\frac{2}{3} \right\} + C_A \left\{ \frac{11}{3} \right\}, \\
B_{g,2}^A &= C_Fn_f \left\{ -2 \right\} + C_An_f \left\{ -\frac{8}{3} \right\} + C_A^2 \left\{ \frac{32}{3} + 12\zeta_3 \right\}, \\
B_{g,3}^A &= C_Fn_f^2 \left\{ \frac{11}{9} \right\} + C_F^2n_f + C_An_f^2 \left\{ \frac{29}{18} \right\} + C_AC_Fn_f \left\{ -\frac{241}{18} \right\} + C_A^2n_f \left\{ -\frac{233}{18} \right. \\
&\quad \left. - \frac{80}{3}\zeta_3 - \frac{8}{3}\zeta_2 - \frac{4}{3}\zeta_2^2 \right\} + C_A^3 \left\{ \frac{79}{2} - 80\zeta_5 + \frac{536}{3}\zeta_3 + \frac{8}{3}\zeta_2 - 16\zeta_2\zeta_3 + \frac{22}{3}\zeta_2^2 \right\}. \quad (C.3)
\end{aligned}$$

$$\begin{aligned}
f_{g,1}^A &= 0, \\
f_{g,2}^A &= C_A^2 \left\{ -\frac{22}{3}\zeta_2 - 28\zeta_3 + \frac{808}{27} \right\} + C_An_f \left\{ \frac{4}{3}\zeta_2 - \frac{112}{27} \right\}, \\
f_{g,3}^A &= C_A^3 \left\{ \frac{352}{5}\zeta_2^2 + \frac{176}{3}\zeta_2\zeta_3 - \frac{12650}{81}\zeta_2 - \frac{1316}{3}\zeta_3 + 192\zeta_5 + \frac{136781}{729} \right\} \\
&\quad + C_A^2n_f \left\{ -\frac{96}{5}\zeta_2^2 + \frac{2828}{81}\zeta_2 + \frac{728}{27}\zeta_3 - \frac{11842}{729} \right\} \\
&\quad + C_AC_Fn_f \left\{ \frac{32}{5}\zeta_2^2 + 4\zeta_2 + \frac{304}{9}\zeta_3 - \frac{1711}{27} \right\} + C_An_f^2 \left\{ -\frac{40}{27}\zeta_2 + \frac{112}{27}\zeta_3 - \frac{2080}{729} \right\}. \quad (C.4)
\end{aligned}$$

$$\mathbf{D}_{d,g,1}^A = 0,$$

$$\begin{aligned}
\mathbf{D}_{d,g,2}^A &= C_{An_f} \left\{ \frac{112}{27} - \frac{8}{3} \zeta_2 \right\} + C_A^2 \left\{ -\frac{808}{27} + 28\zeta_3 + \frac{44}{3} \zeta_2 \right\}, \\
\mathbf{D}_{d,g,3}^A &= C_{An_f}^2 \left\{ -\frac{1856}{729} - \frac{32}{27} \zeta_3 + \frac{160}{27} \zeta_2 \right\} + C_A C_{Fn_f} \left\{ \frac{1711}{27} - \frac{304}{9} \zeta_3 - 8\zeta_2 - \frac{32}{5} \zeta_2^2 \right\} \\
&\quad + C_{An_f}^2 \left\{ \frac{62626}{729} - \frac{536}{9} \zeta_3 - \frac{7760}{81} \zeta_2 + \frac{208}{15} \zeta_2^2 \right\} + C_A^3 \left\{ -\frac{297029}{729} - 192\zeta_5 + \frac{14264}{27} \zeta_3 \right. \\
&\quad \left. + \frac{27752}{81} \zeta_2 - \frac{176}{3} \zeta_2 \zeta_3 - \frac{616}{15} \zeta_2^2 \right\}. \tag{C.5}
\end{aligned}$$

D Results of SV rapidity distribution to third order

$$\Delta_{d,g,1}^{A,SV} = \delta\bar{\delta} \left\{ C_A (4 + 6\zeta_2) \right\} + \bar{\mathcal{D}}_0 \mathcal{D}_0 \left\{ C_A (2) \right\} + \delta\bar{\mathcal{D}}_1 \left\{ C_A (4) \right\} + (z_1 \leftrightarrow z_2), \tag{D.1}$$

$$\begin{aligned}
\Delta_{d,g,2}^{A,SV} &= \delta\bar{\delta} \left[\left\{ C_{Fn_f} \left(-\frac{80}{3} + 6 \ln \left(\frac{\mu_R^2}{m_t^2} \right) + 8\zeta_3 \right) \right\} + \left\{ C_{An_f} \left(-\frac{41}{3} - 4\zeta_3 - \frac{20}{3} \zeta_2 \right) \right\} \right] \\
&\quad + \left\{ C_A^2 \left(\frac{247}{3} - 22\zeta_3 + \frac{278}{3} \zeta_2 + \frac{126}{5} \zeta_2^2 \right) \right\} + \bar{\mathcal{D}}_0 \mathcal{D}_0 \left[\left\{ C_{An_f} \left(-\frac{20}{9} \right) \right\} \right] \\
&\quad + \left\{ C_A^2 \left(\frac{278}{9} + 4\zeta_2 \right) \right\} + \bar{\mathcal{D}}_1 \mathcal{D}_0 \left[\left\{ C_{An_f} \left(\frac{8}{3} \right) \right\} + \left\{ C_A^2 \left(-\frac{44}{3} \right) \right\} \right] \\
&\quad + \mathcal{D}_0 \bar{\mathcal{D}}_2 \left\{ C_A^2 (24) \right\} + \bar{\mathcal{D}}_1 \mathcal{D}_1 \left\{ C_A^2 (24) \right\} + \delta\bar{\mathcal{D}}_0 \left[\left\{ C_{An_f} \left(+\frac{112}{27} - \frac{8}{3} \zeta_2 \right) \right\} \right. \\
&\quad \left. + \left\{ C_A^2 \left(-\frac{808}{27} + 60\zeta_3 + \frac{44}{3} \zeta_2 \right) \right\} \right] + \delta\bar{\mathcal{D}}_1 \left[\left\{ C_{An_f} \left(-\frac{40}{9} \right) \right\} + \left\{ C_A^2 \left(\frac{556}{9} \right. \right. \right. \\
&\quad \left. \left. + 8\zeta_2 \right) \right\} \right] + \delta\bar{\mathcal{D}}_2 \left[\left\{ C_{An_f} \left(\frac{4}{3} \right) \right\} + \left\{ C_A^2 \left(-\frac{22}{3} \right) \right\} \right] + \delta\bar{\mathcal{D}}_3 \left\{ C_A^2 (8) \right\} + (z_1 \leftrightarrow z_2), \tag{D.2}
\end{aligned}$$

$$\begin{aligned}
\Delta_{d,g,3}^{A,SV} &= \delta\bar{\delta} \left[\left\{ n_f \left(-2C_J^{(2)} \right) \right\} + \left\{ C_{Fn_f}^2 \left(\frac{749}{9} - \frac{8}{9} \zeta_4 - \frac{112}{3} \zeta_3 - \frac{20}{9} \zeta_2 \right) \right\} \right] \\
&\quad + \left\{ C_{Fn_f}^2 \left(\frac{457}{6} - 160\zeta_5 + 104\zeta_3 \right) \right\} + \left\{ C_{An_f}^2 \left(\frac{3457}{81} - \frac{152}{9} \zeta_4 + \frac{56}{3} \zeta_3 - 8\zeta_2 \right. \right. \\
&\quad \left. \left. - \frac{8}{45} \zeta_2^2 \right) \right\} + \left\{ C_A C_{Fn_f} \left(-\frac{1797}{2} + 48 \ln \left(\frac{\mu_R^2}{m_t^2} \right) + 80\zeta_5 + \frac{44}{9} \zeta_4 + \frac{904}{3} \zeta_3 - \frac{3205}{9} \zeta_2 \right. \right. \\
&\quad \left. \left. + 72\zeta_2 \ln \left(\frac{\mu_R^2}{m_t^2} \right) + 144\zeta_2 \zeta_3 \right) \right\} + \left\{ C_A^2 n_f \left(-\frac{56683}{81} + \frac{596}{9} \zeta_5 + \frac{5258}{27} \zeta_4 + \frac{188}{27} \zeta_3 \right. \right. \\
&\quad \left. \left. - \frac{5138}{27} \zeta_2 - 136\zeta_2 \zeta_3 - \frac{824}{15} \zeta_2^2 \right) \right\} + \left\{ C_A^3 \left(\frac{57284}{27} - \frac{4006}{3} \zeta_6 + \frac{682}{9} \zeta_5 - \frac{15257}{27} \zeta_4 \right) \right\}
\end{aligned}$$

$$\begin{aligned}
& - \frac{33098}{27} \zeta_3 + \frac{800}{3} \zeta_3^2 + \frac{40235}{27} \zeta_2 - 44 \zeta_2 \zeta_3 + \frac{25982}{45} \zeta_2^2 + \frac{12688}{35} \zeta_2^3 \Big) \Big] \\
& + \delta \bar{\mathcal{D}}_0 \left\{ C_A n_f^2 \left(-\frac{1856}{729} - \frac{32}{27} \zeta_3 + \frac{160}{27} \zeta_2 \right) \right\} + \delta \bar{\mathcal{D}}_0 \left\{ C_A C_{Fnf} \left(\frac{1711}{27} - \frac{304}{9} \zeta_3 - 8 \zeta_2 \right. \right. \\
& \left. \left. - \frac{32}{5} \zeta_2^2 \right) \right\} + \delta \bar{\mathcal{D}}_0 \left\{ C_A^2 n_f \left(\frac{86818}{729} - \frac{392}{3} \zeta_3 - \frac{8144}{81} \zeta_2 + \frac{16}{5} \zeta_2^2 \right) \right\} + \delta \bar{\mathcal{D}}_0 \left\{ C_A^3 \left(-\frac{471557}{729} \right. \right. \\
& \left. \left. + 192 \zeta_5 + \frac{40088}{27} \zeta_3 + \frac{27560}{81} \zeta_2 - \frac{608}{3} \zeta_2 \zeta_3 + \frac{88}{5} \zeta_2^2 \right) \right\} + \delta \bar{\mathcal{D}}_1 \left\{ C_A n_f^2 \left(\frac{400}{81} - \frac{32}{9} \zeta_2 \right) \right\} \\
& + \delta \bar{\mathcal{D}}_1 \left\{ C_A C_{Fnf} \left(-250 + 48 \ln \left(\frac{\mu_R^2}{m_t^2} \right) + 96 \zeta_3 \right) \right\} + \delta \bar{\mathcal{D}}_1 \left\{ C_A^2 n_f \left(-\frac{19940}{81} + 32 \zeta_3 \right. \right. \\
& \left. \left. + \frac{64}{3} \zeta_2 \right) \right\} + \delta \bar{\mathcal{D}}_1 \left\{ C_A^3 \left(\frac{103654}{81} - 704 \zeta_3 + \frac{680}{9} \zeta_2 - \frac{64}{5} \zeta_2^2 \right) \right\} + \delta \bar{\mathcal{D}}_2 \left\{ C_A n_f^2 \left(-\frac{80}{27} \right) \right\} \\
& + \delta \bar{\mathcal{D}}_2 \left\{ C_A C_{Fnf4} \right\} + \delta \bar{\mathcal{D}}_2 \left\{ C_A^2 n_f \left(\frac{2116}{27} - \frac{112}{3} \zeta_2 \right) \right\} + \delta \bar{\mathcal{D}}_2 \left\{ C_A^3 \left(-\frac{9992}{27} + 488 \zeta_3 \right. \right. \\
& \left. \left. + \frac{616}{3} \zeta_2 \right) \right\} + \delta \bar{\mathcal{D}}_3 \left\{ C_A n_f^2 \left(\frac{16}{27} \right) \right\} + \delta \bar{\mathcal{D}}_3 \left\{ C_A^2 n_f \left(-\frac{656}{27} \right) \right\} + \delta \bar{\mathcal{D}}_3 \left\{ C_A^3 \left(\frac{5428}{27} - 64 \zeta_2 \right) \right\} \\
& + \delta \bar{\mathcal{D}}_4 \left\{ C_A^2 n_f \left(\frac{40}{9} \right) \right\} + \delta \bar{\mathcal{D}}_4 \left\{ C_A^3 \left(-\frac{220}{9} \right) \right\} + \delta \bar{\mathcal{D}}_5 \left\{ C_A^3 (8) \right\} + \bar{\mathcal{D}}_0 \mathcal{D}_0 \left\{ C_A n_f^2 \left(\frac{200}{81} - \frac{16}{9} \zeta_2 \right) \right\} \\
& + \bar{\mathcal{D}}_0 \mathcal{D}_0 \left\{ C_A C_{Fnf} \left(-125 + 24 \ln \left(\frac{\mu_R^2}{m_t^2} \right) + 48 \zeta_3 \right) \right\} + \bar{\mathcal{D}}_0 \mathcal{D}_0 \left\{ C_A^2 n_f \left(-\frac{9970}{81} + 16 \zeta_3 \right. \right. \\
& \left. \left. + \frac{32}{3} \zeta_2 \right) \right\} + \bar{\mathcal{D}}_0 \mathcal{D}_0 \left\{ C_A^3 \left(\frac{51827}{81} - 352 \zeta_3 + \frac{340}{9} \zeta_2 - \frac{32}{5} \zeta_2^2 \right) \right\} + \bar{\mathcal{D}}_1 \mathcal{D}_0 \left\{ C_A n_f^2 \left(-\frac{160}{27} \right) \right\} \\
& + \bar{\mathcal{D}}_1 \mathcal{D}_0 \left\{ C_A C_{Fnf} (8) \right\} + \bar{\mathcal{D}}_1 \mathcal{D}_0 \left\{ C_A^2 n_f \left(\frac{4232}{27} - \frac{224}{3} \zeta_2 \right) \right\} + \bar{\mathcal{D}}_1 \mathcal{D}_0 \left\{ C_A^3 \left(-\frac{19984}{27} + 976 \zeta_3 \right. \right. \\
& \left. \left. + \frac{1232}{3} \zeta_2 \right) \right\} + \mathcal{D}_0 \bar{\mathcal{D}}_2 \left\{ C_A n_f^2 \left(\frac{16}{9} \right) \right\} + \mathcal{D}_0 \bar{\mathcal{D}}_2 \left\{ C_A^2 n_f \left(-\frac{656}{9} \right) \right\} + \mathcal{D}_0 \bar{\mathcal{D}}_2 \left\{ C_A^3 \left(\frac{5428}{9} - 192 \zeta_2 \right) \right\} \\
& + \mathcal{D}_0 \bar{\mathcal{D}}_3 \left\{ C_A^2 n_f \left(\frac{160}{9} \right) \right\} + \mathcal{D}_0 \bar{\mathcal{D}}_3 \left\{ C_A^3 \left(-\frac{880}{9} \right) \right\} + \mathcal{D}_0 \bar{\mathcal{D}}_4 \left\{ C_A^3 (40) \right\} + \bar{\mathcal{D}}_1 \mathcal{D}_1 \left\{ C_A n_f^2 \left(\frac{16}{9} \right) \right\} \\
& + \bar{\mathcal{D}}_1 \mathcal{D}_1 \left\{ C_A^2 n_f \left(-\frac{656}{9} \right) \right\} + \bar{\mathcal{D}}_1 \mathcal{D}_1 \left\{ C_A^3 \left(\frac{5428}{9} - 192 \zeta_2 \right) \right\} + \mathcal{D}_1 \bar{\mathcal{D}}_2 \left\{ C_A^2 n_f \left(\frac{160}{3} \right) \right\} \\
& + \mathcal{D}_1 \bar{\mathcal{D}}_2 \left\{ C_A^3 \left(-\frac{880}{3} \right) \right\} + \mathcal{D}_1 \bar{\mathcal{D}}_3 \left\{ C_A^3 (160) \right\} + \bar{\mathcal{D}}_2 \mathcal{D}_2 \left\{ C_A^3 (120) \right\} + (z_1 \leftrightarrow z_2).
\end{aligned} \tag{D.3}$$

Here, $\mathcal{D}_j = \left[\frac{\ln^j(1-z_1)}{(1-z_1)} \right]_+$, $\bar{\mathcal{D}}_j = \left[\frac{\ln^j(1-z_2)}{(1-z_2)} \right]_+$, $\delta = \delta(1-z_1)$ and $\bar{\delta} = \delta(1-z_2)$.

E The Resummation constant $\tilde{g}_{d,g,0}^A$

$$\tilde{g}_{d,g,0}^A(a_s(\mu_R^2)) = \sum_{i=0}^{\infty} a_s^i(\mu_R^2) \tilde{g}_{d,g,0,i}^A \quad . \tag{E.1}$$

$$\tilde{g}_{d,g,0,0}^A = 1, \quad (\text{E.2})$$

$$\tilde{g}_{d,g,0,1}^A = n_f \left\{ \frac{4}{3} L_{fr} \right\} + C_A \left\{ 8 + 16\zeta_2 - \frac{22}{3} L_{fr} \right\} + \gamma_E C_A \left\{ -8L_{qr} + 8L_{fr} \right\} + \gamma_E^2 C_A \left\{ 8 \right\}, \quad (\text{E.3})$$

$$\begin{aligned} \tilde{g}_{d,g,0,2}^A = & n_f C_F \left\{ -\frac{160}{3} + 12L_{rmt} + 16\zeta_3 + 4L_{fr} \right\} + n_f^2 \left\{ \frac{4}{3} L_{fr}^2 \right\} + C_A n_f \left\{ -\frac{82}{3} - \frac{88}{9} \zeta_3 \right. \\ & - \frac{160}{9} \zeta_2 + \frac{20}{3} L_{qr} + \frac{32}{3} L_{qr} \zeta_2 + 16L_{fr} + \frac{64}{3} L_{fr} \zeta_2 - \frac{44}{3} L_{fr}^2 \left. \right\} + C_A^2 \left\{ \frac{494}{3} - \frac{308}{9} \zeta_3 \right. \\ & + \frac{2224}{9} \zeta_2 + 92\zeta_2^2 - \frac{92}{3} L_{qr} + 24L_{qr} \zeta_3 - \frac{176}{3} L_{qr} \zeta_2 - 80L_{fr} - 24L_{fr} \zeta_3 - \frac{352}{3} L_{fr} \zeta_2 \\ & + \frac{121}{3} L_{fr}^2 \left. \right\} + \gamma_E C_A n_f \left\{ -\frac{224}{27} + \frac{80}{9} L_{qr} - \frac{8}{3} L_{qr}^2 - \frac{80}{9} L_{fr} - \frac{32}{3} L_{fr} L_{qr} + \frac{40}{3} L_{fr}^2 \right. \\ & \left. \right\} + \gamma_E C_A^2 \left\{ \frac{1616}{27} - 56\zeta_3 - \frac{1112}{9} L_{qr} - 112L_{qr} \zeta_2 + \frac{44}{3} L_{qr}^2 + \frac{1112}{9} L_{fr} + 112L_{fr} \zeta_2 \right. \\ & + \frac{176}{3} L_{fr} L_{qr} - \frac{220}{3} L_{fr}^2 \left. \right\} + \gamma_E^2 C_A n_f \left\{ -\frac{80}{9} + \frac{16}{3} L_{qr} + \frac{32}{3} L_{fr} \right\} + \gamma_E^2 C_A^2 \left\{ \frac{1112}{9} \right. \\ & + 112\zeta_2 - \frac{88}{3} L_{qr} + 32L_{qr}^2 - \frac{176}{3} L_{fr} - 64L_{fr} L_{qr} + 32L_{fr}^2 \left. \right\} + \gamma_E^3 C_A n_f \left\{ -\frac{32}{9} \right\} \\ & + \gamma_E^3 C_A^2 \left\{ \frac{176}{9} - 64L_{qr} + 64L_{fr} \right\} + \gamma_E^4 C_A^2 \left\{ 32 \right\}, \quad (\text{E.4}) \end{aligned}$$

$$\begin{aligned} \tilde{g}_{d,g,0,3}^A = & n_f \left\{ -4C_J^{(2)} \right\} + n_f C_F^2 \left\{ \frac{457}{3} - 320\zeta_5 + 208\zeta_3 - 2L_{fr} \right\} + n_f^2 C_F \left\{ \frac{1498}{9} - \frac{16}{9} \zeta_4 \right. \\ & - \frac{224}{3} \zeta_3 - \frac{40}{9} \zeta_2 - \frac{640}{9} L_{qr} + 16L_{qr} L_{rmt} + \frac{64}{3} L_{qr} \zeta_3 - \frac{662}{9} L_{fr} + 16L_{fr} L_{rmt} \\ & + \frac{64}{3} L_{fr} \zeta_3 + \frac{28}{3} L_{fr}^2 \left. \right\} + n_f^3 \left\{ \frac{32}{27} L_{fr}^3 \right\} + C_A n_f C_F \left\{ -1797 + 96L_{rmt} + \frac{88}{9} \zeta_4 \right. \\ & + 160\zeta_5 + \frac{1792}{3} \zeta_3 - \frac{8660}{9} \zeta_2 + 192\zeta_2 L_{rmt} + 384\zeta_2 \zeta_3 + \frac{3628}{9} L_{qr} - 88L_{qr} L_{rmt} \\ & - \frac{352}{3} L_{qr} \zeta_3 + 32L_{qr} \zeta_2 + \frac{4049}{9} L_{fr} - 88L_{fr} L_{rmt} - \frac{352}{3} L_{fr} \zeta_3 + 64L_{fr} \zeta_2 - \frac{154}{3} L_{fr}^2 \\ & \left. \right\} + C_A n_f^2 \left\{ \frac{6914}{81} - \frac{304}{9} \zeta_4 + \frac{3344}{81} \zeta_3 - \frac{896}{81} \zeta_2 - \frac{64}{45} \zeta_2^2 - \frac{976}{27} L_{qr} - \frac{352}{27} L_{qr} \zeta_3 \right. \\ & - \frac{640}{27} L_{qr} \zeta_2 + \frac{40}{9} L_{qr}^2 + \frac{64}{9} L_{qr}^2 \zeta_2 - \frac{119}{3} L_{fr} - \frac{352}{27} L_{fr} \zeta_3 - \frac{640}{27} L_{fr} \zeta_2 + \frac{80}{9} L_{fr} L_{qr} \\ & + \frac{128}{9} L_{fr} L_{qr} \zeta_2 + \frac{212}{9} L_{fr}^2 + \frac{64}{3} L_{fr}^2 \zeta_2 - \frac{176}{9} L_{fr}^3 \left. \right\} + C_A^2 n_f \left\{ -\frac{113366}{81} + \frac{10516}{27} \zeta_4 \right. \\ & + \frac{808}{9} \zeta_5 - \frac{7336}{81} \zeta_3 - \frac{50768}{81} \zeta_2 - \frac{784}{3} \zeta_2 \zeta_3 - \frac{8576}{45} \zeta_2^2 + \frac{13064}{27} L_{qr} - \frac{736}{27} L_{qr} \zeta_3 \\ & + \frac{14288}{27} L_{qr} \zeta_2 + 120L_{qr} \zeta_2^2 - \frac{404}{9} L_{qr}^2 + 16L_{qr}^2 \zeta_3 - \frac{704}{9} L_{qr}^2 \zeta_2 + \frac{4397}{9} L_{fr} \\ & + \frac{2144}{27} L_{fr} \zeta_3 + \frac{14864}{27} L_{fr} \zeta_2 + \frac{376}{3} L_{fr} \zeta_2^2 - \frac{808}{9} L_{fr} L_{qr} + 32L_{fr} L_{qr} \zeta_3 \end{aligned}$$

$$\begin{aligned}
& - \frac{1408}{9} L_{fr} L_{qr} \zeta_2 - \frac{2146}{9} L_{fr}^2 - 48 L_{fr}^2 \zeta_3 - \frac{704}{3} L_{fr}^2 \zeta_2 + \frac{968}{9} L_{fr}^3 \left. \right\} + C_A^3 \left\{ \frac{114568}{27} \right. \\
& - \frac{8012}{3} \zeta_6 - \frac{30514}{27} \zeta_4 + \frac{3476}{9} \zeta_5 - \frac{158620}{81} \zeta_3 + 96 \zeta_3^2 + \frac{345064}{81} \zeta_2 - \frac{2024}{3} \zeta_2 \zeta_3 \\
& + \frac{6224}{3} \zeta_2^2 + \frac{6080}{7} \zeta_2^3 - \frac{36064}{27} L_{qr} - 160 L_{qr} \zeta_5 + \frac{21608}{27} L_{qr} \zeta_3 - \frac{54256}{27} L_{qr} \zeta_2 \\
& + 352 L_{qr} \zeta_2 \zeta_3 - 660 L_{qr} \zeta_2^2 + \frac{1012}{9} L_{qr}^2 - 88 L_{qr}^2 \zeta_3 + \frac{1936}{9} L_{qr}^2 \zeta_2 - \frac{13115}{9} L_{fr} \\
& + 160 L_{fr} \zeta_5 - \frac{8056}{27} L_{fr} \zeta_3 - \frac{58288}{27} L_{fr} \zeta_2 - 352 L_{fr} \zeta_2 \zeta_3 - \frac{2068}{3} L_{fr} \zeta_2^2 \\
& + \frac{2024}{9} L_{fr} L_{qr} - 176 L_{fr} L_{qr} \zeta_3 + \frac{3872}{9} L_{fr} L_{qr} \zeta_2 + \frac{5390}{9} L_{fr}^2 + 264 L_{fr}^2 \zeta_3 \\
& + \frac{1936}{3} L_{fr}^2 \zeta_2 - \frac{5324}{27} L_{fr}^3 \left. \right\} + \gamma_E C_A n_f C_F \left\{ - \frac{3422}{27} + \frac{608}{9} \zeta_3 + \frac{64}{5} \zeta_2^2 + 500 L_{qr} \right. \\
& - 96 L_{qr} L_{rmt} - 192 L_{qr} \zeta_3 - 8 L_{qr}^2 - 500 L_{fr} + 96 L_{fr} L_{rmt} + 192 L_{fr} \zeta_3 - 32 L_{fr} L_{qr} \\
& + 40 L_{fr}^2 \left. \right\} + \gamma_E C_A n_f^2 \left\{ \frac{3712}{729} + \frac{64}{9} \zeta_3 - \frac{800}{81} L_{qr} + \frac{160}{27} L_{qr}^2 - \frac{32}{27} L_{qr}^3 - \frac{992}{81} L_{fr} \right. \\
& + \frac{320}{27} L_{fr} L_{qr} - \frac{32}{9} L_{fr} L_{qr}^2 - \frac{160}{9} L_{fr}^2 - \frac{32}{3} L_{fr}^2 L_{qr} + \frac{416}{27} L_{fr}^3 \left. \right\} + \gamma_E C_A^2 n_f \left\{ \right. \\
& - \frac{173636}{729} + \frac{1808}{27} \zeta_3 - \frac{9104}{81} \zeta_2 - \frac{32}{5} \zeta_2^2 + \frac{39880}{81} L_{qr} + \frac{704}{9} L_{qr} \zeta_3 + \frac{2240}{9} L_{qr} \zeta_2 \\
& - \frac{4328}{27} L_{qr}^2 - \frac{352}{3} L_{qr}^2 \zeta_2 + \frac{352}{27} L_{qr}^3 - \frac{17096}{81} L_{fr} - \frac{2048}{9} L_{fr} \zeta_3 - \frac{2240}{9} L_{fr} \zeta_2 \\
& - \frac{5920}{27} L_{fr} L_{qr} - 64 L_{fr} L_{qr} \zeta_2 + \frac{352}{9} L_{fr} L_{qr}^2 + \frac{3416}{9} L_{fr}^2 + \frac{544}{3} L_{fr}^2 \zeta_2 + \frac{352}{3} L_{fr}^2 L_{qr} \\
& - \frac{4576}{27} L_{fr}^3 \left. \right\} + \gamma_E C_A^3 \left\{ \frac{943114}{729} + 384 \zeta_5 - \frac{36752}{27} \zeta_3 + \frac{64784}{81} \zeta_2 - \frac{2336}{3} \zeta_2 \zeta_3 \right. \\
& - \frac{176}{5} \zeta_2^2 - \frac{207308}{81} L_{qr} + \frac{5632}{9} L_{qr} \zeta_3 - \frac{23072}{9} L_{qr} \zeta_2 - \frac{2752}{5} L_{qr} \zeta_2^2 + \frac{16912}{27} L_{qr}^2 \\
& - 192 L_{qr}^2 \zeta_3 + \frac{1936}{3} L_{qr}^2 \zeta_2 - \frac{968}{27} L_{qr}^3 + \frac{136204}{81} L_{fr} + \frac{1760}{9} L_{fr} \zeta_3 + \frac{23072}{9} L_{fr} \zeta_2 \\
& + \frac{2752}{5} L_{fr} \zeta_2^2 + \frac{22448}{27} L_{fr} L_{qr} + 384 L_{fr} L_{qr} \zeta_3 + 352 L_{fr} L_{qr} \zeta_2 - \frac{968}{9} L_{fr} L_{qr}^2 \\
& - \frac{13120}{9} L_{fr}^2 - 192 L_{fr}^2 \zeta_3 - \frac{2992}{3} L_{fr}^2 \zeta_2 - \frac{968}{3} L_{fr}^2 L_{qr} + \frac{12584}{27} L_{fr}^3 \left. \right\} \\
& + \gamma_E^2 C_A n_f C_F \left\{ - 500 + 96 L_{rmt} + 192 \zeta_3 + 16 L_{qr} + 32 L_{fr} \right\} + \gamma_E^2 C_A n_f^2 \left\{ \frac{800}{81} \right. \\
& - \frac{320}{27} L_{qr} + \frac{32}{9} L_{qr}^2 - \frac{320}{27} L_{fr} + \frac{64}{9} L_{fr} L_{qr} + \frac{32}{3} L_{fr}^2 \left. \right\} + \gamma_E^2 C_A^2 n_f \left\{ - \frac{39880}{81} \right. \\
& - \frac{704}{9} \zeta_3 - \frac{2240}{9} \zeta_2 + \frac{9008}{27} L_{qr} + \frac{448}{3} L_{qr} \zeta_2 - \frac{992}{9} L_{qr}^2 + \frac{64}{3} L_{qr}^3 + \frac{1856}{9} L_{fr} \\
& + \frac{448}{3} L_{fr} \zeta_2 + 64 L_{fr} L_{qr} + \frac{64}{3} L_{fr} L_{qr}^2 - \frac{1696}{9} L_{fr}^2 - \frac{320}{3} L_{fr}^2 L_{qr} + 64 L_{fr}^3 \left. \right\} \\
& + \gamma_E^2 C_A^3 \left\{ \frac{207308}{81} - \frac{5632}{9} \zeta_3 + \frac{23072}{9} \zeta_2 + \frac{2752}{5} \zeta_2^2 - \frac{13376}{9} L_{qr} + 640 L_{qr} \zeta_3 \right.
\end{aligned}$$

$$\begin{aligned}
& -\frac{2464}{3}L_{qr}\zeta_2 + 840L_{qr}^2 + 384L_{qr}^2\zeta_2 - \frac{352}{3}L_{qr}^3 - \frac{16144}{27}L_{fr} - 640L_{fr}\zeta_3 \\
& -\frac{2464}{3}L_{fr}\zeta_2 - \frac{11248}{9}L_{fr}L_{qr} - 768L_{fr}L_{qr}\zeta_2 - \frac{352}{3}L_{fr}L_{qr}^2 + \frac{9496}{9}L_{fr}^2 \\
& + 384L_{fr}^2\zeta_2 + \frac{1760}{3}L_{fr}^2L_{qr} - 352L_{fr}^3 \left\} + \gamma_E^3 C_A n_f C_F \left\{ -\frac{32}{3} \right\} + \gamma_E^3 C_A n_f^2 \left\{ \frac{640}{81} \right. \\
& - \frac{128}{27}L_{qr} - \frac{128}{27}L_{fr} \left. \right\} + \gamma_E^3 C_A^2 n_f \left\{ -\frac{16928}{81} - \frac{128}{3}\zeta_2 + \frac{5248}{27}L_{qr} - 64L_{qr}^2 \right. \\
& - \frac{2432}{27}L_{fr} - \frac{128}{3}L_{fr}L_{qr} + \frac{320}{3}L_{fr}^2 \left. \right\} + \gamma_E^3 C_A^3 \left\{ \frac{79936}{81} - 448\zeta_3 + \frac{704}{3}\zeta_2 \right. \\
& - \frac{43424}{27}L_{qr} - 768L_{qr}\zeta_2 + 352L_{qr}^2 - \frac{256}{3}L_{qr}^3 + \frac{35680}{27}L_{fr} + 768L_{fr}\zeta_2 \\
& + \frac{704}{3}L_{fr}L_{qr} + 256L_{fr}L_{qr}^2 - \frac{1760}{3}L_{fr}^2 - 256L_{fr}^2L_{qr} + \frac{256}{3}L_{fr}^3 \left. \right\} + \gamma_E^4 C_A n_f^2 \left\{ \frac{64}{27} \right. \\
& \left. \right\} + \gamma_E^4 C_A^2 n_f \left\{ -\frac{2624}{27} + \frac{640}{9}L_{qr} + \frac{128}{9}L_{fr} \right\} + \gamma_E^4 C_A^3 \left\{ \frac{21712}{27} + 384\zeta_2 - \frac{3520}{9}L_{qr} \right. \\
& + 256L_{qr}^2 - \frac{704}{9}L_{fr} - 512L_{fr}L_{qr} + 256L_{fr}^2 \left. \right\} + \gamma_E^5 C_A^2 n_f \left\{ -\frac{256}{9} \right\} + \gamma_E^5 C_A^3 \left\{ \right. \\
& \left. \frac{1408}{9} - 256L_{qr} + 256L_{fr} \right\} + \gamma_E^6 C_A^3 \left\{ +\frac{256}{3} \right\}. \tag{E.5}
\end{aligned}$$

F NSV Resummation exponents $\bar{g}_{d,g,i}^A(\omega)$

$$\bar{g}_{d,g,1}^A(\omega) = 0, \quad \bar{g}_{d,g,2}^A(\omega) = \frac{1}{\beta_0} C_A \left\{ 2L_\omega \right\}, \tag{F.1}$$

$$\begin{aligned}
\bar{g}_{d,g,3}^A(\omega) &= \frac{\beta_1}{\beta_0^2} C_A \left\{ 2\omega + 2L_\omega \right\} + \frac{1}{\beta_0} C_A n_f \left\{ \frac{20}{9}\omega \right\} + \frac{1}{\beta_0} C_A^2 \left\{ -\frac{134}{9}\omega + 4\omega\zeta_2 \right\} + C_A \left\{ -2 \right. \\
& \left. + 2L_{qr} - 2L_{fr} + 2L_{fr}\omega - 4\gamma_E \right\}, \tag{F.2}
\end{aligned}$$

$$\begin{aligned}
\bar{g}_{d,g,4}^A(\omega) &= \frac{\beta_1^2}{\beta_0^3} C_A \left\{ \omega^2 - L_\omega^2 \right\} + \frac{\beta_2}{\beta_0^2} C_A \left\{ -\omega^2 \right\} + \frac{\beta_1}{\beta_0^2} C_A n_f \left\{ -\frac{20}{9}\omega + \frac{10}{9}\omega^2 - \frac{20}{9}L_\omega \right\} \\
& + \frac{\beta_1}{\beta_0^2} C_A^2 \left\{ \frac{134}{9}\omega - 4\omega\zeta_2 - \frac{67}{9}\omega^2 + 2\omega^2\zeta_2 + \frac{134}{9}L_\omega - 4L_\omega\zeta_2 \right\} + \frac{1}{\beta_0} C_A n_f^2 \left\{ \frac{8}{27}\omega \right. \\
& - \frac{4}{27}\omega^2 \left. \right\} + \frac{1}{\beta_0} C_A C_F n_f \left\{ \frac{55}{3}\omega - 16\omega\zeta_3 - \frac{55}{6}\omega^2 + 8\omega^2\zeta_3 \right\} + \frac{1}{\beta_0} C_A^2 n_f \left\{ \frac{418}{27}\omega \right. \\
& + \frac{56}{3}\omega\zeta_3 - \frac{80}{9}\omega\zeta_2 - \frac{209}{27}\omega^2 - \frac{28}{3}\omega^2\zeta_3 + \frac{40}{9}\omega^2\zeta_2 \left. \right\} + \frac{1}{\beta_0} C_A^3 \left\{ -\frac{245}{3}\omega - \frac{44}{3}\omega\zeta_3 \right. \\
& + \frac{536}{9}\omega\zeta_2 - \frac{88}{5}\omega\zeta_2^2 + \frac{245}{6}\omega^2 + \frac{22}{3}\omega^2\zeta_3 - \frac{268}{9}\omega^2\zeta_2 + \frac{44}{5}\omega^2\zeta_2^2 \left. \right\} + \frac{\beta_1}{\beta_0} C_A \left\{ 2L_\omega \right. \\
& - 2L_\omega L_{qr} + 4L_\omega \gamma_E \left. \right\} + C_A n_f \left\{ \frac{116}{27} - \frac{2}{3}\zeta_2 - \frac{20}{9}L_{qr} + \frac{20}{9}L_{fr} - \frac{40}{9}L_{fr}\omega \right. \\
& + \frac{20}{9}L_{fr}\omega^2 + \frac{40}{9}\gamma_E \left. \right\} + C_A^2 \left\{ -\frac{806}{27} + 14\zeta_3 + \frac{23}{3}\zeta_2 + \frac{134}{9}L_{qr} - 4L_{qr}\zeta_2 \right.
\end{aligned}$$

$$\begin{aligned}
& -\frac{134}{9}L_{fr} + 4L_{fr}\zeta_2 + \frac{268}{9}L_{fr}\omega - 8L_{fr}\omega\zeta_2 - \frac{134}{9}L_{fr}\omega^2 + 4L_{fr}\omega^2\zeta_2 - \frac{268}{9}\gamma_E \\
& + 8\gamma_E\zeta_2 \Big\} + \beta_0 C_A \Big\{ -\zeta_2 + 2L_{qr} - L_{qr}^2 + L_{fr}^2 - 2L_{fr}^2\omega + L_{fr}^2\omega^2 - 4\gamma_E \\
& + 4\gamma_E L_{qr} - 4\gamma_E^2 \Big\}, \tag{F.3}
\end{aligned}$$

G NSV Resummation exponents $h_{d,g,ij}^A(\omega)$ and $\tilde{h}_{d,g,ij}^A(\omega, \omega_l)$

$$h_{d,g,00}^A(\omega) = \frac{1}{\beta_0} C_A \Big\{ -4L_\omega \Big\} \quad h_{d,g,01}^A(\omega) = 0, \tag{G.1}$$

$$\begin{aligned}
h_{d,g,10}^A(\omega) = & \frac{1}{2\beta_0^2(\omega-1)} \Big[\beta_1 C_A \Big\{ 8\omega + 8L_\omega \Big\} + \beta_0 C_A n_f \Big\{ \frac{80}{9}\omega \Big\} + \beta_0 C_A^2 \Big\{ -\frac{536}{9}\omega \\
& + 16\omega\zeta_2 - 32\gamma_E\omega \Big\} + \beta_0^2 C_A \Big\{ -4 - 8L_{fr} + 8L_{fr}\omega + 8L_{qr} - 16\gamma_E \Big\} \Big], \tag{G.2}
\end{aligned}$$

$$\tilde{h}_{d,g,11}^A(\omega, \omega_l) = \frac{C_A^2}{\beta_0} \Big\{ -\frac{4\omega_l}{(\omega-1)^2} - \frac{16\omega}{(\omega-1)} \Big\}, \tag{G.3}$$

$$\begin{aligned}
h_{d,g,20}^A(\omega) = & \frac{1}{2\beta_0^3(\omega-1)^2} \Big[\beta_1^2 C_A \Big\{ -4\omega^2 + 4L_\omega^2 \Big\} + \beta_0\beta_2 C_A \Big\{ 4\omega^2 \Big\} + \beta_0\beta_1 C_A n_f \Big\{ \frac{80}{9}\omega \\
& - \frac{40}{9}\omega^2 + \frac{80}{9}L_\omega \Big\} + \beta_0\beta_1 C_A^2 \Big\{ -\frac{536}{9}\omega + 16\omega\zeta_2 + \frac{268}{9}\omega^2 - 8\omega^2\zeta_2 - 32\gamma_E\omega \\
& + 16\gamma_E\omega^2 - \frac{536}{9}L_\omega + 16L_\omega\zeta_2 - 32L_\omega\gamma_E \Big\} + \beta_0^2 C_A n_f^2 \Big\{ -\frac{32}{27}\omega + \frac{16}{27}\omega^2 \Big\} \\
& + \beta_0^2 C_A C_F n_f \Big\{ -\frac{172}{3}\omega + 64\omega\zeta_3 + \frac{86}{3}\omega^2 - 32\omega^2\zeta_3 \Big\} + \beta_0^2 C_A^2 n_f \Big\{ -\frac{1096}{27}\omega \\
& - \frac{224}{3}\omega\zeta_3 + \frac{320}{9}\omega\zeta_2 + \frac{548}{27}\omega^2 + \frac{112}{3}\omega^2\zeta_3 - \frac{160}{9}\omega^2\zeta_2 - \frac{640}{9}\gamma_E\omega \\
& + \frac{320}{9}\gamma_E\omega^2 \Big\} + \beta_0^3 C_A^3 \Big\{ \frac{724}{3}\omega - \frac{112}{3}\omega\zeta_3 - \frac{2144}{9}\omega\zeta_2 + \frac{352}{5}\omega\zeta_2^2 - \frac{362}{3}\omega^2 \\
& + \frac{56}{3}\omega^2\zeta_3 + \frac{1072}{9}\omega^2\zeta_2 - \frac{176}{5}\omega^2\zeta_2^2 + \frac{4288}{9}\gamma_E\omega - 128\gamma_E\omega\zeta_2 - \frac{2144}{9}\gamma_E\omega^2 \\
& + 64\gamma_E\omega^2\zeta_2 \Big\} + \beta_0^2\beta_1 C_A \Big\{ 8\omega - 4\omega^2 - 4L_\omega + 8L_\omega L_{qr} - 16L_\omega\gamma_E \Big\} \\
& + \beta_0^3 C_A n_f \Big\{ -\frac{272}{27} + \frac{32}{3}\zeta_2 - \frac{80}{9}L_{fr} + \frac{160}{9}L_{fr}\omega - \frac{80}{9}L_{fr}\omega^2 + \frac{80}{9}L_{qr} \\
& - \frac{148}{9}\gamma_E \Big\} + \beta_0^3 C_A^2 \Big\{ \frac{1808}{27} - 56\zeta_3 - \frac{224}{3}\zeta_2 + \frac{536}{9}L_{fr} - 16L_{fr}\zeta_2 \\
& - \frac{1072}{9}L_{fr}\omega + 32L_{fr}\omega\zeta_2 + \frac{536}{9}L_{fr}\omega^2 - 16L_{fr}\omega^2\zeta_2 - \frac{536}{9}L_{qr} + 16L_{qr}\zeta_2 \\
& + \frac{1060}{9}\gamma_E - 32\gamma_E\zeta_2 + 32\gamma_E L_{fr} - 64\gamma_E L_{fr}\omega + 32\gamma_E L_{fr}\omega^2 - 32\gamma_E L_{qr} \Big\}
\end{aligned}$$

$$\begin{aligned}
& + 56\gamma_E^2 \Big\} + \beta_0^4 C_A \Big\{ 16\zeta_2 - 4L_{fr}^2 + 8L_{fr}^2\omega - 4L_{fr}^2\omega^2 - 4L_{qr} + 4L_{qr}^2 + 8\gamma_E \\
& - 16\gamma_E L_{qr} + 16\gamma_E^2 \Big\} \Big], \tag{G.4}
\end{aligned}$$

$$\begin{aligned}
h_{d,g,21}^A(\omega) = & \frac{1}{2\beta_0^2(\omega-1)^2} \Big[\beta_1 C_A^2 \Big\{ -32\omega + 16\omega^2 - 32L_\omega \Big\} + \beta_0 C_A^2 n_f \Big\{ -\frac{640}{9}\omega + \frac{320}{9}\omega^2 \\
& \Big\} + \beta_0 C_A^3 \Big\{ \frac{4288}{9}\omega - 128\omega\zeta_2 - \frac{2144}{9}\omega^2 + 64\omega^2\zeta_2 \Big\} + \beta_0^2 C_A n_f \Big\{ \frac{4}{3} \Big\} \\
& + \beta_0^2 C_A^2 \Big\{ -\frac{4}{3} + 32L_{fr} - 64L_{fr}\omega + 32L_{fr}\omega^2 - 32L_{qr} + 48\gamma_E \Big\} \Big], \tag{G.5}
\end{aligned}$$

$$\tilde{h}_{d,22}^g(\omega, \omega_l) = \frac{\omega_l}{\beta_0(\omega-1)^3} \Big[C_A^2 n_f \Big\{ \frac{32}{27} \Big\} + C_A^3 \Big\{ -\frac{176}{27} \Big\} \Big], \tag{G.6}$$

where γ_E is the Euler-Mascheroni constant. Here, $L_\omega = \ln(1-\omega)$ with $\omega = \beta_0 a_s(\mu_R^2) \ln N_1 N_2$, $\omega_l = \beta_0 a_s(\mu_R^2) \ln N_l$ with $l = 1, 2$, $L_{qr} = \ln\left(\frac{q}{\mu_R^2}\right)$ and $L_{fr} = \ln\left(\frac{\mu_F^2}{\mu_R^2}\right)$.

References

- [1] A. H. Ajjath, P. Mukherjee, V. Ravindran, A. Sankar and S. Tiwari, On next to soft corrections for Drell-Yan and Higgs boson rapidity distributions beyond N³LO, [2010.00079](#).
- [2] ATLAS collaboration, G. Aad et al., Observation of a new particle in the search for the Standard Model Higgs boson with the ATLAS detector at t [Phys. Lett. **B716** \(2012\) 1–29](#), [[1207.7214](#)].
- [3] CMS collaboration, S. Chatrchyan et al., Observation of a New Boson at a Mass of 125 GeV with the CMS Experiment at the LHC, [Phys. Lett. **B 716** \(2012\) 30–61](#), [[1207.7235](#)].
- [4] P. W. Higgs, Broken symmetries, massless particles and gauge fields, [Phys. Lett. **12** \(1964\) 132–133](#).
- [5] P. W. Higgs, Broken Symmetries and the Masses of Gauge Bosons, [Phys. Rev. Lett. **13** \(1964\) 508–509](#).
- [6] P. W. Higgs, Spontaneous Symmetry Breakdown without Massless Bosons, [Phys. Rev. **145** \(1966\) 1156–1163](#).
- [7] F. Englert and R. Brout, Broken Symmetry and the Mass of Gauge Vector Mesons, [Phys. Rev. Lett. **13** \(1964\) 321–323](#).
- [8] G. S. Guralnik, C. R. Hagen and T. W. B. Kibble, Global Conservation Laws and Massless Particles, [Phys. Rev. Lett. **13** \(1964\) 585–587](#).
- [9] P. Fayet, Supergauge Invariant Extension of the Higgs Mechanism and a Model for the electron and Its Neutrino, [Nucl. Phys. **B 90** \(1975\) 104–124](#).
- [10] P. Fayet, Supersymmetry and Weak, Electromagnetic and Strong Interactions, [Phys. Lett. **B 64** \(1976\) 159](#).

- [11] P. Fayet, Spontaneously Broken Supersymmetric Theories of Weak, Electromagnetic and Strong Interactions, [Phys. Lett. B](#) **69** (1977) 489.
- [12] S. Dimopoulos and H. Georgi, Softly Broken Supersymmetry and SU(5), [Nucl. Phys. B](#) **193** (1981) 150–162.
- [13] N. Sakai, Naturalness in Supersymmetric Guts, [Z. Phys. C](#) **11** (1981) 153.
- [14] K. Inoue, A. Kakuto, H. Komatsu and S. Takeshita, Aspects of Grand Unified Models with Softly Broken Supersymmetry, [Prog. Theor. Phys.](#) **68** (1982) 927.
- [15] K. Inoue, A. Kakuto, H. Komatsu and S. Takeshita, Renormalization of Supersymmetry Breaking Parameters Revisited, [Prog. Theor. Phys.](#) (1984) .
- [16] K. Inoue, A. Kakuto, H. Komatsu and S. Takeshita, Low-Energy Parameters and Particle Masses in a Supersymmetric Grand Unified Model, [Prog. Theor. Phys.](#) **67** (1982) 1889.
- [17] CMS collaboration, S. Chatrchyan et al., Observation of a New Boson at a Mass of 125 GeV with the CMS Experiment at the LHC, [Phys. Lett. B](#) **716** (2012) 30–61, [[1207.7235](#)].
- [18] C. Anastasiou and K. Melnikov, Higgs boson production at hadron colliders in NNLO QCD, [Nucl. Phys. B](#) **646** (2002) 220–256, [[hep-ph/0207004](#)].
- [19] R. V. Harlander and W. B. Kilgore, Next-to-next-to-leading order Higgs production at hadron colliders, [Phys. Rev. Lett.](#) **88** (2002) 201801, [[hep-ph/0201206](#)].
- [20] V. Ravindran, J. Smith and W. L. van Neerven, NNLO corrections to the total cross-section for Higgs boson production in hadron hadron collisions, [Nucl. Phys. B](#) **665** (2003) 325–366, [[hep-ph/0302135](#)].
- [21] C. Anastasiou, C. Duhr, F. Dulat, F. Herzog and B. Mistlberger, Higgs Boson Gluon-Fusion Production in QCD at Three Loops, [Phys. Rev. Lett.](#) **114** (2015) 212001, [[1503.06056](#)].
- [22] J. R. Ellis, M. K. Gaillard and D. V. Nanopoulos, A Phenomenological Profile of the Higgs Boson, [Nucl. Phys. B](#) **106** (1976) 292.
- [23] M. A. Shifman, A. I. Vainshtein, M. B. Voloshin and V. I. Zakharov, Low-Energy Theorems for Higgs Boson Couplings to Photons, [Sov. J. Nucl. Phys.](#) **30** (1979) 711–716.
- [24] B. A. Kniehl and M. Spira, Low-energy theorems in Higgs physics, [Z. Phys. C](#) **69** (1995) 77–88, [[hep-ph/9505225](#)].
- [25] R. P. Kauffman and W. Schaffer, QCD corrections to production of Higgs pseudoscalars, [Phys. Rev. D](#) **49** (1994) 551–554, [[hep-ph/9305279](#)].
- [26] A. Djouadi, M. Spira and P. M. Zerwas, Two photon decay widths of Higgs particles, [Phys. Lett. B](#) **311** (1993) 255–260, [[hep-ph/9305335](#)].

- [27] R. V. Harlander and W. B. Kilgore,
Production of a pseudoscalar Higgs boson at hadron colliders at next-to-next-to leading order,
[JHEP](#) **10** (2002) 017, [[hep-ph/0208096](#)].
- [28] C. Anastasiou and K. Melnikov,
Pseudoscalar Higgs boson production at hadron colliders in NNLO QCD, [Phys. Rev.](#) **D67**
(2003) 037501, [[hep-ph/0208115](#)].
- [29] K. G. Chetyrkin, B. A. Kniehl, M. Steinhauser and W. A. Bardeen,
Effective QCD interactions of CP odd Higgs bosons at three loops, [Nucl. Phys. B](#) **535**
(1998) 3–18, [[hep-ph/9807241](#)].
- [30] M. Spira, A. Djouadi, D. Graudenz and P. M. Zerwas,
SUSY Higgs production at proton colliders, [Phys. Lett. B](#) **318** (1993) 347–353.
- [31] M. Spira, A. Djouadi, D. Graudenz and P. Zerwas, Higgs boson production at the LHC,
[Nucl. Phys. B](#) **453** (1995) 17–82, [[hep-ph/9504378](#)].
- [32] T. Ahmed, T. Gehrmann, P. Mathews, N. Rana and V. Ravindran,
Pseudo-scalar Form Factors at Three Loops in QCD, [JHEP](#) **11** (2015) 169, [[1510.01715](#)].
- [33] V. Ravindran, On Sudakov and soft resummations in QCD, [Nucl. Phys.](#) **B746** (2006)
58–76, [[hep-ph/0512249](#)].
- [34] V. Ravindran, Higher-order threshold effects to inclusive processes in QCD, [Nucl. Phys.](#)
B752 (2006) 173–196, [[hep-ph/0603041](#)].
- [35] T. Ahmed, M. Mahakhud, N. Rana and V. Ravindran,
Drell-Yan Production at Threshold to Third Order in QCD, [Phys. Rev. Lett.](#) **113** (2014)
112002, [[1404.0366](#)].
- [36] T. Ahmed, M. C. Kumar, P. Mathews, N. Rana and V. Ravindran,
Pseudo-scalar Higgs boson production at threshold N^3 LO and N^3 LL QCD, [Eur. Phys. J.](#)
C76 (2016) 355, [[1510.02235](#)].
- [37] T. Ahmed, M. Bonvini, M. C. Kumar, P. Mathews, N. Rana, V. Ravindran and L. Rottoli,
Pseudo-scalar Higgs boson production at N^3 LO_A + N^3 LL', [Eur. Phys. J.](#) **C76** (2016) 663,
[[1606.00837](#)].
- [38] C. Anastasiou, C. Duhr, F. Dulat, E. Furlan, T. Gehrmann, F. Herzog, A. Lazopoulos and
B. Mistlberger,
High precision determination of the gluon fusion Higgs boson cross-section at the LHC,
[JHEP](#) **05** (2016) 058, [[1602.00695](#)].
- [39] V. Ravindran, J. Smith and W. L. van Neerven,
Two-loop corrections to Higgs boson production, [Nucl. Phys.](#) **B704** (2005) 332–348,
[[hep-ph/0408315](#)].
- [40] D. de Florian, M. Grazzini and Z. Kunszt,
Higgs production with large transverse momentum in hadronic collisions at next-to-leading order,
[Phys. Rev. Lett.](#) **82** (1999) 5209–5212, [[hep-ph/9902483](#)].
- [41] B. Field, J. Smith, M. E. Tejeda-Yeomans and W. L. van Neerven,
NLO corrections to differential cross-sections for pseudoscalar Higgs boson production,
[Phys. Lett. B](#) **551** (2003) 137–145, [[hep-ph/0210369](#)].
- [42] G. F. Sterman,

- Summation of Large Corrections to Short Distance Hadronic Cross-Sections, [Nucl. Phys. B281](#) (1987) 310–364.
- [43] S. Catani and L. Trentadue, Resummation of the QCD Perturbative Series for Hard Processes, [Nucl. Phys. B327](#) (1989) 323–352.
- [44] S. Catani, D. de Florian, M. Grazzini and P. Nason, Soft gluon resummation for Higgs boson production at hadron colliders, [JHEP 07](#) (2003) 028, [[hep-ph/0306211](#)].
- [45] S. Moch and A. Vogt, Higher-order soft corrections to lepton pair and Higgs boson production, [Phys. Lett. B631](#) (2005) 48–57, [[hep-ph/0508265](#)].
- [46] A. Idilbi, X.-d. Ji, J.-P. Ma and F. Yuan, Threshold resummation for Higgs production in effective field theory, [Phys. Rev. D73](#) (2006) 077501, [[hep-ph/0509294](#)].
- [47] V. Ahrens, T. Becher, M. Neubert and L. L. Yang, Renormalization-Group Improved Prediction for Higgs Production at Hadron Colliders, [Eur. Phys. J. C 62](#) (2009) 333–353, [[0809.4283](#)].
- [48] D. de Florian and M. Grazzini, Higgs production through gluon fusion: Updated cross sections at the Tevatron and the LHC, [Phys. Lett. B 674](#) (2009) 291–294, [[0901.2427](#)].
- [49] M. Bonvini and S. Marzani, Resummed Higgs cross section at N³LL, [JHEP 09](#) (2014) 007, [[1405.3654](#)].
- [50] S. Catani, L. Cieri, D. de Florian, G. Ferrera and M. Grazzini, Threshold resummation at N³LL accuracy and soft-virtual cross sections at N³LO, [Nucl. Phys. B888](#) (2014) 75–91, [[1405.4827](#)].
- [51] D. de Florian and J. Zurita, Soft-gluon resummation for pseudoscalar Higgs boson production at hadron colliders, [Phys. Lett. B659](#) (2008) 813–820, [[0711.1916](#)].
- [52] N. Agarwal, P. Banerjee, G. Das, P. K. Dhani, A. Mukhopadhyay, V. Ravindran and A. Tripathi, Resummed transverse momentum distribution of pseudo-scalar Higgs boson at NNLO_A+NNLL, [JHEP 12](#) (2018) 105, [[1805.12553](#)].
- [53] V. Ravindran, J. Smith and W. L. van Neerven, QCD threshold corrections to di-lepton and Higgs rapidity distributions beyond N² LO, [Nucl. Phys. B767](#) (2007) 100–129, [[hep-ph/0608308](#)].
- [54] P. Banerjee, G. Das, P. K. Dhani and V. Ravindran, Threshold resummation of the rapidity distribution for Higgs production at NNLO+NNLL, [Phys. Rev. D97](#) (2018) 054024, [[1708.05706](#)].
- [55] P. Banerjee, G. Das, P. K. Dhani and V. Ravindran, Threshold resummation of the rapidity distribution for Drell-Yan production at NNLO+NNLL, [Phys. Rev. D98](#) (2018) 054018, [[1805.01186](#)].
- [56] E. Laenen and G. F. Sterman, Resummation for Drell-Yan differential distributions, in 7th Meeting of the APS Division of Particles Fields, pp. 987–989, 11, 1992.

- [57] G. F. Sterman and W. Vogelsang, Threshold resummation and rapidity dependence, [JHEP](#) **02** (2001) 016, [[hep-ph/0011289](#)].
- [58] A. Mukherjee and W. Vogelsang, Threshold resummation for W-boson production at RHIC, [Phys. Rev. D](#) **73** (2006) 074005, [[hep-ph/0601162](#)].
- [59] P. Bolzoni, Threshold resummation of Drell-Yan rapidity distributions, [Phys. Lett. B](#) **643** (2006) 325–330, [[hep-ph/0609073](#)].
- [60] T. Becher and M. Neubert, Threshold resummation in momentum space from effective field theory, [Phys. Rev. Lett.](#) **97** (2006) 082001, [[hep-ph/0605050](#)].
- [61] T. Becher, M. Neubert and G. Xu, Dynamical Threshold Enhancement and Resummation in Drell-Yan Production, [JHEP](#) **07** (2008) 030, [[0710.0680](#)].
- [62] M. Bonvini, S. Forte, G. Ridolfi and L. Rottoli, Resummation prescriptions and ambiguities in SCET vs. direct QCD: Higgs production as a case study, [JHEP](#) **01** (2015) 046, [[1409.0864](#)].
- [63] M. A. Ebert, J. K. L. Michel and F. J. Tackmann, Resummation Improved Rapidity Spectrum for Gluon Fusion Higgs Production, [JHEP](#) **05** (2017) 088, [[1702.00794](#)].
- [64] M. Cacciari and S. Catani, Soft gluon resummation for the fragmentation of light and heavy quarks at large x, [Nucl. Phys. B](#) **617** (2001) 253–290, [[hep-ph/0107138](#)].
- [65] E. Laenen, L. Magnea and G. Stavenga, On next-to-eikonal corrections to threshold resummation for the Drell-Yan and DIS cross sections, [Phys. Lett. B](#) **669** (2008) 173–179, [[0807.4412](#)].
- [66] E. Laenen, L. Magnea, G. Stavenga and C. D. White, Next-to-Eikonal Corrections to Soft Gluon Radiation: A Diagrammatic Approach, [JHEP](#) **01** (2011) 141, [[1010.1860](#)].
- [67] D. Bonocore, E. Laenen, L. Magnea, L. Vernazza and C. D. White, The method of regions and next-to-soft corrections in Drell-Yan production, [Phys. Lett. B](#) **742** (2015) 375–382, [[1410.6406](#)].
- [68] D. Bonocore, E. Laenen, L. Magnea, S. Melville, L. Vernazza and C. White, A factorization approach to next-to-leading-power threshold logarithms, [JHEP](#) **06** (2015) 008, [[1503.05156](#)].
- [69] D. Bonocore, E. Laenen, L. Magnea, L. Vernazza and C. White, Non-abelian factorisation for next-to-leading-power threshold logarithms, [JHEP](#) **12** (2016) 121, [[1610.06842](#)].
- [70] V. Del Duca, E. Laenen, L. Magnea, L. Vernazza and C. White, Universality of next-to-leading power threshold effects for colourless final states in hadronic collisions, [JHEP](#) **11** (2017) 057, [[1706.04018](#)].
- [71] N. Bahjat-Abbas, D. Bonocore, J. Sinninghe Damsté, E. Laenen, L. Magnea, L. Vernazza and C. White,

- Diagrammatic resummation of leading-logarithmic threshold effects at next-to-leading power, [JHEP 11 \(2019\) 002](#), [[1905.13710](#)].
- [72] G. Soar, S. Moch, J. Vermaseren and A. Vogt, [On Higgs-exchange DIS, physical evolution kernels and fourth-order splitting functions at large x](#), [Nucl. Phys. B 832 \(2010\) 152–227](#), [[0912.0369](#)].
- [73] S. Moch and A. Vogt, [On non-singlet physical evolution kernels and large-x coefficient functions in perturbative QCD](#), [JHEP 11 \(2009\) 099](#), [[0909.2124](#)].
- [74] D. de Florian, J. Mazzitelli, S. Moch and A. Vogt, [Approximate N³LO Higgs-boson production cross section using physical-kernel constraints](#), [JHEP 10 \(2014\) 176](#), [[1408.6277](#)].
- [75] M. Beneke, A. Broggio, M. Garny, S. Jaskiewicz, R. Szafron, L. Vernazza and J. Wang, [Leading-logarithmic threshold resummation of the Drell-Yan process at next-to-leading power](#), [JHEP 03 \(2019\) 043](#), [[1809.10631](#)].
- [76] M. Beneke, M. Garny, S. Jaskiewicz, R. Szafron, L. Vernazza and J. Wang, [Leading-logarithmic threshold resummation of Higgs production in gluon fusion at next-to-leading power](#), [JHEP 01 \(2020\) 094](#), [[1910.12685](#)].
- [77] M. Beneke, A. Broggio, S. Jaskiewicz and L. Vernazza, [Threshold factorization of the Drell-Yan process at next-to-leading power](#), [1912.01585](#).
- [78] A. H. Ajjath, P. Mukherjee and V. Ravindran, [Going beyond soft plus virtual](#), [Phys. Rev. D 105 \(2022\) L091503](#), [[2204.09012](#)].
- [79] A. H. Ajjath, P. Mukherjee and V. Ravindran, [Next to soft corrections to Drell-Yan and Higgs boson productions](#), [Phys. Rev. D 105 \(2022\) 094035](#), [[2006.06726](#)].
- [80] A. H. Ajjath, P. Mukherjee, V. Ravindran, A. Sankar and S. Tiwari, [On next to soft threshold corrections to DIS and SIA processes](#), [2007.12214](#).
- [81] A. H. Ajjath, P. Mukherjee, V. Ravindran, A. Sankar and S. Tiwari, [Next-to SV resummed Drell-Yan cross section beyond leading-logarithm](#), [Eur. Phys. J. C 82 \(2022\) 234](#), [[2107.09717](#)].
- [82] A. H. Ajjath, P. Mukherjee, V. Ravindran, A. Sankar and S. Tiwari, [Resummed Higgs boson cross section at next-to SV to NNLO + \$\overline{\text{NNLL}}\$](#) , [2109.12657](#).
- [83] A. H. Ajjath, P. Mukherjee, V. Ravindran, A. Sankar and S. Tiwari, [Next-to SV resummed rapidity distribution for Drell-Yan to NNLO + \$\overline{\text{NNLL}}\$](#) , [2112.14094](#).
- [84] V. Ravindran, A. Sankar and S. Tiwari, [Resummed next-to-soft corrections to rapidity distribution of Higgs Boson to NNLO + \$\overline{\text{NNLL}}\$](#) , [2205.11560](#).
- [85] A. Bhattacharya, M. C. Kumar, P. Mathews and V. Ravindran, [Next-to-soft-virtual resummed prediction for pseudoscalar Higgs boson production at NNLO+ \$\overline{\text{NNLL}}\$](#) , [Phys. Rev. D 105 \(2022\) 116015](#), [[2112.02341](#)].
- [86] S. L. Adler, [Axial vector vertex in spinor electrodynamics](#), [Phys. Rev. 177 \(1969\) 2426–2438](#).

- [87] O. Tarasov, A. Vladimirov and A. Zharkov,
The Gell-Mann-Low Function of QCD in the Three Loop Approximation, [Phys. Lett. B](#) **93** (1980) 429–432.
- [88] T. Kinoshita, Mass singularities of Feynman amplitudes, [J. Math. Phys.](#) **3** (1962) 650–677.
- [89] T. Lee and M. Nauenberg, Degenerate Systems and Mass Singularities, [Phys. Rev.](#) **133** (1964) B1549–B1562.
- [90] G. Altarelli and G. Parisi, Asymptotic Freedom in Parton Language, [Nucl. Phys. B](#) **126** (1977) 298–318.
- [91] C. Anastasiou, L. J. Dixon and K. Melnikov,
NLO Higgs boson rapidity distributions at hadron colliders, [Nucl. Phys. B Proc. Suppl.](#) **116** (2003) 193–197, [[hep-ph/0211141](#)].
- [92] K. G. Chetyrkin, B. A. Kniehl and M. Steinhauser,
Hadronic Higgs decay to order α_s^{*4} , [Phys. Rev. Lett.](#) **79** (1997) 353–356, [[hep-ph/9705240](#)].
- [93] C. Anastasiou, C. Duhr, F. Dulat, F. Herzog and B. Mistlberger,
Higgs Boson Gluon-Fusion Production in QCD at Three Loops, [Phys. Rev. Lett.](#) **114** (2015) 212001, [[1503.06056](#)].
- [94] C. Anastasiou, K. Melnikov and F. Petriello,
Fully differential Higgs boson production and the di-photon signal through next-to-next-to-leading order, [Nucl. Phys. B](#) **724** (2005) 197–246, [[hep-ph/0501130](#)].
- [95] F. Dulat, B. Mistlberger and A. Pelloni,
Precision predictions at N³LO for the Higgs boson rapidity distribution at the LHC, [Phys. Rev. D](#) **99** (2019) 034004, [[1810.09462](#)].
- [96] V. Sudakov, Vertex parts at very high-energies in quantum electrodynamics, [Sov. Phys. JETP](#) **3** (1956) 65–71.
- [97] A. H. Mueller, On the Asymptotic Behavior of the Sudakov Form-factor, [Phys. Rev. D](#) **20** (1979) 2037.
- [98] J. C. Collins, Algorithm to Compute Corrections to the Sudakov Form-factor, [Phys. Rev. D](#) **22** (1980) 1478.
- [99] A. Sen, Asymptotic Behavior of the Sudakov Form-Factor in QCD, [Phys. Rev. D](#) **24** (1981) 3281.
- [100] S. Moch, J. A. M. Vermaseren and A. Vogt,
The Three loop splitting functions in QCD: The Nonsinglet case, [Nucl. Phys. B](#) **688** (2004) 101–134, [[hep-ph/0403192](#)].
- [101] A. Vogt, S. Moch and J. A. M. Vermaseren,
The Three-loop splitting functions in QCD: The Singlet case, [Nucl. Phys. B](#) **691** (2004) 129–181, [[hep-ph/0404111](#)].
- [102] S. Catani and L. Trentadue, Comment on QCD exponentiation at large x, [Nucl. Phys. B](#) **353** (1991) 183–186.
- [103] A. Vogt,
Next-to-next-to-leading logarithmic threshold resummation for deep inelastic scattering and the Drell-Yan process, [Phys. Lett. B](#) **497** (2001) 228–234, [[hep-ph/0010146](#)].

- [104] T. Becher and M. Neubert, Infrared singularities of scattering amplitudes in perturbative QCD, [*Phys. Rev. Lett.* **102** \(2009\) 162001](#), [[0901.0722](#)].
- [105] E. Gardi and L. Magnea, Factorization constraints for soft anomalous dimensions in QCD scattering amplitudes, [*JHEP* **03** \(2009\) 079](#), [[0901.1091](#)].
- [106] A. Gonzalez-Arroyo, C. Lopez and F. Yndurain, Second Order Contributions to the Structure Functions in Deep Inelastic Scattering. 1. Theoretical Calculations, [*Nucl. Phys. B* **153** \(1979\) 161–186](#).
- [107] G. Curci, W. Furmanski and R. Petronzio, Evolution of Parton Densities Beyond Leading Order: The Nonsinglet Case, [*Nucl. Phys. B* **175** \(1980\) 27–92](#).
- [108] W. Furmanski and R. Petronzio, Singlet Parton Densities Beyond Leading Order, [*Phys. Lett. B* **97** \(1980\) 437–442](#).
- [109] R. Hamberg and W. van Neerven, The Correct renormalization of the gluon operator in a covariant gauge, [*Nucl. Phys. B* **379** \(1992\) 143–171](#).
- [110] R. Ellis and W. Vogelsang, The Evolution of parton distributions beyond leading order: The Singlet case, [hep-ph/9602356](#).
- [111] J. Ablinger, A. Behring, J. Blümlein, A. De Freitas, A. von Manteuffel and C. Schneider, The three-loop splitting functions $P_{qq}^{(2)}$ and $P_{qq}^{(2,N_F)}$, [*Nucl. Phys. B* **922** \(2017\) 1–40](#), [[1705.01508](#)].
- [112] S. Moch, B. Ruijl, T. Ueda, J. A. M. Vermaseren and A. Vogt, Four-Loop Non-Singlet Splitting Functions in the Planar Limit and Beyond, [*JHEP* **10** \(2017\) 041](#), [[1707.08315](#)].
- [113] P. Banerjee, P. K. Dhani, M. C. Kumar, P. Mathews and V. Ravindran, NNLO QCD corrections to production of a spin-2 particle with nonuniversal couplings in the Drell-Yan process, [*Phys. Rev. D* **97** \(2018\) 094028](#), [[1710.04184](#)].
- [114] T. Ahmed, A. A. H., P. Mukherjee, V. Ravindran and A. Sankar, Soft-virtual correction and threshold resummation for n -colorless particles to fourth order in QCD: Part II, [2010.02980](#).
- [115] L. A. Harland-Lang, A. D. Martin, P. Motylinski and R. S. Thorne, Parton distributions in the LHC era: MMHT 2014 PDFs, [*Eur. Phys. J.* **C75** \(2015\) 204](#), [[1412.3989](#)].
- [116] A. Buckley, J. Ferrando, S. Lloyd, K. Nordström, B. Page, M. Rüfenacht, M. Schönherr and G. Watt, LHAPDF6: parton density access in the LHC precision era, [*Eur. Phys. J.* **C75** \(2015\) 132](#), [[1412.7420](#)].
- [117] PARTICLE DATA GROUP collaboration, P. A. Zyla et al., Review of Particle Physics, [*PTEP* **2020** \(2020\) 083C01](#).